Gas Phase Hydrodynamics inside a Circulating Fluidized Bed

by

James C Moran

M.S., Mechanical Engineering, Massachusetts Institute of Technology (1996)

B.S., Mechanical Engineering, University College Dublin (1994)

Submitted to the Department of Mechanical Engineering
in partial fulfillment of the requirements for the degree of

Doctor of Philosophy in Mechanical Engineering

at the

MASSACHUSETTS INSTITUTE OF TECHNOLOGY

February 2001

Author .....

Department of Mechanical Engineering
January 9, 2001

Certified by .....

Leon R. Glicksman
Professor of Architecture and Mechanical Engineering
Thesis Supervisor

Accepted by .....

Ain A. Sonin
Chairman, Graduate Committee

Gas Phase Hydrodynamics inside a Circulating Fluidized Bed

by

James C Moran

Submitted to the Department of Mechanical Engineering
on January 9, 2001, in partial fulfillment of the
requirements for the degree of
Doctor of Philosophy in Mechanical Engineering

Abstract

Circulating Fluidized Beds (CFB's) offer many advantages over traditional pulverized coal burners in the power generation industry. They operate at lower temperatures, have better environmental emissions and better fuel flexibility.

The motion of solids inside a CFB has been studied extensively over the previous twenty years. However the motion of gas is less well understood. There has previously only been indirect measurements of gas velocities and fluctuations. The gas phase is important as the motion of the particles is controlled by the gas. Accurate simulations of CFB's are not possible without accurate information on the gas phase.

Instrumentation was developed for use in measuring gas phase fluctuations inside a scale model CFB. Results were unexpected in that gas fluctuations were substantially larger than expected. The fluctuation level without particle flow was around $0.15m/s$. This was expected to stay constant or decrease with the introduction of particles. However with particle introduction the fluctuation level increased to $0.7m/s$, an increase of over 400%. This is more than likely due to the clustering of particles which produces large scale structures with the resulting vortex shedding. A smaller riser was built which allowed the introduction of single individual clusters into the unit. The effect of single clusters on the surrounding gas flow was studied and modeled. These results indicate a mechanism by which, previously unknown, large scale fluctuations are generated inside a CFB.

Thesis Supervisor: Leon R. Glicksman
Title: Professor of Architecture and Mechanical Engineering

Acknowledgments

I would first and foremost like to thank my advisor Professor Leon Glicksman. His constant enthusiasm and sound advice kept me motivated and focused especially during the frustrating periods encountered throughout this project.

I would also like to offer a sincere thank you to my committee, Professors John Lienhard, Ain Sonin and Janos Beer, who gave me invaluable advice and guidance at critical stages of this work.

I would also like to thank Tony Caloggero and Jim Bales from the Edgerton center for allowing me to use their high speed digital video camera any time I needed it.

To my lab-mates, in particular Matt Sweetland and Maribel Vazquez with whom I discussed many technical problems, some of which were related to this thesis and who were my lunch partners on many occasions.

To my parents who have always stood by my side and supported me with whatever I wanted to do. My two younger brothers also deserve a mention.

And finally to the best Math teacher I ever had - Mr. Jimmy Johnston.

This work was sponsored by the National Science Foundation under grant number CTS-9712053.

Contents

List of Figures

List of Tables

Chapter 1

Introduction

1.1 Thesis layout

This section introduces the structure and layout of this thesis. Chapter 1 contains a general description of fluidization and its commercial applications. Chapter 2 deals more specifically with circulating fluidized beds and gives an account of previous research in that area, the direction future research is heading and the motivation behind the research contained throughout this thesis. Chapter 3 contains information on the specific experimental apparatus and equipment used for the majority of experiments. Chapter 4 contains results and models of initial experiments on flow visualization. Chapter 5, 6 deals with the gas phase measurements, results and discussions. Chapter 7 deals with a separate experimental procedure along with a numerical model to help understand previous puzzling data. Chapter 8 summarizes and discusses the main conclusions resulting from this work while also suggesting potential avenues for future research.

1.2 Description of Fluidization

Fluidization involves passing a fluid vertically upward through a quantity of solid particles contained in some chamber. This chamber is often know as a "riser", and the particles are commonly referred to as a "bed" of particles, D.Kunii and O.Levenspiel [30]. As the fluid velocity increases the the particles will segregate somewhat and begin to behave qualitatively as a fluid. This gives rise to the term "fluidized bed", a chamber filled with particles where a fluid is passing at or above a certain velocity. The reason for doing this is to allow interaction between the fluid and the particles. Commercial development initially focused on chemical reactions, in which the solid material was a catalyst for some desired chemical transformation of the fluid. Commercial systems first appeared in the early 1940's and functioned as chemical reactors for fluid catalytic cracking processes.

1.3 Fluidization Regimes

The fluid-like behavior of a bed of solid particles can vary greatly depending on the gas superficial velocity (volume flow rate per unit area), and in some cases on the flow rate of the solid particles themselves. The basic flow regimes are shown in figure (1-1).

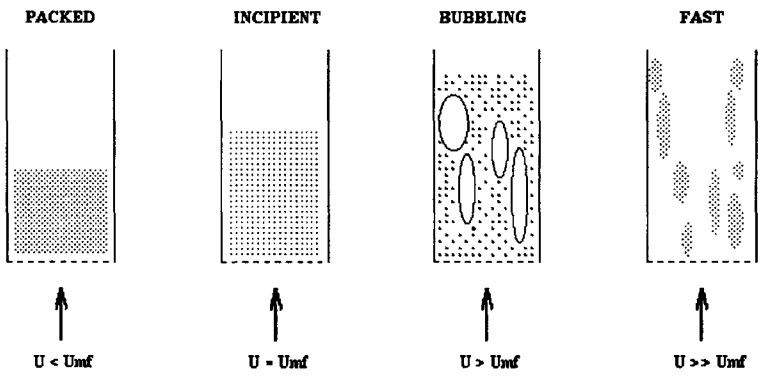

Figure 1-1: Regimes of fluidization

1.3.1 Fixed Bed

At low superficial gas velocities, the particles remain fixed in the bed. This gives rise to the term "Fixed Bed" or "Packed Bed". The flow rate of the gas is so low that the particles remain relatively undisturbed and the gas flows through the interstitial gaps between the particles. Fixed beds function much like a filter. Automobile catalytic converters are examples of fixed bed reactors.

1.3.2 Minimum Fluidization

At slightly higher velocities, the minimum fluidization point is reached which is the point where the hydrodynamic forces on the particles balance the weight of the particles. This superficial velocity is know as the "incipient" or "minimum" fluidization. The particles in this state behave in many ways similar to a liquid. The minimum fluidization velocity is a characteristic of solid particles of a certain density and size and of a particular gas in a given thermodynamic state.

1.3.3 Bubbling Fluidization

At velocities slightly higher than the minimum fluidization velocity the bubbling regime is encountered. The extra gas flows in the form of void pockets or bubbles. The bed of particles takes on a fluid-like behavior, Paul Farrell [13]. This is the regime in which bubbling fluidized beds (BFB) operate. A BFB looks very much like a boiling pot of a heavy liquid except the heavy liquid is in fact a pile of granular particles. Bubbling fluidized beds shall be discussed in more detail later on.

1.3.4 Fast Fluidization

At much higher superficial velocities the fast fluidization regime is encountered. This transition is marked by an increasing rate of particle entrainment with increasing gas velocity which eventually becomes so high that unless the entrained particles are

returned to the bed, the inventory of particles is soon depleted. In order to maintain a steady state in this regime, particles must be introduced into the bottom of the bed at the same rate they are being dragged out, J.Grace, A.Avidan and T.Knowlton [22]. Fast fluidized beds can also be characterized by the rate at which solid particles are introduced and whether or not those solid particles are coming from a fresh source or are being recycled from the riser discharge. A pneumatic transport line, for example, is characterized by a relatively high superficial velocity and a relatively low solids flux with the solid particles supplied from a fresh source and transported elsewhere. A circulating fluidized bed (CFB), on the other hand, will have a recirculation loop to return the particles from the discharge of the riser to the entrance of the riser. CFBs typically run at lower superficial velocities or higher rates of solid replenishment than pneumatic transport lines.

1.4 Applications for Fluidization Processes

Fluidized beds are used in promoting physical interactions such as heat and/or mass transfer; or else used in promoting chemical reactions, in which the solid may be the catalyst or the primary reactant. Some of the more common ones are discussed below.

Catalytic Converters

Catalytic converters are not fluidized but they present an interesting point from which to begin the discussion of applications of gas-solid reaction systems. They are analogous to packed bed reactors where the catalyst is in the form of porous pellets of size ranging from 1 to $15mm$ in diameter. This gives a large surface area per unit volume. They are used to remove CO, NO and unburnt hydrocarbons from automobile exhausts by having the exhaust gases flow through the narrow passages in the catalyst.

A Sterling engine also uses a porous matrix which is analogous to a packed bed. In this application heat is alternatively stored and removed as the working fluid is moved by a piston, E.Gyftopoulos and G.Beretta [23]. The porous matrix

also offers a high surface to volume ratio to absorb or reject the heat, as well as a relatively high heat capacity such that little heat is lost between stages of a cycle.

Fluid Catalytic Cracking

Fluid catalytic cracking (FCC) was one of the first applications of fluidization. It differs from those beds which promote physical interactions, such as heat and/or mass transfer, in that FCC's promote chemical interactions. The solid is a catalyst. FCC units convert heavy fuel oil and petroleum residue to lighter products. Major FCC products are gasoline, diesel fuel, heating oil and light gases such as propane, [22]. The total worldwide capacity of FCC units is over 16 million barrels per day. Zeolite cracking catalysts are the typical solids utilized in FCC's. The gas flow consists of vaporized fuel and steam. The fuel reacts upon contact with the catalyst. Cyclones at the top of the unit separate out the products, in gaseous form, from the catalyst.

Power Generation using pulverized coal technology

Coal is a common fuel used in boilers and the steam produced from these boilers can be used in industrial processes or for generating electrical power. Pulverized coal technology is the most prevalent boiler type for coal combustion. Its a mature technology in which the coal is ground and dried, pneumatically transported to the burners and injected in the form of a particle-laden jet into the combustion chamber. The coal mixes with the hot combustion products and ignites, L.Douglas and D.Platt [10]. A 500MW chamber may have dimensions $10x10m$ and be 30-40 meters in height. The walls are cooled by steam generating tubes. A disadvantage to this approach is that typical bed temperatures reach 1400°C and the temperature profile is highly non-uniform. Such conditions are favorable for the production of nitrogen oxide and limit the unit to combustion of relatively high grade fossil fuels.

Bubbling Fluidized Beds

The physical and chemical benefits of fluidized beds have prompted their use in power generation systems. Bubbling fluidized beds operate in the bubbling regime. They are used as boilers for steam production. The bed consists of particles of calcium carbonate and a small fraction of coal which captures up to 90% of the sulphur produced from combustion. They are typically shorter and wider than circulating fluidized beds. This geometry leads to smaller gas superficial velocities. The heat transfer surfaces are located inside the bed. The surfaces are usually pipes through which steam flows. Good mixing leads to a high combustion efficiency of around ninety five percent. BFBs were originally developed in the 1950s.

1.5 Circulating Fluidized Beds

A circulating fluidized bed (often abbreviated as CFB) is a device for generating steam by burning fossil fuels in a furnace operated under a special hydrodynamic conditions. Fine solids are transported through the furnace by gas flowing at a velocity exceeding the average terminal velocity of the particles, yet at a low enough velocity to allow a degree of refluxing of solids adequate to ensure uniformity of temperature in the furnace, M.Hyre [26], N.Gelperin and V.Einstein [41].

Figure (1-2) illustrates the basic components of a CFB system. The component of major interest is the vertical riser, wherein the desired gas solid contacting is achieved. Solids introduced at the base of the riser are entrained by means of upward flowing gas. The resulting gas-solid suspension within the riser forms the CFB. This gas-solid suspension then exits the top of the riser and enters a gas solid separation system, indicated as a cyclone. The captured solid particles are then returned to the base of the riser by means of a return line and solid feed system to complete the closed-loop path of the solids particle flow. The gas makes only a single pass through the riser and exhausts through the top of the cyclone.

The creation of special hydrodynamic conditions of particle refluxing, is the key to the CFB process. The combination of gas velocity, solids recirculation rate,

solids characteristics, volume of solids and the geometry of the system gives rise to this special hydrodynamic conditions under which solid particles are fluidized at a velocity greater than the terminal velocity of individual particles. Yet these particles are not entrained immediately as expected in pneumatic transport systems. Solids move up and down in the form of aggregates, causing a high degree of refluxing. These aggregates are continuously formed, dispersed and formed again, D.Westphalen [62].

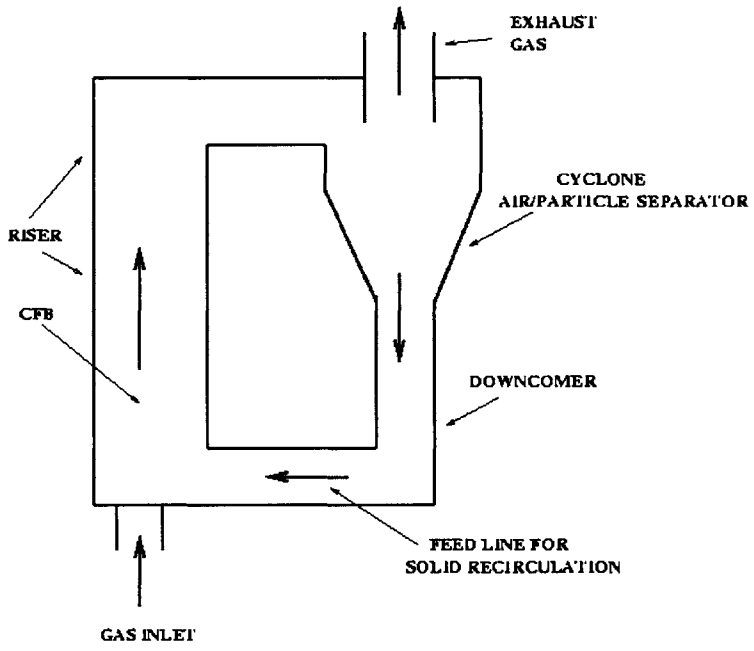

Figure 1-2: Schematic for a typical circulating fluidized bed

1.5.1 Power generation with circulating fluidized beds

Circulating fluidized beds over the past twenty years have found a major application in the power generation industry. They have several advantages over traditional coal powered technologies. Combustion temperatures vary according to the type of fuel being burned but are typically between 750°C and 900°C. There is excellent mixing inside the bed which produces a uniform bed temperature. At full load the difference between the hottest and coldest points may be as little as 30°C. These properties lead to improved environmental emissions.

The cycle efficiency for power generation for conventional atmospheric fluidized bed combustors is comparable with pulverized coal technology. Typical values run in the range of 35%. With more advanced CFB technology such as pressurized fluidized beds coupled with more advanced cycles such as the integrated gasification combined cycle this value can climb as high as 45%, [22]. CFB combustion efficiency of over 96% is also comparable with pulverized coal technology.

The turndown ability and load following capability is very good for CFB's. The bed temperature must remain constant for good combustion and emissions performance yet to reduce the steam generation rate, the rate of heat transfer to the heat transfer surfaces must be reduced. This can be done by adjusting the solids recycle rate. Some units also have an external heat exchanger. The larger the inventory the higher the heat transfer coefficient. The fuel flexibility is also very good. "Dirty" coal which produces a significant amount of ash and is not suitable for pulverized coal units can be used. Municipal waste can also be the fuel of choice although because of the high variability from its heating value it usually is used with 80% coal to provide a more stable power output. Another benefit to CFBs is that fewer feed points are needed because of good gas-solids mixing and an extended combustion zone through the riser.

Throughout the seventies bubbling fluidized beds were preferred over circulating fluidized beds. This was because the technology in CFB's had not yet been perfected. Over the past 10 years however CFB's have been the preferred choice. This is due largely to the perception that they represent a better technology for exhaust gas clean up. A CFB has a more dilute concentration of solid particles than a BFB,

Characteristic	Stoker	Bubbling	Circulating	Pulverized
Height of bed or fuel burning zone (m)	0.2	1-2	15-40	27-45
NO_x emission (ppm)	400 - 600	300 - 400	50 - 200	400 - 600
SO_2 capture in furnace (%)	None	80 - 90	80 - 90	Small
Combustion efficiency	85 - 90	90 - 96	95 - 99	99
Superficial velocity (m/s)	1.2	1.5 - 2.5	4 - 8	4 - 6
Turn down ratio	4:1	3:1	3-4:1	n/a

Table 1.1: Comparison Between Different Combustion Technologies

and the particles in a CFB are typically smaller and therefore have a larger surface-volume ratio. Both of these attributes provide for a better opportunity for better gas solid contact, better utilization of calcium and enhancement of the absorption of SO_x. Furthermore a CFB will typically occupy less square footage on the ground. However CFBs are generally taller and more complex to operate which is why some users still prefer BFBs. A comparison of the different coal combustion technologies is given in table (C.1).

To summarize the features of CFB boilers:

- Fuel flexibility due to excellent gas-solid and solid-solid mixing
- Low NO_x emissions due to lower combustion temperatures
- Good turndown and load following capability by adjusting the solid recycle rate
- Efficient sulfur removal due to small sorbent sizes and good gas-solids mixing
- High combustion efficiency due to recycling of unburned fuel particles back to the furnace and high gas-solid mixing
- Small furnace cross section because of high heat release rates due to high superficial gas velocities and intense mixing

1.6 Typical Boiler Sizes

1.6.1 Large scale hydrodynamics

In this study a cold flow scale model of a 2-MW CFB boiler was used. A 2-MW boiler means that it consumes fuel at a rate of 2 MW at peak capacity. The riser of this bed has a square cross section of 0.64 m on each side and is 8m tall, P.Noymer [45], D.Westphalen [62]. Atmospheric pressure CFB technology has matured to the point where manufacturers are offering units of up to 300 MW size which are designed to meet all current thermal and emissions requirements. Since the power level scales roughly with the bed area then a given linear dimension roughly scales by the square root of the increase in power. A large boiler may be 50m in height and several meters in diameter. Height to diameter ratios range from about 10:1 to 50:1 and the height is driven by the design for the combustion and pollutant absorption reactions. The upward traveling gas must have enough time to interact with the particles. Figure (1-3) presents a picture of a full sized atmospheric CFB boiler with an energy output rate of $160MW_{th}$; for an estimate of its scale notice the person in the lower left corner. For the past 10 years there has been typically 20-40 annual installations of fluidized bed boilers.

1.6.2 Mid-scale CFB hydrodynamics

Closer inspection of a CFB behavior yields what is commonly called a "core-annulus" structure, Yerushalmi and Cankurt [66]. The core of the riser consists of perhaps 80% of the cross sectional area and is based at the center of the riser. It contains a relatively dilute upward flowing region of gas and particles. The particles are both single and grouped together in "cluster" formation. The exact percentage in each is the subject of ongoing research. The remaining 20% of the area is the annular region and it consists of a relatively dense downward moving layer of particles. They travel as cluster or streamers and provide the mechanism by which particles give their heat to the water cooled walls. this is also the main mechanism for solid recycling with a CFB. The reason the flow is downward is due to the lack of gas momentum in

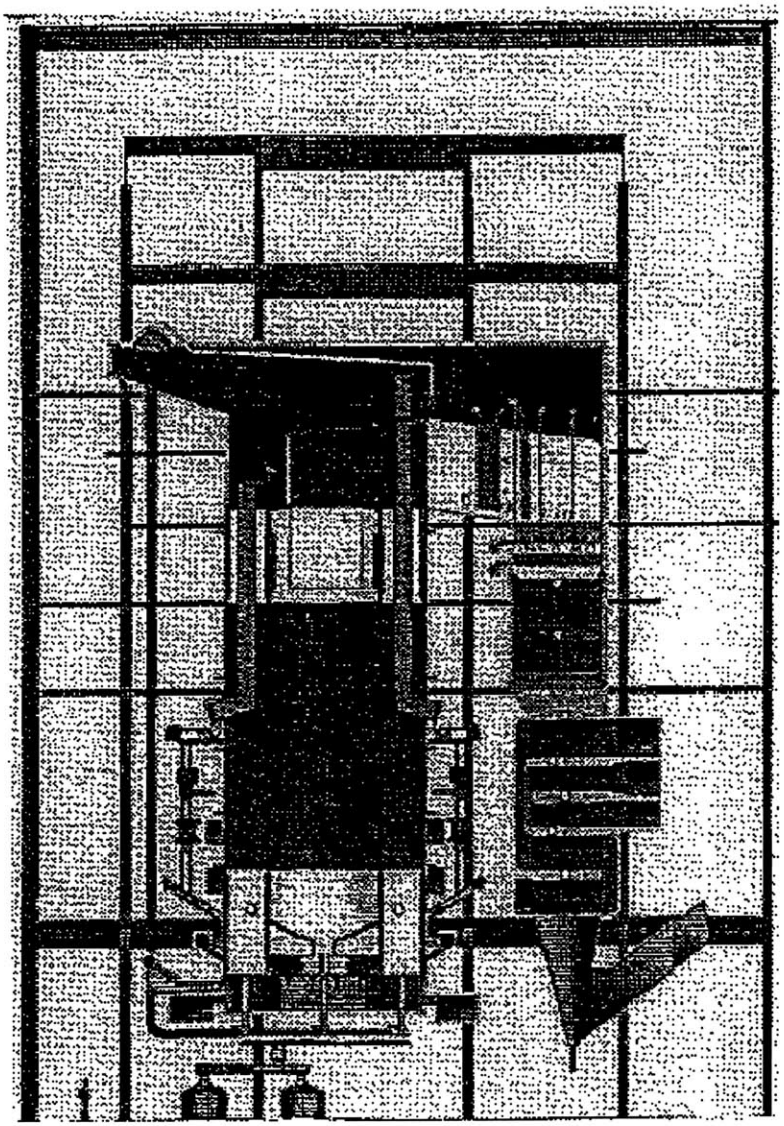

Figure 1-3: Full-sized CFB boiler; from Kokko et al.[28]

that area. The velocity required to transport the particles upwards is not present in the annulus. The particles in this region move downward under their own weight. Particles from the core are transported to the annulus via particle-particle interactions and gas phase turbulence which together provide a diffusion mechanism. The flow of gas in the annular region is very poorly understood and this is one of the subjects addressed later on in this thesis.

1.6.3 Small-scale CFB hydrodynamics

Beyond the mesoscale "core-annulus" flow structure the flow inside a CFB becomes one of gas and particles and their interactions with each other. Both enter the riser at the bottom, interact with each other and are eventually removed at the top. This interaction is used either to provide heat transfer and/or mass transfer from one phase to the other. The solids form cluster in the center, travel upwards, break up, disperse, some solids diffuse to the wall where they flow in a downward direction before returning to the core - a phenomena known as refluxing.

1.6.4 Research on CFBs

Research in the past has focused on understanding the physical phenomena underlying the technology. Particular attention has been paid to understanding the heat transfer process and the chemical reactions, P.Noymer and L.Glicksman [44, 43], H.Mickley and D.Fairbanks [38], C.Lockhart et al. [35]. Both of these involve characterizing and understanding the gas-solids mixing. This would lead to an improvement in the design and operation of CFB boilers. Many early design efforts simply extended correlations for earlier BFB technology or extrapolated from the limited knowledge base of CFBs without regard to fundamental physical changes. The development of valid small scale experimental models, (see Glicksman [20]), have contributed greatly to a better understanding of the physical mechanisms governing heat transfer by using similitude to conduct experiments on small scale cold models and applying the results to larger more expensive units.

As computers have become more and more powerful they are becoming

widely used in CFB research, Y.Tsuji et al. [60], J.Ouyang and J.Li [46]. Computer models typically involve the time/volume and/or ensemble averaging of mass, momentum and energy balance relations. This results in a separate set of equations for each of the flow components. These equations are connected by terms for interaction between the phases in the forms of drag, heat and mass transfer. These set of equations are very complex and usually require experimental data to provide closure. As a result these models are valid only from the bed where the experimental coefficients were obtained. Computers will play a larger role in modern CFB research but they are not yet powerful enough nor do they contain all the physical information necessary to provide a general computational model of a generic CFB.

Chapter 2

Current Research on Fluidized Bed Combustors

2.1 Present Difficulties with CFBs

One of the biggest challenges facing CFBs is the issue of scale up. This involves the ability to accurately scale up small commercial units to large units. Small commercial beds do not scale up linearly to larger commercial sized units. This has limited the introduction of large ($\sim 300MW$) commercial units in the past because of the large investment risk as these units can cost upwards of 50 million dollars. If the performance of these units cannot be accurately predicted in advance, development of large units remains slow. For example, in smaller units the heat transfer coefficient measured at the wall is always higher than larger units. The reason for this shall be explained later when discussing the flow hydrodynamics at the wall. How the heat transfer coefficient scales with bed height or bed diameter is still unknown. Simply building and operating a model with the same geometric shape as the full scale bed will not lead to valid results. Presently in-house empirical correlations and accumulated design expertise are used to try and design larger units but it still remains more of an art than a science.

2.2 Scale Modeling of CFBs

Designers concern about the relationship between the performance of large commercial beds and results obtained from much smaller pilot plants led to the development of scaling laws, Glicksman et al. [20]. These use similitude or dimensional analysis to allow results from small beds simulate a much larger bed. Similitude has been used in many fields to allow small controlled experiments to closely simulate physical phenomena. Wind tunnels are commonly used to determine the aerodynamic properties of aircraft and automobiles. Towing tanks are used to examine proposed ship designs. Small scale structures are used to determine the performance of building structures in high winds or earthquakes.

This approach offers many advantages. Time and money is saved building prototypes as opposed to large scale units. Cold flow (no combustion) scale models have the advantage that their environment is less hostile and more therefore more suited to sensitive data acquisition equipment.

2.2.1 Scaling Laws

The first step in deriving scale relationships for CFB's is the identification of all the independent parameters important to the system. Independent parameters are only those that can be controlled directly by design. They are then combined into a number of dimensionless parameters. For example, if there are n independent parameters consisting of r basic physical dimensions then there will be $n - r$ independent dimensionless groups. For further information on dimensional analysis see most introductory fluid mechanics books such as Fay [14]. Another procedure which produces the exact same results is to write down the set of differential equations that govern the system and after non-dimensionalization the independent parameters are obtained, L.Glicksman [36].

From a hydrodynamic standpoint there are several independent parameters inside a circulating fluidized bed. Given the intense mixing inside the riser most of the gas flow can be represented by exhaust products at a certain temperature and

pressure. Since only 2 variables are required to specify a particular thermodynamic state the temperature and pressure can be represented by the density and viscosity (ρ_f and μ). The average size and density of the particles (d_p and ρ_s) used are important as is the dimensions of the bed, length and diameter (L and D). The gas flow rate is specified by the gas superficial velocity (U_o) and the flow rate of solids is specified by the solids recycle rate which is a solid flow rate per unit riser area (G_s). Gravity (g) also plays an important role so this parameter is included. There are several other parameters which may be included such as particle sphericity (ϕ_s) and particle size distribution (PSD). Westphalen and Glicksman [63] found that these parameters were important while parameters relating to electrostatic or particle collisions were not as important.

This gives 11 independent parameters which are important for hydrodynamic similitude. There are three independent physical dimensions between them - mass, time and length. This gives 8 dimensionless groups from the Buckingham Pi theorem.

$$\frac{L}{D}, \frac{\rho_s}{\rho_f}, \frac{d_p}{D}, \frac{U_o^2}{gD}, \frac{\rho_f U_o D}{\mu}, \frac{G_s}{\rho_s U_o}, PSD, \phi_s \tag{2.1}$$

Equation(2.1) is known as the full set of scaling laws. These groups can also be obtained by non-dimensionalizing the ensemble-averaged equations of motion for the particles and fluid in a fluidized bed along with their boundary conditions or else by non-dimensionalizing the single particle equation of motion. To construct a model which will give behavior similar to another bed all of these groups must have the same value. The requirement of similar bed geometry is met by geometrically similar beds, the ratio of all linear bed dimensions to a reference dimension such as bed diameter must be the same for the model and combustor. The dimensions of the elements external to the bed such as the particle return loop do not have to be matched as long as the return loop is designed to provide the proper external solids flow rate, inlet conditions and size distribution, Chang and Louge [7].

These design parameters do not solve all problems. They can be restrictive. For example if they are rigidly followed then the state of the gas and the size of the bed cannot be specified independently. If an atmospheric scale model is desired

to simulate the behavior of a bed running at 10atm pressure we get the following equation for the length ratios - where the subscript s corresponds to the scaled unit and the subscript r corresponds to the real unit:

$$\frac{D_s}{D_r} = \left(\frac{\mu_s \rho_{fr}}{\mu_r \rho_{fs}}\right)^{2/3} \tag{2.2}$$

For a 10atm pressurized combustor the atmospheric cold scale model must have a diameter similar in size to the bed it is simulating. This is not very convenient and leads to a more simplified version of the scaling laws. Glicksman et al. [37] performed a simplification analysis on the full scaling laws. Upper and lower bounds on the Reynolds number Re, based on gas superficial velocity and particle diameter were found to yield a similar set of parameters. This resulted in the following set of dimensionless groups:

$$\frac{L}{D}, \frac{\rho_s}{\rho_f}, \frac{U_o}{U_{mf}}, \frac{U_o^2}{gD}, \frac{G_s}{\rho_s U_o}, PSD, \phi_s \tag{2.3}$$

where U_{mf} is the minimum fluidization velocity. As a result of this simplification the additional degree of freedom allows for the linear scale factor of the fluidized bed to be specified in addition to specifying the gas and its properties. Similar to the full set of laws the electrostatic forces and other inter-particle forces are not considered important. Geometrically similar beds and the use of particulate material that are denser (for atmospheric CFBC) and finer than the material used in the full scale bed are the main practical design issues extracted from the simplified scaling relationships.

2.3 Heat Transfer in CFBs

The hydrodynamics of a large scale unit can be modeled in small scale laboratory models using the above full and simplified scaling laws. Understanding the hydrodynamics leads to an better comprehension of heat transfer as they are both coupled. Radiation also plays an important role in the heat transfer to the walls of the bed

but it cannot be directly simulated in a cold bed since it is dependent on temperature level. For fluidized beds, simulation of the convective component is the most important part to understanding the overall heat transfer. Radiation heat transfer can be estimated analytically with more confidence than can convective heat transfer. In addition the convective component has a higher magnitude especially in the more dense regions of the bed.

Heat transfer by convection to the walls of a circulating fluidized bed can generally be broken into two terms. Particle heat transfer results from particles near the surface transferring their heat to the surface. Gas convection is the heat transfer from the surface due to gas motion and its corresponding heat capacity. For some cases the distinction between these two mechanisms is not precise. As stated earlier radiation is a separate physical mechanism but it may interact with the other forms of heat transfer.

Numerous researchers have studied heat transfer in fluidized beds. Noymer et al. [43] studied cluster motion near the wall and its effect on the heat transfer. Lints [32] studied closely the mechanism by which particles at the wall transfer their heat to the wall while Leckner et al. [1] discussed experimental methods for estimating the heat transfer. C.Lockhart et al. attempted to correlate the heat transfer with cluster motion at the walls [35]. Some books have also been written, J.Grace et al. [22], D.Kunii and O.Levenspiel [30] and N.Gelperin and V.Einstein [41]. There are many more - to numerous to mention who have contributed to this field. Some generally accepted trends from this research are that higher heat transfer coefficients are observed in CFBs running at higher temperature. This is likely due to more radiative heat transfer. Increasing the solids concentration also increases the heat transfer as there is increased conduction from the particles. Smaller beds with shorter surfaces also tend to have higher heat transfer coefficients because the temperature difference between the walls and the solids at the wall does not have time to converge. These are the generally accepted trends. There are other effects such as the influence of riser diameter which are not as clear due to variations in the operating conditions of published experiments.

2.3.1 Modeling Heat Transfer

The gas and particle clusters flow independently along the heat transfer surface. They contribute independently to the convection heat transfer, Subbarao and Basu [57]. Neglecting the radiation component, this gives a time averaged heat transfer coefficient as:

$$h_{convective} = f.h_{pc} + (1 - f).h_{gc} \tag{2.4}$$

where, f represents the fraction of the wall covered by clusters, h_{pc} represents the heat transfer coefficient from the particles to the wall and h_{gc} represents the heat transfer coefficient from the gas to the wall which can be roughly obtained from forced convection heat transfer correlations. The gas convective portion is typically quite small in comparison to the particle component. It only becomes significant at small particle concentrations. Mickley and Fairbanks [38] developed an expression for transient heat transfer between packets of particles which remain at the wall for a time t then are periodically displaced from the heat transfer surface:

$$h_{cluster} = \sqrt{\frac{(k\rho c)_{cluster}}{\pi t}} \tag{2.5}$$

Equation(2.5) shows the dependence of the heat transfer coefficient on several hydrodynamic parameters such as the concentration of solids in each cluster and the cluster wall contact time. The heat capacity of a cluster can be approximated by:

$$(\rho c)_{cluster} = (1 - \varepsilon_{cluster})(\rho c)_{solid} \tag{2.6}$$

where $\varepsilon_{cluster}$ represents the volumetric concentration of air in the cluster and is dependent upon the operating conditions in the CFB. Equation (2.6) remains accurate so long as $\varepsilon_{cluster} < 0.99$. The thermal conductivity of a cluster can be obtained from an expression developed by Gelperin and Einstein [41].

$$\frac{k_{cluster}}{k_{gas}} = 1 + \frac{(1 - \varepsilon_{cluster}).(1 - \frac{k_{gas}}{k_{solid}})}{\frac{k_{gas}}{k_{solid}} + 0.28\varepsilon_{cluster}^{0.63(k_{gas}/k_{solid})^{-0.18}}} \tag{2.7}$$

It can be shown that $k_{cluster}$ is about 1.5 to 2 times k_{gas} for typical CFB conditions.

Baskakov [3] introduced an additional "contact" resistance between the wall and the cluster. This resistance results from a gap or gas layer between the cluster and the wall. This resistance prevents the heat transfer coefficient from equation (2.5) approaching infinity as the cluster wall contact time approaches zero. This resistance is modeled using the concept of a small distance, y_{gap}, between the cluster and the wall.

$$R_w = \frac{y_{gap}}{k_{gas}} \tag{2.8}$$

The exact expression for transient conduction from a semi-infinite body to a constant temperature surface with a series resistance is complicated. However a simpler expression can be obtained by modeling the contact resistance and the transient conduction to a homogeneous cluster of particles as independent and in series with each other. This simplification still represents a close approximation to the actual heat transfer.

$$h_{cluster} = \left[\frac{y_{gap}}{k_{gas}} + \sqrt{\frac{\pi t}{(k\rho c)_{cluster}}} \right]^{-1} \tag{2.9}$$

Substituting equation (2.9) into equation (2.4) yields the following expression for the heat transfer to the walls of a CFB.

$$h_{convective} = f. \left[\frac{y_{gap}}{k_{gas}} + \sqrt{\frac{\pi t}{(k\rho c)_{cluster}}} \right]^{-1} + (1 - f).h_{gc} \tag{2.10}$$

Equation (2.10) has five parameters which must be determined, f, the fraction of the wall covered by clusters, y_{gap}, the effective gas layer thickness between the cluster and the wall, t, the time of contact between the cluster and the wall, $\varepsilon_{cluster}$, the volumetric concentration of air inside the cluster and h_{gc}, the dilute phase heat transfer coefficient.

The dilute phase heat transfer coefficient has been shown to be reasonably well approximated by correlations for single phase gas convection, see Lints [32]. The gas superficial velocity, the bed diameter and the gas properties need to be specified. The effective gas layer between the cluster and the wall was measured by Lints and Glicksman [34] in a cold scale model CFB. They used a phonograph needle attached to a magnetic cartridge. When particles struck the needle a signal was generated by the cartridge. By mounting the probe on a linear translation stage its position was precisely located relative to the wall. To an order of magnitude the size of the gap is equal to about one particle diameter. This was found to be dependent on the local cross-sectional solids concentration and to a lesser extent the superficial velocity.

The volumetric concentration of solids inside a cluster, $1-\varepsilon_{cluster}$, was measured by Soong et al. [53] using a capacitance probe. Solid fractions of clusters between 10% and 30% were measured. Lockhart et al. [35] used a similar technique and measured concentration levels between 15% and 25%. Lints and Glicksman [34] developed a correlation based on published data which gave the following expression:

$$(1-\varepsilon_{cluster}) \approx (1-\varepsilon)_{avg}^{1/2} \tag{2.11}$$

This indicates that the solid concentration of clusters can be approximated by taking the square-root of the average cross sectional solids concentration which is a parameter easier to measure. None of these experiments or mathematical models provide a proper physical understanding of what governs cluster solid concentration.

The time a cluster spends in contact with the wall, t, is more difficult to measure. Local cluster velocities have been measured previously by Moran and Glicksman [40], Noymer et al. [18] and Zhang et al. [68]. These velocities are independent of the gas superficial velocity and the cross sectional solids concentration which is quite a surprising result. Moran and Glicksman [40] also reported video evidence of clusters accelerating to a final terminal velocity - a result which was originally postulated by Glicksman [19]. This meant that measuring a contact length between the cluster and the wall and dividing by the average velocity would not give the contact time as the velocity was not constant over the time period. These problems were solved by Noymer and Glicksman [42] with a thermal image velocimetry technique. This

involved heating the clusters over a certain section of the wall and observing them beneath that section with an infrared camera. As the camera is moved further away from the heater section the observations of heated clusters in a given time interval decrease. Using statistical methods the number of observed heated clusters at a given level can be converted into a contact time. Contact times on the order of 1 second were found but this was for a cold scale model CFB. It is unclear how to scale contact times to larger commercial units.

2.3.2 Fractional Wall Coverage

The most important parameter in equation (2.10) is probably the fractional wall coverage, f. Making representative estimates for all parameters except the cluster wall contact time and the cluster fractional wall coverage, the plot is obtained in figure (2-1):

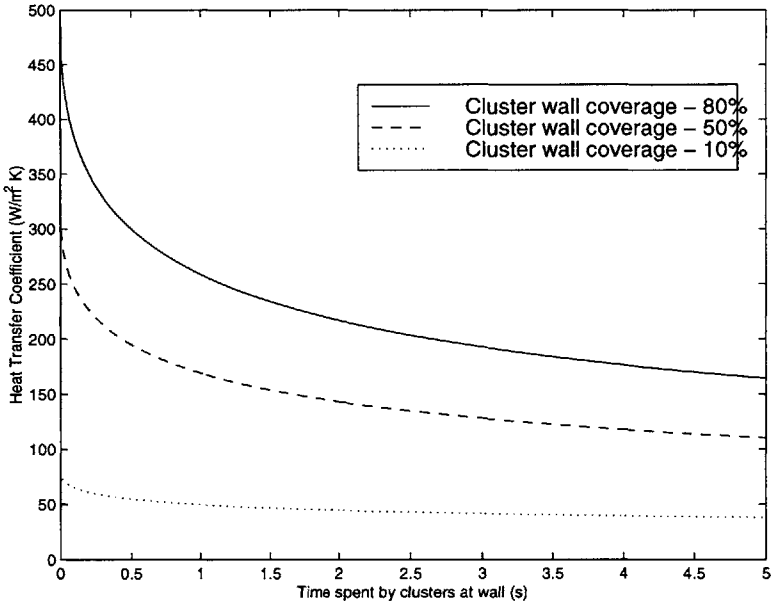

Figure 2-1: Heat transfer coefficient versus cluster contact time for different fractional wall coverage

It is important to remember that the heat transfer coefficient as shown in figure (2-1) does not include the radiation component. The fraction wall coverage has a larger effect on the heat transfer coefficient than the cluster contact time. A larger

increase in the heat transfer coefficient comes from attempting to raise the fractional wall coverage rather than reducing the time spent at the wall by clusters. Of course if its possible to do both at the same time, this clearly is optimal.

Obtaining the highest possible heat transfer coefficient is good from an efficiency standpoint. However what is even more important from a design standpoint is the ability to predict in advance what the heat transfer coefficient will be. An ability to predict the fractional wall coverage in advance is therefore needed. Hyre [26] analyzed existing data and concluded that the fractional wall coverage was dependent on the superficial velocity, the solids density ratio, bed size and the cross sectional solids concentration - with the solids concentration being the most important parameter.

2.4 Proposed Research

An ability to model accurately the fractional wall coverage means an ability to accurately predict particle arrival from the core of the bed to the wall. This will lead to a better prediction from a fundamental perspective of the heat transfer coefficient. However, the mechanisms which remove clusters from the wall and which deliver particles to the wall are poorly understood. It is generally taken for granted that gas turbulence and particle-particle interactions provide the transport mechanism of particles from the center of the bed to the wall, but this has not yet been experimentally studied in depth and many authors have called for further research in this area J. Kuipers et al. [29], G. Palchonok et al. [16], H. Enwald and A.E.Almstedt [12].

To further the fundamental understanding and quantitative prediction of the heat transfer in a CFB, this research proposes to experimentally measure and study gas phase fluctuations in the riser of a circulating fluidized bed. It is suspected that gas phase turbulence plays a role in the separation of clusters from the heat transfer surface. In addition, particle deposition from the core to the surface is governed by particle to particle collisions and particle interactions with gas eddies, [26]. Gas phase turbulence has never been experimentally studied in fluidized beds before and remains one of the most poorly understood phenomena associated with this field M.Hyre [26], R.A.Gore and C.T.Crowe [8]. Difficulties in experimentally studying the gas phase

arise due to the corrosive, optically poor environment inside a fluidized bed. This study intends to overcome such difficulties using a non-conventional experimental approach. A more developed understanding of the gas phase would allow local details of the two-phase flow to be modeled more accurately than present techniques which necessitate the use of averaging with the gas phase behavior assumed to be the same as that in a single phase turbulent gas flow. Such information would be of benefit to both designers of fluidized beds and the numerical codes used to model fluidized bed dynamics. It would also aid in our understanding of particle dynamics and hence heat transfer. Current correlations, for heat transfer, when compared to data from commercial risers are found to be in error of 50 percent or more. A fundamental understanding of the parameters governing gas phase turbulence may prove essential in improving such models. A lack of prior research into this area makes it difficult to predict with certainty what additional benefits may occur. It is certain however that the majority of research up to this point has dealt primarily with the particle or dispersed phase. Studying the gas phase behavior will at the very least aid in our understanding of one of the fundamental mechanisms governing the dynamics of fluidized beds.

Chapter 3

Experimental Apparatus

3.1 General Description

The experiments were conducted on a cold scale-model CFB (see figure (3-1)) which was originally built as a 1/4 scale model of a $2-MW_{th}$ atmospheric combustor [18, 45]. The riser is $2.44m$ high with a square cross-section measuring $0.159m$ on each side; the walls are made of clear 12.5mm thick polycarbonate plastic. Clear wall materials were used to facilitate visualization of internal hydrodynamic behavior. The upper half of one of the four walls is removable. This allows for different wall geometries to be used as well as installation of surfaces for heat transfer measurements.

3.1.1 Bed Operation

Air is supplied to the riser from a blower. The volumetric capacity of the blower is $0.5m^3/s$ although for these experiments a flow rate of $0.1m^3/s$ was used with the air being supplied at a temperature of $45°C$ and 2.5psi.

When the particles and gas exit the riser they need to be separated so the particles can be reused and the air can be safely exhausted to the atmosphere. This separation occurs in two stages. The exiting products first of all enter an inertial

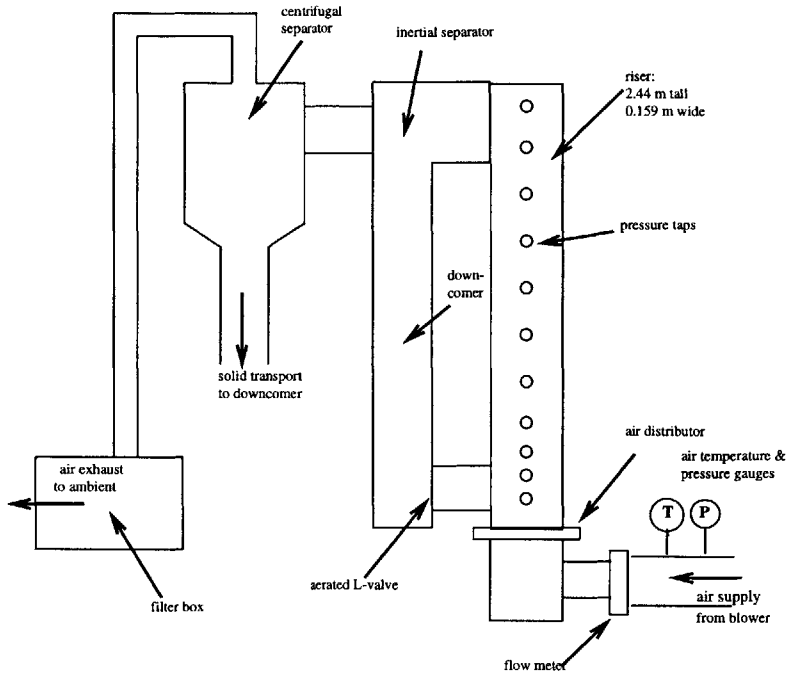

Figure 3-1: Schematic of experimental CFB

separator. This consists of a vertical array of plates. The air flows horizontally around the plates while the particles having larger inertia crash into the plates and are directed downwards toward the downcomer. The finer particles not separated from the flow by the inertial separator travel through a cyclone separator. This operates by the centrifugal force causing the particles to move toward the outside of the cyclone. They accelerate out and down and are gathered in a standpipe. Meanwhile the air is passed upward through the center of the cyclone. At the bottom of the cyclone the particles gather and are transported to the downcomer via a pneumatic transport line.

Downcomer

The downcomer or standpipe is a 10-cm clear acrylic pipe. The separated particles are returned here. They are then fed back to the riser via a 90° extension from the bottom of the downcomer. This feed system is commonly know as an "L-valve". The particles can be observed traveling down the downcomer through the clear plastic. This allows measurement of the rate at which solids are being fed into the riser. To

control the feed rate the L-valve is aerated with a small air jet at roughly 30psi. This pressure may be adjusted to increase or decrease the solids flow rate.

As the air exits the cyclone it is fed into a filter box. The filter box traps the finer particles that have been entrained by the air flow and did not get captured by the inertial separator or the cyclone. The filter box contains two filters for redundancy after which the air exhausts to ambient.

3.1.2 Particle Description

The particles used for these experiments were sand particles with an average size of $164\mu m$. In addition to the particle size there are other important particle properties that need to be specified as they determine bed operating parameters. These include, particle minimum fluidization, particle sphericity and particle density.

Particle Size

The average particle size was determined using a shaker table, (model CL-305 from ELE International) containing a set of sieves. The shaker is powered on and vibrates the stack of sieves. The particles distribute themselves throughout the meshes. By assigning the average of the mesh sizes to the mass of particles remaining, a statistical distribution of particle sizes can be determined. Typically for fluidized beds the mean particle size corresponds to the average surface to volume ratio given by the following expression:

$$\frac{1}{d_p} = \sum \frac{x_i}{d_i} \tag{3.1}$$

Where d_p is the mean particle size, x_i is the mass fraction of the ith sample and d_i is the diameter corresponding to the ith sample. Figure 3-2 shows the particle size distribution for the sand used in these experiments.

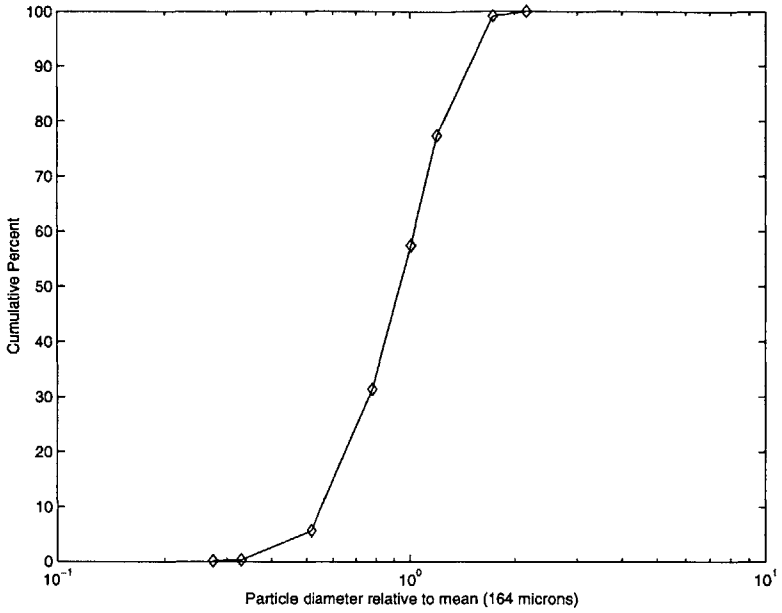

Figure 3-2: Particle-size distribution for 164μm sand particles

Particle Sphericity

The sphericity of the particles need to be measured as it is an important parameter for geometric similarity in fluidized beds. It is defined as the ratio between the surface area of a sphere and the surface area of a particle having the same volume as the sphere. Farrell [13] measured sphericity by measuring the particle circularity (sphericity in two dimensions) using microscopic photographs of many particles. A similar technique was used to determine that the sphericity of these particles was 0.79 ± 0.05. This value is quite typical for particles in fluidized beds.

Particle Density

The particle density is a critical parameter in determining the solids recycle rate and the volumetric solids concentration. A helium pycnometer was used to measure this quantity. It functions by placing a known mass of particles inside a small chamber. A identical chamber is filled with helium gas at a particular pressure. That quantity of helium is transferred to the chamber with the particles. The pressure of the helium will be greater due to the reduced volume available in the second chamber. Since

the system is isothermal the volume taken by the particles can be obtained from the pressure of the helium. The sand particles had a density, ρ_s, of approximately $2650kg/m^3$.

Particle Void Fraction

The particle loosely packed void fraction, ε_{lp}, is needed in order to calculate the solid recycle rate. It is measured by pouring a know mass of particles into a graduated cylinder, tapping it several times to pack the particles closely and then measuring the volume occupied. The loosely packed void fraction was found to be 0.43 for these particles.

3.1.3 Operating Parameters

There are several operating parameter that need measuring during experiments. These are the gas superficial velocity, solids recycle rate and the average volumetric solids concentration.

Gas Superficial Velocity

The gas superficial velocity is defined as the gas volume rate divided by the cross sectional area of the riser. An orifice plate is located in the air supply line. This creates a pressure drop which can then be related to the flow rate. The air supply line has a $10cm$ diameter while the orifice plate has a $5.62cm$ diameter. The pressure difference is measured with a water manometer located one pipe diameter upstream and half a pipe diameter downstream. The initial air stream temperature and pressure are measured using gauges located in the piping. These properties are then used to determine the gas density and viscosity.

Solids Recirculation

The solid recirculation rate is measured by observing the speed at which particles descend the downcomer. This technique was originally used by Westphalen [62]. It is based on the assumption that the particles descend in uniform or plug flow. With a stopwatch, the length of time it takes a particular particle, visible at the wall, to travel a fixed distance (usually 5 inches) is measured. At steady state dividing the distance by the time gives the velocity of particles in the downcomer, u_{dc}. The solid recycle rate expressed as mass flow per unit area is given by:

$$G_s = \frac{\rho_s(1-\varepsilon_{lp})u_{dc}A_{dc}}{A_{riser}} \tag{3.2}$$

where ε_{lp} is the loosely packed void fraction, A_{dc} is the cross sectional area of the downcomer, ρ_s is the solids density, A_{riser} is the cross sectional area of the riser and u_{dc} is the particle velocity in the downcomer.

Solids Concentration

The volumetric solids concentration is one of the most important parameters. This is the concentration of solids in the riser and the variation of concentration along the riser. It is a parameter of great interest to CFB designers because it directly influences the heat transfer coefficient and the input power requirements. It can be measured by recording the drop in air pressure along the riser. Any loss in gas momentum will manifest itself as a drop in pressure. The greatest contribution toward the pressure drop is from the weight of the particles. They play a much larger role than wall shear stresses even at low (0.1%) concentrations. Mixing effects at the entrance to the riser are minimized by the distribution plate, so neglecting the small effect of wall shear, the pressure drop can be equated to the average solids concentration $(1-\varepsilon_{avg})$ as follows:

$$\triangle P = \rho_s(1-\varepsilon_{avg})g\triangle x \tag{3.3}$$

The experimental apparatus has eleven pressure taps along the length of

the riser. This allows for ten differential pressure measurements along the length of the riser. Appendix B contains precise information concerning tap location and transducer calibration. The pressure transducers were purchased from Autotran Inc. and the data acquisition hardware was a DAS-16 board from Keithley Instruments with the software testpoint also from Keithley Instruments. The riser openings for the transducers were slanted at an angle of 45° to prevent being blocked by particles close to the wall. Purged air was also run through the lines to eliminate blockages. The purged air was turned off before data was taken. Manipulating equation (3.3) to get the solids concentration:

$$(1 - \varepsilon_{avg}) = \frac{\triangle P}{\rho_s g \triangle x} \tag{3.4}$$

Pressure readings were taken at a rate of 100Hz for 15 seconds and then averaged for that span to obtain $\triangle P$ in equation (3.4) and hence the local solid fraction in the riser.

The relationship between the gas superficial velocity, solids recycle rate and cross sectional solids concentration depends on several parameters including, particle density, size and shape, bed geometry, exit effects, plate distributor design and so forth. At higher superficial velocities the air has more energy to transport the particles from the riser. Therefore one would expect for a given solids recycle rate the cross sectional solids concentration should decrease while the gas superficial velocity is increasing. In this particular bed the range of gas superficial velocities is very limited (1.9 - 2.5 m/s) due to pressure restrictions in the piping system. Nevertheless the relationship between the three parameters is best displayed in graph form as shown in figure (3-3).

As can be seen from figure (3-3) for a fixed solids recycle rate the cross sectional solids concentration decreases with increasing gas superficial velocity as expected.

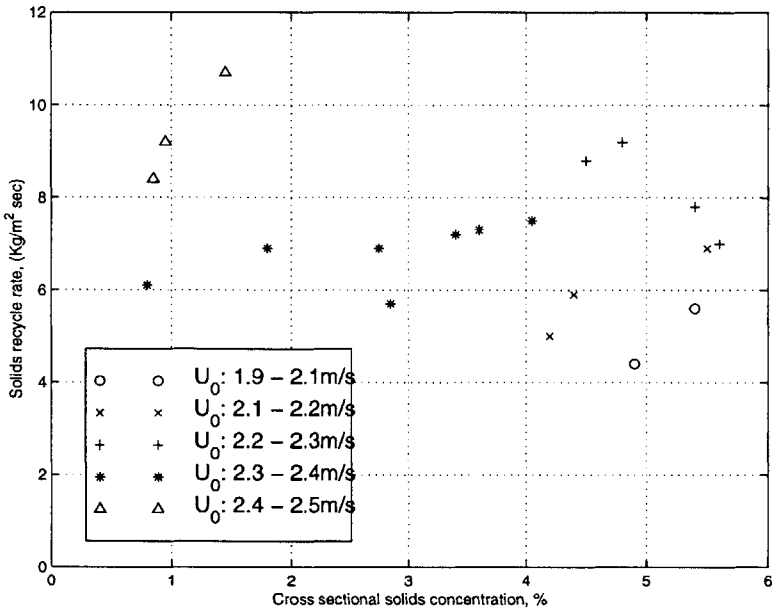

Figure 3-3: Relationship between cross sectional solids concentration, solids recycle rate and gas superficial velocity U_0

Chapter 4

Membrane Wall Experiments

4.1 Introduction

As a prelude to studying the effects of gas phase turbulence inside a circulating fluidized bed, the behavior of clusters on a membrane wall was studied. It was the study of cluster behavior on a membrane wall that led to our interest in gas-cluster turbulence interactions. The motivation for performing these experiments came from a lack of previous research on membrane walls. Direct photographic evidence of the near wall hydrodynamics had never been previously obtained on a membrane wall. This is important because a number of heat transfer parameters in equation (2.10) are functions of the hydrodynamics in a CFB such as f, the fraction of the wall covered by clusters, y_{gap}, the contact resistance between the cluster and wall and t, the contact time between the cluster and wall respectively. Therefore to understand the heat transfer mechanisms depends on the ability to understand the hydrodynamic parameters in CFB's.

The majority of commercial fluidized bed combustors have membrane walls. Membrane walls are composed of vertical tubes connected by fins, see figures (4-1, 4-2). They are commonly employed as heat transfer surfaces to remove heat from circulating fluidized bed (CFB) combustors. The membrane tubes influence the dynamics of gas and particle flow and these particles or clusters play a very important

role in the heat transfer mechanism of a circulating fluidized bed. The velocity at which the clusters travel and the amount of time the clusters spend at the wall are important parameters that aid in our understanding of the hydrodynamics at the wall. The velocity of clusters both at the fin and tube sections of membrane walls was experimentally determined. The contact time of clusters on the tube surface was also estimated.

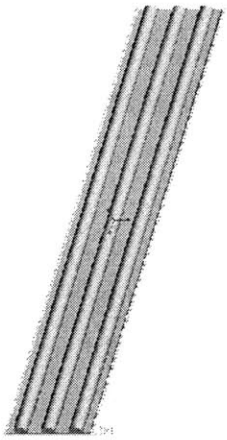

Figure 4-1: 3D construction details of riser wall used in experiments

4.2 Background

Cluster velocities can affect the cluster-wall contact time, or t in equation (2.10). Local cluster velocities have been measured previously on straight (plane,flat) walls of a CFB, Glicksman and Noymer [18] and M.Rhodes et al. [49] and particle velocity on membrane walls have been measured W.Zhang et al. [68] and J.Zhou et al. [69], although it was indirectly measured using a flux and momentum probe in the case of Zhang et al.[68], but cluster velocities on membrane walls have not been directly measured or observed yet. Likewise cluster wall contact times have been measured by Noymer et al. [42] on a straight wall but this parameter has not been experimentally determined for a membrane wall. This is due to the natural difficulty of visualizing

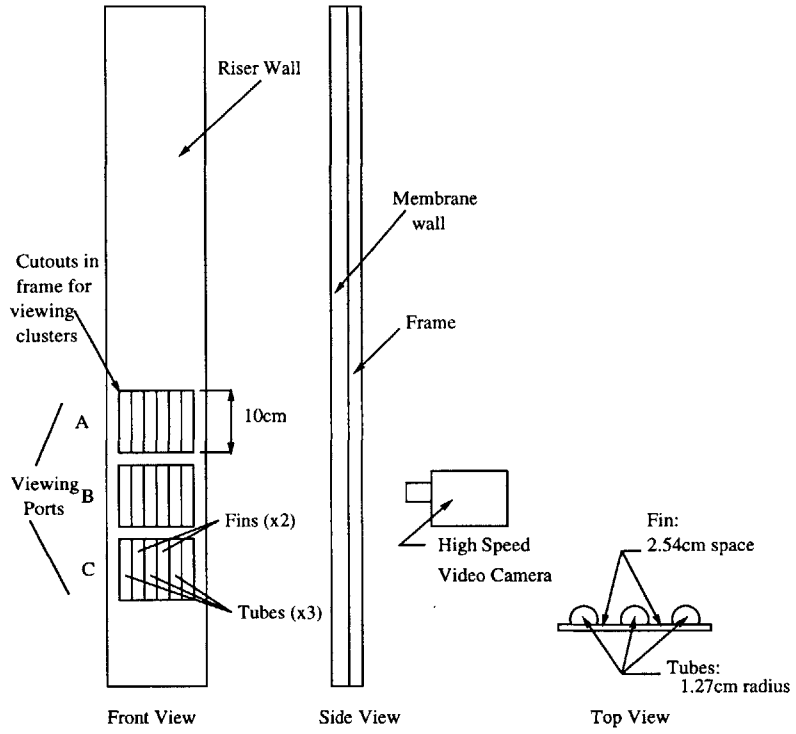

Figure 4-2: Dimensional details of riser wall used in experiments

flow inside a hot fluidized bed. In our particular experiment a cold scale model bed was used with the wall section made from transparent plastic (polycarbonate) which allowed for direct observation of clusters at the wall. Care was taken to construct the membrane wall with no rough elements or gaps along its length as this would disrupt cluster flow at the wall.

4.3 Experiment Procedure

In order to view clusters a high speed digital camera was used to videotape falling particles at the wall. The field of view was a rectangular window, $10cm$ tall by $10cm$ wide, see figure (4-2). The camera was operated at an exposure rate of 1000Hz which allowed for detailed observations of clusters at the wall. The average velocity of a particular cluster was calculated from the distance a cluster traveled divided by the time spent traveling that distance. A 1000Hz exposure rate meant that the accuracy in evaluating the time a cluster spent in the field of view was $\pm\frac{1}{2000}$ seconds. The

camera can store 2500 images in its memory which allowed for 2.5 seconds of video for each experiment.

Experiments were run at a variety of different cross sectional solids concentration, 0.4% - 0.7%, with gas superficial velocities in the range of 2.0m/s - 2.45m/s. The solids concentration data corresponds to the local solids concentration in the field of view of the camera. The actual solids concentration averaged over the entire riser height ranges from 3% - 5%. For a description on how these parameters were measured the reader is referred to chapter 3. The experiments were run in the cold scale model CFB that was described in section (3.1). The results from these experiments are discussed next.

4.4 Results

It is important to note that these results are based on observations of what the authors perceive to be as "clusters". There is no exact scientific method of determining what is or is not a cluster. It was decided only to consider clusters of particles which were considerably more dense than their background and treat them as "clusters". The first observation from the images was the lack of particles on the tube surface. There always seemed to be a relatively dense arrangement of particles on the fin section in comparison. Therefore by the above definition, clusters on the fin section would always be larger and more dense than clusters on the tube section. For each experimental run (2.5 seconds of video) approximately 16 clusters were observed on the fin compared with just 4 on the tube. In some experiments no clusters were seen on the tube surface. Figures (4-3, 4-4) show typical video frames of clusters at the wall.

The second observation is that the average velocity of clusters seems to be independent of the local cross sectional solids concentration in the bed as can be seen in figures (4-5, 4-6). The average cluster velocity on the fin region was calculated to be 1.76m/s, see figure 4-5, while the average velocity on the tube was 1.02m/s, figure 4-6. This is quite a large difference (72%) which is not explained by the statistical variations in the data.

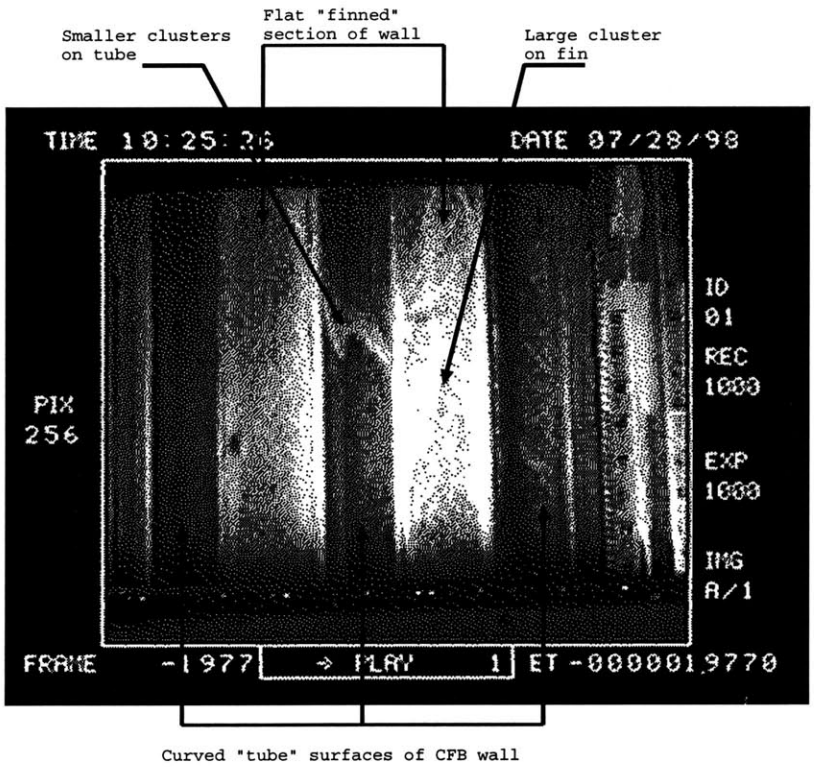

Figure 4-3: Clusters on the wall of the CFB, for a gas superficial velocity of $2.34m/s$, local cross sectional solids concentration of 0.58% and a solids recycle rate of $8.59kg/m^2s$

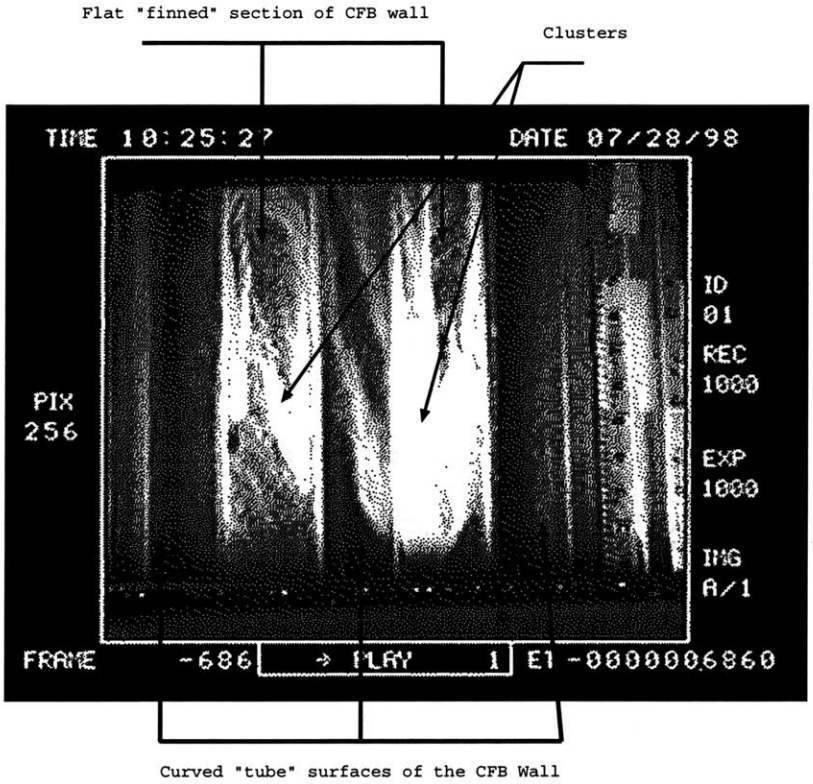

Figure 4-4: Clusters on the wall of the CFB, for a gas superficial velocity of $2.34m/s$, local cross sectional solids concentration of 0.58% and a solids recycle rate of $8.59kg/m^2s$

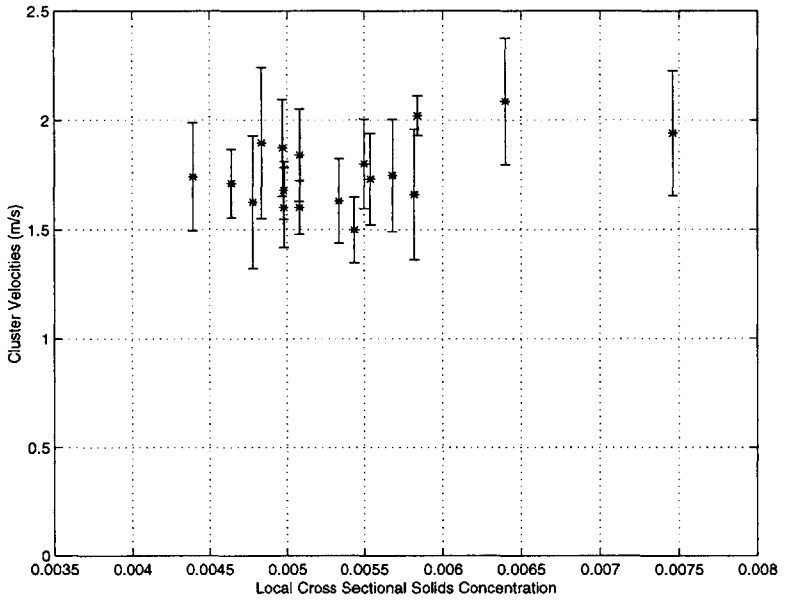

Figure 4-5: Velocity of Clusters on Fin Surface versus Cross Sectional Solids Concentration

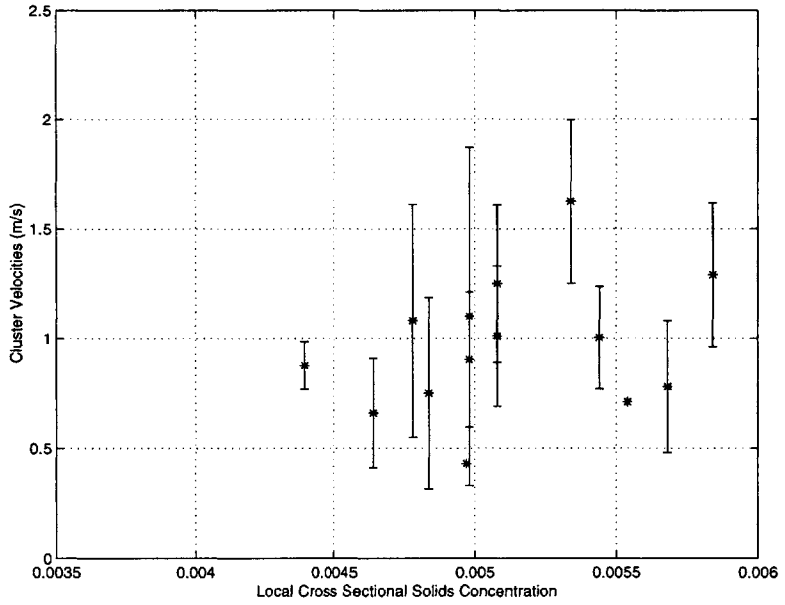

Figure 4-6: Velocity of Clusters on Tube Surface versus Cross Sectional Solids Concentration

The third observation is that almost all of the clusters observed on the fin fell from the top of the camera's field of view to the bottom without leaving the wall (a distance of approximately 10cm) but the clusters on the membrane section did not. Out of a total of 73 clusters observed on the tube sections, only 8 fell through the entire field of view. A further 6 started to form in the middle of the screen and then traveled down to the bottom. Those remaining all started and broke up or disappeared from the wall within the 10cm field of view. The average distance traveled by these clusters on the membrane surface before leaving was 5.5cm.

This distance is much shorter than the distance traveled by the clusters on the finned section. This observation has been noted by others, B.Andersson and B.Leckner [2] C.Lockhart et al. [35] but an exact distance had not been specified. However this observation helps to explain why the above differences in velocity have been observed. It has been previously postulated before L.R.Glicksman [19] that clusters accelerate to a terminal velocity. That would explain the smaller observed average velocity, since the clusters on the tube surface are still accelerating to a terminal velocity. In addition on two separate occasions clusters were observed just about to form at the fin surface. Their velocities were measured (over the short distance, $5cm$, left in the field of view) to be $0.86m/s$ and $1.01m/s$ respectively. This is remarkably similar to the velocities of the clusters at the membrane surface. Therefore, the conclusion that these clusters are, in fact, accelerating to an terminal velocity approaching $1.76m/s$ appears to be accurate. Figure 4-7 also provides auxiliary evidence supporting this conclusion.

An alternative explanation could be that the larger more dense clusters on the fin region have a greater final terminal velocity than the smaller clusters on the tube. The underlying assumption associated with this explanation is that the clusters can be modeled, to a first approximation, as a solid body. It is not yet clear whether this is valid or not. It is also possible the velocity difference is a result of a combination of these two explanations. The smaller clusters accelerate to a slower final velocity but are stripped away from the tube surface before obtaining, or very soon after reaching, this terminal velocity. There is insufficient experimental evidence at present to determine the terminal velocity of the clusters at the tube surface. They are removed from the surface too quickly thus yielding the more scattered data in figure 4-6.

A third possible explanation is that gas velocity gradient between the outer surface of the tube and the free stream flow is more steep than the velocity gradient between the fin and the free stream flow. The tube clusters are subjected to a larger shear force and hence move at a slower velocity. However numerous researchers Glicksman and Noymer [18], J.R.Grace et al. [22], W.Zhang et al. [68], have concluded that cluster velocities are independent of the gas superficial velocity. If the clusters were effected by the gas shear force then increasing the gas superficial velocity would be expected to slow down the clusters. Therefore this explanation is considered to be the least likely of the three.

Another question is why are the clusters on the tube removed so quickly? Is it a result of some turbulent interaction with the core or does the gas velocity gradient strip them away? These are questions which provoked our interest in the gas phase dynamics. It is generally assumed that gas dynamics plays a role in particle transport toward the wall and cluster removal from the wall but there has been no direct experimental measurements of the gas phase fluctuations.

4.5 Modeling Cluster Motion

Given that the cluster velocities have been observed to be independent of operating conditions and that clusters descend near the wall in a region of low gas momentum, they can be thought of as descending in still air (to a first approximation). With this, two models of descending clusters shall be considered in order to predict velocity history. In one model, the cluster is modeled as a free body with no drag. This will provide an upper bound to their velocity. In another model the drag force is linearly proportional to the velocity, resulting in the following equation of motion for the cluster:

$$m_{cl}\frac{du}{dt} = m_{cl}g - C_1 u \tag{4.1}$$

where u is the descent velocity of the cluster and C_1 is the "drag coefficient." Solving eq. (4.1) for the boundary conditions $u(0) = 0$ and $u(\infty) = u_{cl}$ yields:

$$u(t) = u_{cl}\left[1 - exp\left(\frac{-gt}{u_{cl}}\right)\right] \tag{4.2}$$

where u_{cl} is the average terminal velocity of the clusters, 1.76m/s for our particular situation. Figure (4-7) contains both of these models.

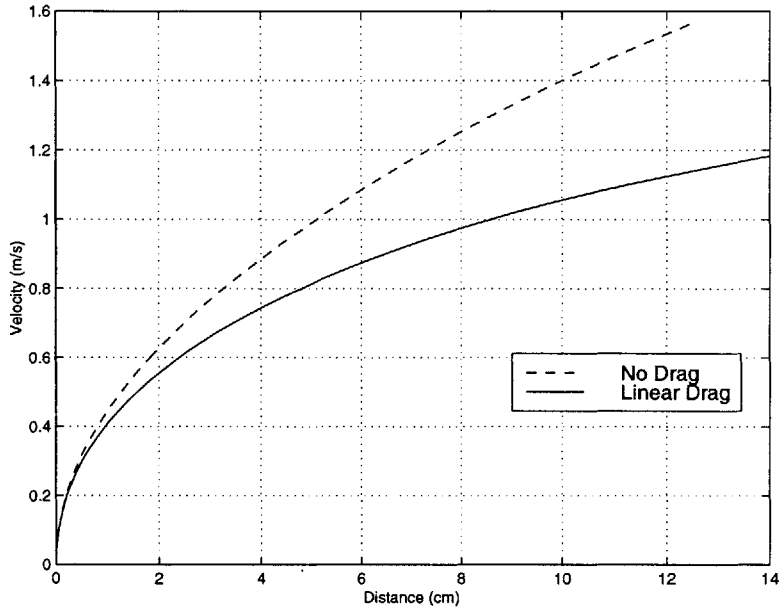

Figure 4-7: Distance traveled by clusters versus velocity for zero drag and linear drag cases

As can be seen for small distances both models are quite similar. After having traveled a distance of 6cm the upper bound on the velocity is 1.08m/s while the linear drag model predicts a value of 0.88m/s. This is less than the average velocity on the membrane wall which is 1.02m/s. Therefore it is possible that the clusters have an initial velocity of estimated to be approximately 0.2m/s. The experimental video images help support the above reasoning as clusters are observed to group together while already moving in a downward direction.

The effect of these results on the heat transfer to the membrane wall needs discussion. Higher particle concentration and lower contact times both increase convective heat transfer, see equation (2.10). The fin sections have higher particle concentration but the tube sections have lower cluster contact times. However, the fin should receive more heat than the tube because the effect of particle concentration

has a larger influence on heat transfer than the cluster contact time which goes as $1/\sqrt{t}$, see figure (2-1). More detailed information is required on the cluster-fin contact time before a quantitative analysis can be performed.

4.6 Summary

Experiments were carried out in a cold scale model CFB with clear polycarbonate walls and clusters were observed on section of the surface of a membrane wall using a high speed digital camera. The main findings from these experiments were:

- The velocities of clusters on the surface of the membrane wall is independent of bed operating conditions.
- Significantly higher particle concentrations were observed on the fin sections in comparison with the tube sections.
- The average velocity of clusters on the fin was 1.76m/s while the average cluster velocity on the tube was 1.02m/s. The difference between these two is attributed to cluster acceleration.
- The distance traveled by a cluster on the tube section before leaving the wall was approximately 5.5cm while clusters on the fins traveled much further.
- The deposition of particles to the wall and the removal of clusters from the wall appear to be random processes which warrant further investigation.

Chapter 5

Gas Phase Measurements

5.1 Problem statement

Cluster motion on a membrane wall spurred interest in the deposition and removal mechanisms from the wall. The fraction of wall covered by clusters, f, and the time spent by clusters on the wall, t, are two of the most important hydrodynamic parameters effecting the heat transfer coefficient, P.Basu and P.K.Nag [4], and T.Erbert et al. [11]. Various parameters such as the particle velocity at the wall L.Glicksman and P.Noymer [18], and K.S.Lim et al. [31], particle velocity at the bed center J.Zhou et al. [70], the thickness of the particle boundary layer at the wall W.Zhang et al. [68] and J.Zhou et al. [69], cluster size at the bed center, C.H.Soong et al. [54] and cluster structure at the wall, M.Lints and L.Glicksman [33] have been studied in the past. However the gas phase remains less well understood. It is generally assumed that gas phase fluctuations and particle-particle collisions play an important role in the transport of particles to the wall and the removal of particles from the wall. Upon further investigation it was discovered that there was a lack of experimental, theoretical and numerical research performed on the behavior of the gas phase inside a circulating fluidized bed. Some authors, most notably Leckner et al. [56, 16], have examined the gas phase. However these experiments only studied turbulence indirectly by studying fluctuations in bed pressure measurements. In fact many authors such as J. Kuipers et al. [29], G. Palchonok et al. [16] and H. Enwald and A.E. Almstedt [12], have called

for further research in this area.

The motion of the gas phase inside a circulating fluidized bed is poorly understood due to a lack of prior investigation. Particle motion in both the annulus and the core has been studied extensively and has been the subject of the vast majority of published papers in CFB's. The gas phase has not been given much attention for several reasons. Firstly, it is difficult to experimentally measure gas motion inside a CFB. Secondly, particles play a dominant role in the heat transfer mechanism and therefore gas motion was considered less important. However, one of the principle mechanisms of particle dispersion to the walls of a CFB is gas phase fluctuations. So an understanding of gas phase motion aids the understanding of particle transport which in turn aids the understanding of heat transfer.

To further the fundamental understanding and quantitative prediction of the heat transfer in a CFB, this research has experimentally measured and studied gas phase fluctuations in the riser of a circulating fluidized bed. Gas phase fluctuations have never been experimentally studied in fluidized beds before and remains one of the most poorly understood phenomena associated with this field a statement validated by such authors as M. Hyre and L. Glicksman [26], and Crowe et al. [8]. Difficulties in experimentally studying the gas phase arise due to the corrosive, optically poor environment inside a fluidized bed. This study intends to overcome such difficulties using a non-conventional experimental approach. A more developed understanding of the gas phase would allow local details of the two-phase flow to be modeled more accurately than present techniques. Current techniques necessitate averaging, with the gas phase behavior assumed to be the same as that in a single phase turbulent gas flow or sometimes even laminar flow. Such information would be of benefit to both designers of fluidized beds and the numerical codes used to model fluidized bed dynamics. It would also aid in our understanding of particle dynamics and hence heat transfer.

5.2 Previous Research

Prior research undertaken in the area of gas-particle interactions is not directly applicable to CFB's. Tsuji et al. [61] performed measurements of gas phase turbulence in a two phase flow. The average cross sectional solids concentration was around 0.5% which is approximately the same order of magnitude as that found in CFB's. He discovered that large particles ($\sim 3mm$) tended to increase the air turbulence while smaller particles ($\sim 200\mu m$) tended to reduce the turbulence. Both effects of promotion and suppression of turbulence were observed at the same time in the presence of particles in between the above sizes. However this research was carried out in a small diameter pipe (3cm) and both phases were moving upward. Experiments were not performed using the common core-annulus flow structure found in CFB's. This is because the laser techniques used by Tsuji will not work with higher concentrations and larger bed diameters. Other research into gas turbulence in two phase flows has been carried out with much lower particle concentrations than those found in circulating fluidized beds, see for example J. Shuen et al. [52] and D. Modarress et al. [39]. Research has also been carried out by Crowe [8] into the gas turbulence of two phase flows but the majority of these flows had overall particle concentrations of 0.04%, which is also considerably smaller than average particle concentrations typically found in fluidized beds. Only one or two experiments were carried out with larger solids concentrations but did not exhibit the core-annulus fluidized bed flow structure and were carried out in very small diameter vertical tubes [61]. Therefore prior research into this area cannot be directly applied to the flow structures found in circulating fluidized beds.

Turbulence in circulating fluidized beds has never been directly measured previously. Other authors have made indirect attempts at inferring that turbulence plays an important role inside a CFB. G.I.Palchonok et al. [16] measured gas convective heat transfer components and found it to be 50% higher than single phase flow correlations with no free stream turbulence. They concluded that turbulence caused the enhanced heat transfer. J. Sterneus et al. [55] performed fast fourier transforms on pressure fluctuations inside a circulating fluidized bed. They noted irregularity in the pressure fluctuations and Kolmogorov power law fall off ($P \sim f^{-5/3}$) at high frequencies in the power spectra which is characteristic of turbulent energy cascad-

ing. This once again provided indirect evidence of turbulence although they admitted that direct measurement of the gas velocity was the only way to accurately measure turbulence.

In order to verify the indirect evidence that turbulence exists inside circulating fluidized beds a fast fourier transform was performed on pressure fluctuation data from our bed. Pressure fluctuations in the freeboard region, 1.5m above the distributor plate were recorded with differential pressure transducers (see section(3.1.3)), at a frequency of 4000Hz. The results of a FFT of this data is shown in figure (8-2) with the Kolmorogov slope shown for comparison. An explanation for this slope is given in section (5.7.1).

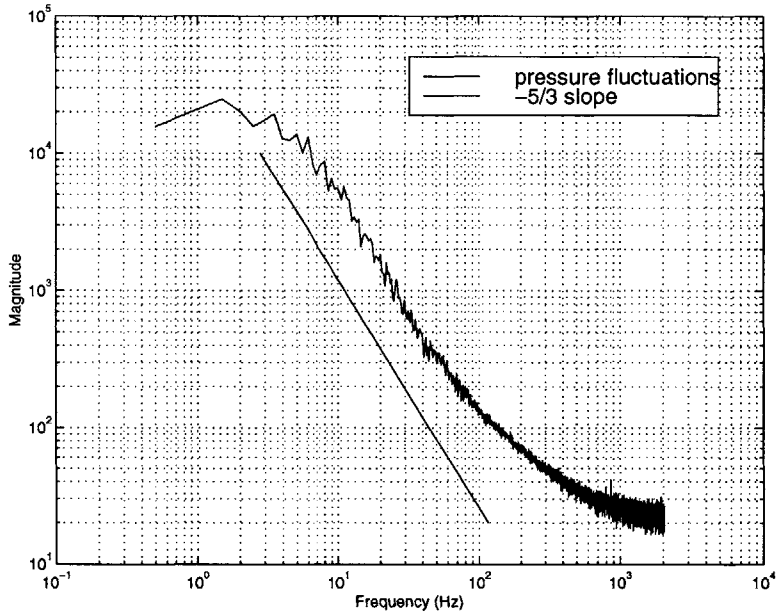

Figure 5-1: Fourier transform of fluctuating pressure measurements in CFB freeboard, gas superficial velocity of 2.35m/s, local cross sectional solids concentration of 0.66%, solids recycle rate of $7.28 Kg/m^2 s$

This confirms indirectly that turbulence effects are there. The local cross sectional solids concentration was 0.66% in the region where the pressure measurements were taken. However a more direct method of measuring the gas phase velocity is preferred and such a method is discussed below.

5.3 Experimental Method

Research into the gas dynamics and turbulence in fluidized beds is difficult due to the hot corrosive environments inside fluidized beds. Even in cold models CFB's, such as the variety at MIT, experimental measurement of the gas dynamics is difficult. Particle dynamics has been studied extensively in the past at MIT and other institutions. Experimental techniques involving capacitance probes, J.Zhou et al. [70, 71] and laser techniques, Masayuki Horio and Hiroaki Kuroki [24] and Y.Tsuji et al. [61], have been utilized to great effect. Capacitance probes cannot be used to determine gas phase turbulence and laser techniques have serious limitations. Particle Image Velocimetry (PIV) measures velocity by determining particle displacement over time using a double pulsed laser technique. The flow structure can thus be determined. Fluidized beds contain large particle concentrations which make optical penetration by laser sheets extremely difficult. With an average cross sectional solids concentration as low as 0.5% and a mean particle diameter of 200 microns the mean free path of a laser is just 2.5cm. This is why researchers using lasers have to either use very low particle concentrations as used by Masayuki Horio and Hiroaki Kuroki [24], or else very small tube diameters, as used by Y.Tsuji et al. [61]. Laser Doppler Velocimetry (LDV) is another well-proven laser technique for measuring fluid velocity. A laser beam is split into two equal intensity beams which are focused at a common point in the flow field. Particles moving through this measuring volume scatter light of varying intensity, some of which is collected by a photodetector. The resulting frequency of the photodetector output is related directly to particle velocity. LDV can be used to obtain particle velocity at the wall of a CFB but if gas turbulence is desired then difficulties exist. Small particles on the order of one or two microns would have to be introduced to the flow. The LDV system would have to have to be capable of distinguishing between the large particles already present in the CFB and the small particles. The assumption is that the smaller particles follow the motion of the gas phase and their velocity corresponds with that of the gas phase. This is a difficult experiment and has never been performed on a fluidized bed although it has been performed for some other two-phase flow configurations [61]. Inserting a large quantity of small particles without disturbing the preexisting flow would be highly challenging. Even if successful the gas flow outside the immediate vicinity of the wall would be almost impossible to determine due to the clusters at the wall blocking

the optical path further into the bed. For these reasons laser techniques were ruled unsuitable for our purposes.

5.3.1 Hot-Wire Anemometry

Eventually thermal hot-wire anemometry is the proposed approach to estimate the gas phase turbulence levels. Hot-wire model 1201 from TSI Inc. was the probe model selected. This is a disposable platinum, $50.8\mu m$ diameter sensor which was attached to a standard probe support model number 1150, dimensions which are given in figure (5-2).

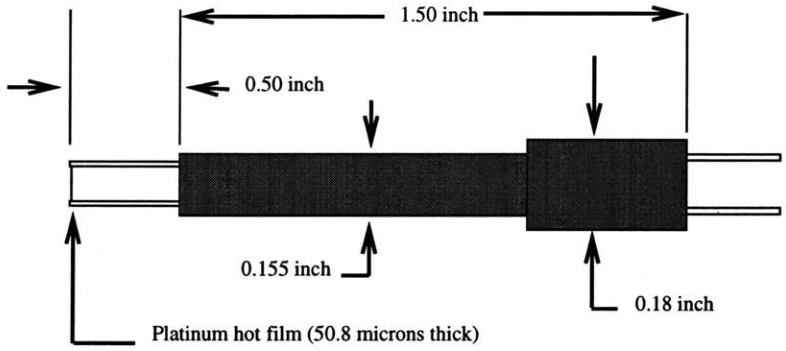

Figure 5-2: Dimensions of standard hot wire model used in experiments

Hot-wire technology measures fluid velocity by sensing the changes in heat transfer from a small, electrically-heated element exposed to the fluid. A key feature of thermal anemometry is its ability to measure very rapid changes in velocity. Time response to flow fluctuations as short as three microseconds can be easily achieved. The delicate nature of the probe sensor up to now has precluded its use in fluidized beds. With a diameter of just 50 microns the platinum hot-wire would break easily in the presence of a particle laden flow. In this experiment the hot-wire is surrounded with a mesh which protects the sensor from the particles but allows through the gas flow. The anemometer probe is placed inside a quarter inch brass tube which has two half inch slots machined out. Air can flow unhindered from one side of the tube to the other through the slots. A $38\mu m$ mesh with a wire size of $25\mu m$ and a 36% open area is fixed around the air slots to prevent particles penetrating into the tube and damaging the hot-wire. This allows measurement of gas velocities at any point

in the circulating fluidized bed simply by placing the protected probe at the desired location.

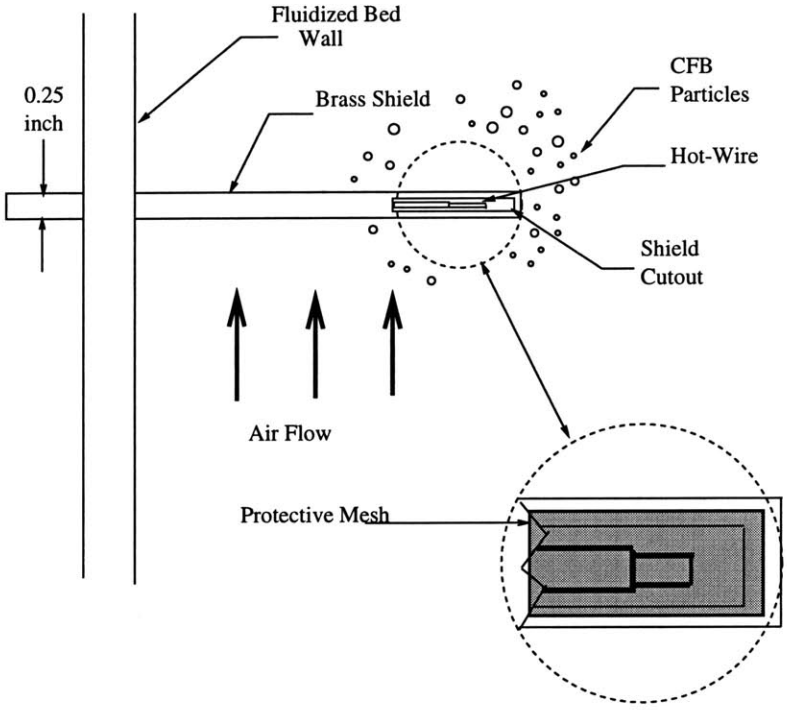

Figure 5-3: Shielded hot-wire anemometer probe

5.3.2 Hot-Wire Calibration

The effectiveness of the mesh at protecting the hot-wire sensor and possible adverse effects on the turbulence readings needs to be questioned at this stage. Tests have been undertaken to answer these questions. In order to ensure the mesh provides adequate protection for the hot-wire the fluidized bed was drained of all inventory. The particles were sieved and any particle with a diameter below $45\mu m$ was removed. Smaller particles may penetrate the wire mesh and cause damage. A small fraction (0.3%) of the overall inventory was removed. This produced little if any effect on the particle size distribution. The shielded hot-wire was placed inside the fast fluidized bed using swagelok fittings to hold the brass support in place and prevent particle leakage. After a short period of time ($\sim$ 2minutes) with an average cross sectional solids concentration of $\sim$0.5%, the anemometer was removed and tested. It was found

to function normally. This test above shows that this strategy adequately protects the anemometer from damage.

The accuracy of velocity measurements using the hot-wire with the surrounding mesh must be addressed. For a start, a calibration procedure was performed on every anemometer purchased. This involved placing the shielded probe inside a wind tunnel which has a velocity range from $0.5m/s$ up to $10m/s$. The width of the test section was $0.5m$ and the air was pulled through the test section via a 20:1 area contraction ratio, which led to a low level of turbulence inside the test section. The air velocity was measured inside the wind tunnel using a pitot probe which has an accuracy of $\pm 0.1m/s$. A pitot probe works on the bernoulli principle with the velocity, v_1, related to the pressure drop along the probe, $P_2 - P_1$, in equation 5.1.

$$v_1 = \sqrt{\frac{2}{\rho_g}(P_2 - P_1)} \tag{5.1}$$

Where ρ_g is the density of the air. The pressure drop was measured using a baratron. This gave the air velocity. The hot wire anemometer works on the principle of heat transfer. The bridge electronics keep the wire resistance constant by keeping the wire temperature constant. The electric current that flows through the wire controls the temperature by balancing joule heating and gas cooling. The voltage across the wire, V_f, is directly related to the probe output, V_{out}, therefore it can be used to indicate flow velocity. If the sensor resistance and temperature are kept constant (which they are) the output voltage is related to the velocity, using an empirical heat transfer correlation, the important features which are shown in in equation 5.2.

$$V_{out}^2 \propto \sqrt{v_1} \tag{5.2}$$

Therefore a plot of V_{out}^2 versus $\sqrt{v_1}$ should be linear. Figure (5-4) shows such a graph for a particular anemometer. Similar calibration curves for different anemometers are available in appendix A.

Figure (5-4) is a linear plot, thereby validating the calibration procedure.

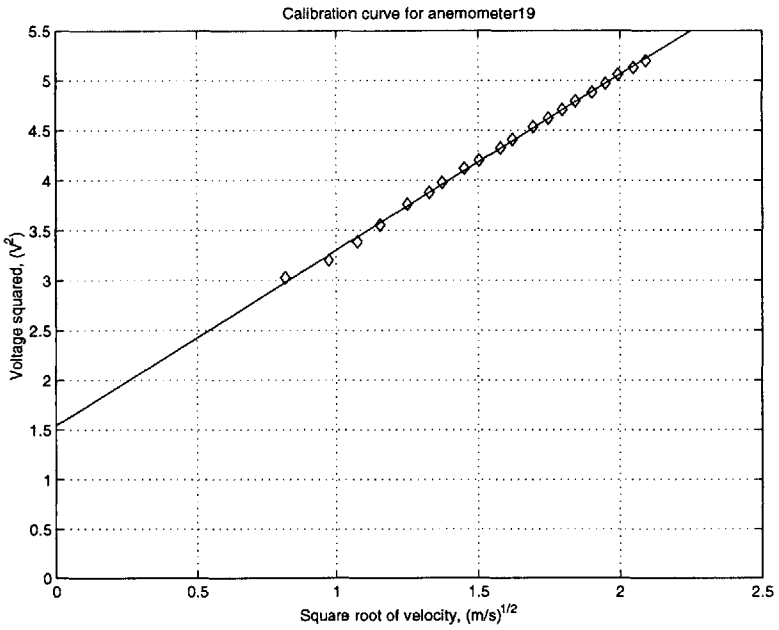

Figure 5-4: Calibration curve for hot-wire anemometer without protective shield

The exact same procedure was repeated except this time the hot wire probe was surrounded by its protective shield. The pitot tube was again used for velocity measurement. The voltage output was plotted versus air speed to obtain the representative calibration curves in figures (5-5, 5-6). Remaining calibration curves for different anemometers are given in appendix A. These plots show a linear relationship between voltage and velocity, for velocities greater than $1m/s$. For velocities below $1m/s$ there is a quadratic relationship between voltage and velocity although the experiments are performed with the gas velocity always higher than $1m/s$.

Calibration curves for the rest of the anemometers used can be found in Appendix A. Using these curves it is possible to convert the voltage output from the hot-wire into a velocity reading. This demonstrates a monotonic relationship for the anemometer holds even when surrounded by the protective shield. Note this does not demonstrate the effectiveness of the apparatus in determining velocity fluctuations merely the fact that velocity measurements are possible. It is however a positive sign.

In order to determine how accurately the velocity fluctuations are measured by the hot-wire while surrounded by the protective shield, a fast fourier transform (FFT) was performed on the velocity data taken in the wind tunnel. The airflow

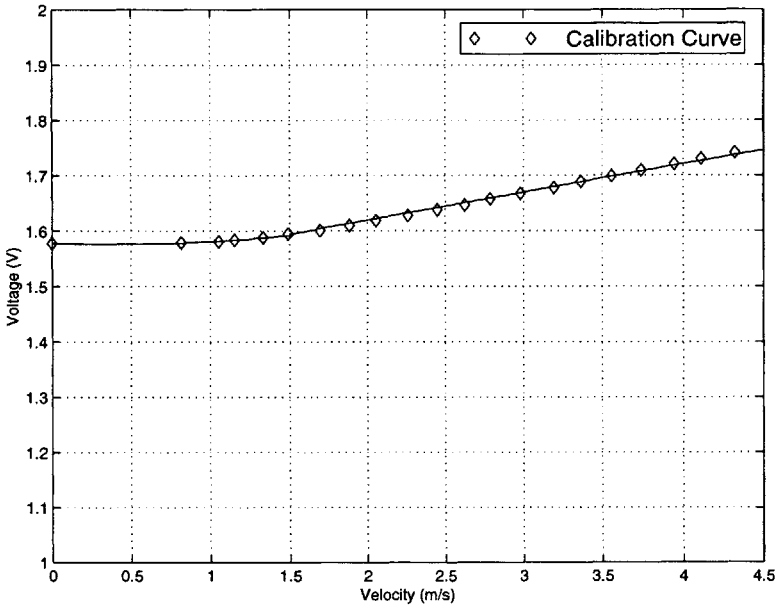

Figure 5-5: Calibration curve for hot-wire anemometer with protective shield

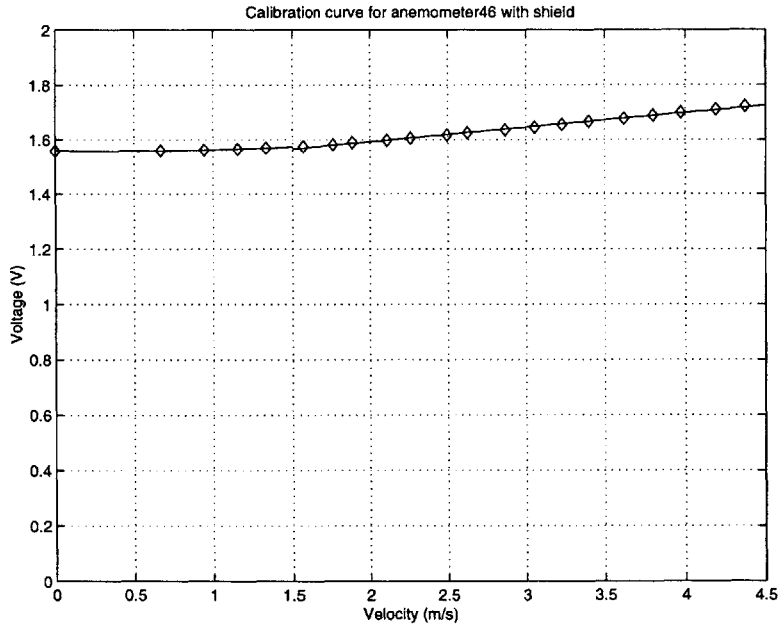

Figure 5-6: Calibration curve for hot-wire anemometer with protective shield

over the assembly was $3.0m/s$, which is approximately the same speed as the gas superficial velocity inside our CFB. The experiment was performed twice, once with the shield surrounding the hot-wire and once with no protective shield surrounding the hot-wire probe. The results are shown in figure (5-7):

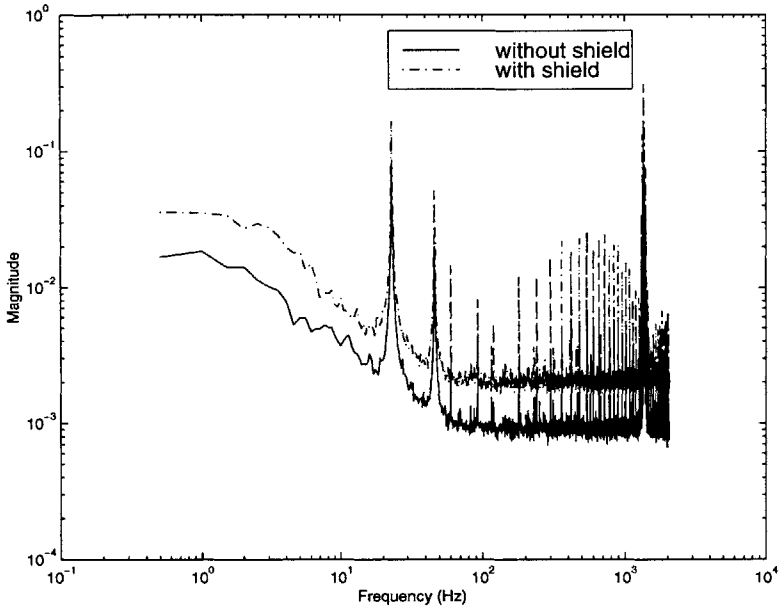

Figure 5-7: FFT of velocity data for hot-wire anemometer with and without protective shield

As can be seen from figure (5-7) up to a frequency of $2kHz$ the shield does not appear to significantly either block, distort or attenuate the signal from the flow field at any frequencies. The slight difference in magnitude between the two signals can be attributed to slightly different air velocities and/or air temperatures between both sets of experiments.

The results from the above experiments show that the shielded hot-wire can be used to measure air flow velocities. Both mean air flow and variations in the air flow are measurable. The purpose for the probe is to examine gas flow structures inside a CFB. Even if there are some slight errors associated with the shielded hot-wire at higher frequencies the preliminary data will be useful to aid understanding of the basic flow structures inside the bed and also serve as a guide to more detailed future experiments.

5.3.3 Temperature Compensation

Hot-wires are sensitive to temperature. They were calibrated inside a large room at a temperature of $24°C$. When the circulating fluidized bed is turned on the air temperature is read from an air temperature sensor embedded in the air supply line. As the air flows through the compressor and flow lines it heats up from room temperature to a steady state temperature of $44°C$. This temperature transition takes several minutes. However as particles, which are at room temperature, are added to the bed they may effect the temperature inside. Therefore a shielded thermocouple was placed inside the bed during operation. The bed was operated at a steady inlet air temperature of $44°C$ and at a variety of solids recycle rates. The shielded thermocouple was placed at the bed center and bed wall. The result was a uniform bed temperature of $32°C$ for all conditions. This should not be surprising as the excellent mixing inside a CFB leads to uniform bed temperatures as published by previous authors, D. Subbarrao et al. [57]. Since each hot-wire probe was calibrated at a room temperature of $24°C$ yet used in an environment of $32°C$ a correction factor needs to be introduced. In order to correct for temperature changes a reasonable assumption is that the bridge voltage squared V_B^2, divided by the temperature difference between the sensor operating temperature and ambient $T_s - T$, remains constant. Or in mathematically form:

$$\frac{V_B^2}{T_s - T} \simeq const \tag{5.3}$$

Therefore it is possible to predict a new bridge voltage, $V_{B'}$, for a new temperature, T', as follows:

$$V_{B'} = V_B \left[\frac{T_s - T'}{T_s - T}\right]^{1/2} \tag{5.4}$$

The sensor operating temperature in our case is $250°C$, therefore what the bridge voltage would read at $24°C$ given that the data was taken at $32°C$ is:

$$V_{B'} = V_B \left[\frac{250 - 24}{250 - 32}\right]^{1/2} \tag{5.5}$$

Giving a correction factor of:

$$V_{B'} = V_B * 1.0182 \tag{5.6}$$

This is a small correction factor being about 2% greater than the actual reading but it is important to take this correction into account before using the calibration curves to convert the voltage into velocity due to the sensitivity of velocity to small changes in voltage.

5.4 Results

Initial experiments were performed with the shielded hot-wire probe placed inside the center of the circulating fluidized bed. The hot wire measured the gas velocity at a height of 1.5m above the distributor plate, which is inside the freeboard region. The sampling rate used for the data acquisition was $10kHz$, which allowed all gas frequencies up to $5kHz$ to be measured. For more information on sampling theory the reader is referred to Beckwith et al. [5]. The gas superficial velocity, measured with the orifice plate is in the range of $2 - 3m/s$. Initially, experiments were run with air only and the air velocity was measured at the bed center. The average velocity from the hot-wire was always found to be very close to the actual gas superficial velocity, with a turbulence level comparable with that expected from single phase flow, ($\sim 7\%$) as can be seen in figure (5-8). The average velocity at the bed center as measured by the hot wire is $2.1m/s$ with the corresponding gas superficial velocity of $2.06m/s$.

This provides further evidence validating this experimental approach. The next step involved introducing particles into the flow, forming the typical core-annulus flow structure, and measuring the gas velocity at the center of the bed. The graph showing the hot-wire velocity over a period of 7 seconds is shown in figure (5-9):

For this experiment in figure (5-9) the local averaged cross section solids concentration was 0.924%, with a solids recycle rate of $6.544kg/m^2$. The difference in the air flow between both cases is striking. The particles appear to increase the air velocity at the centerline and also produce much greater fluctuations. In order

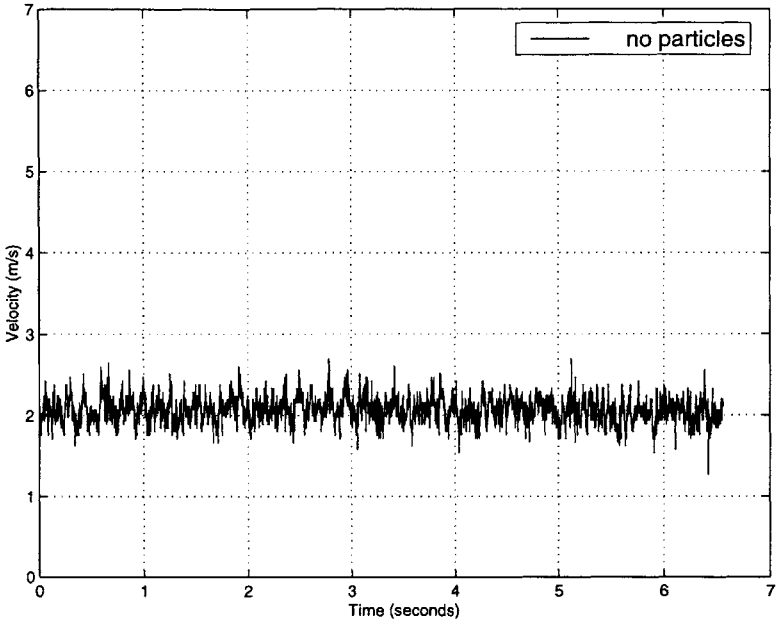

Figure 5-8: Hot wire velocity measurements at bed center with no particle flow, see appendix C test 2 for flow conditions

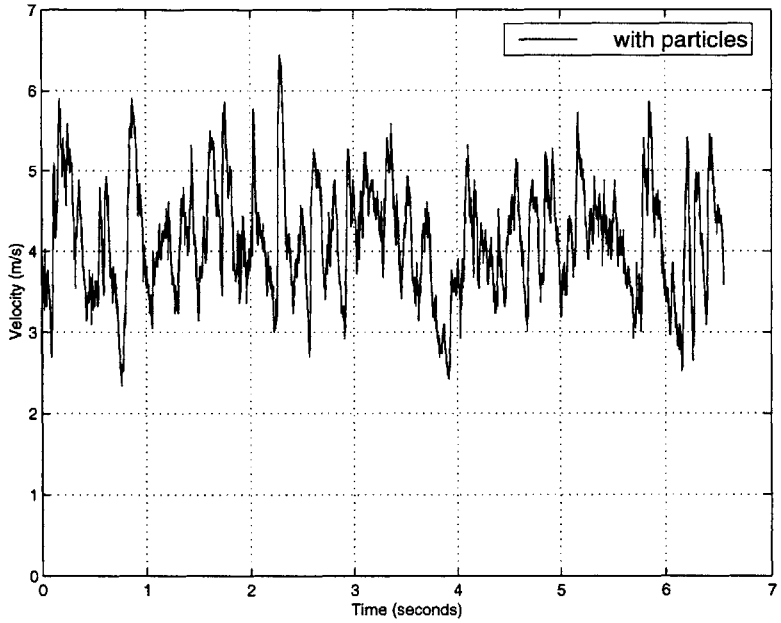

Figure 5-9: Air velocity at bed center with particle flow, see appendix C test 1 for flow conditions

to better compare both graphs they were both plotted on the same axes as shown in figure (5-10).

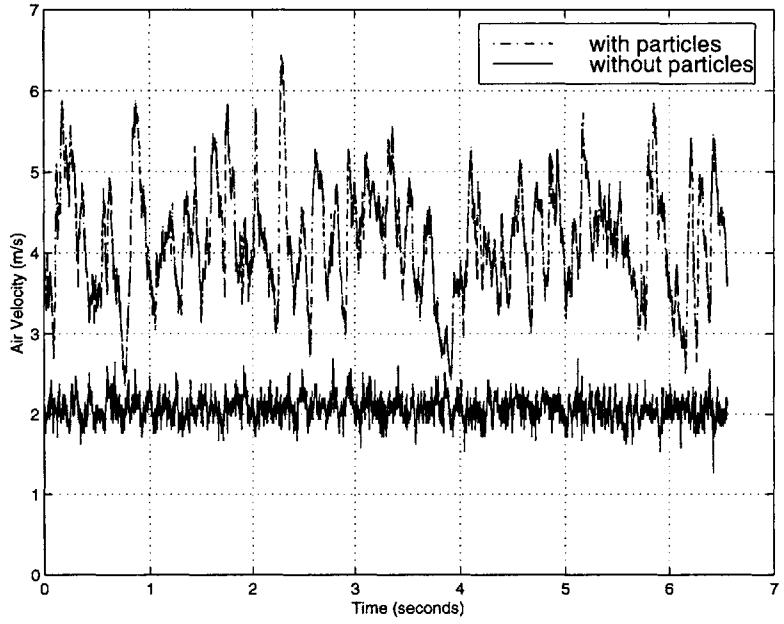

Figure 5-10: Air velocity parallel to bulk gas flow, at bed center, with and without particle flow, see appendix C test 1&2 for flow conditions

The fluctuations range from 3 - 6 m/s, a difference of 3 m/s. When there is no particle flow the air fluctuation is only 0.5 m/s. If the hot-wire probe is oriented at an angle of 90° to the direction of the air flow, so that it measures fluctuations perpendicular to the flow, a similar result is achieved:

Once again velocity fluctuations are increased substantially by the presence of particles, even in the lateral direction. For this experiment in figure (5-11) the local averaged cross section solids concentration was 0.75%, with a solids recycle rate of $4.68 kg/m^2$. This phenomena has not been observed directly by previous authors. All theses readings were taken at the center of the bed where one might expect higher levels of fluctuations than at the walls. In the lateral direction the mean velocity is not zero as one might expect since there is no net flow in that direction. The reason for this apparent inaccuracy is that the hot wire probe is not capable of distinguishing velocity direction, a positive velocity value is recorded regardless of direction.

A series of experiments were performed with the shielded hot wire probe

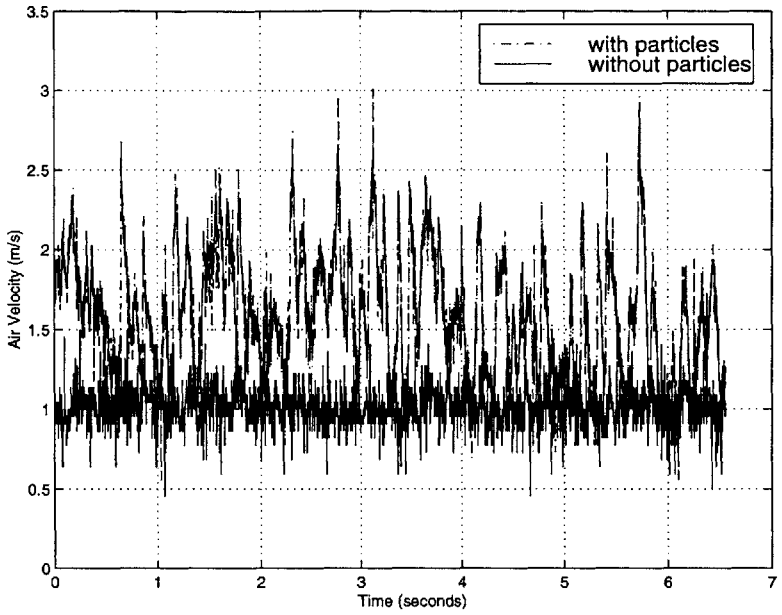

Figure 5-11: Air velocity perpendicular to bulk gas flow at bed center, with and without particle flow, see appendix C test 3&4 for flow conditions

located $0.25cm$ from the wall surface. Results from these experiments can be seen in figure (5-12).

In all cases in figure (5-12) the data with the greater velocity and higher fluctuations represents the case where there is particle flow in comparison to the case without any particles. It is interesting to note in all cases the apparent increase in velocity. This increase shall be discussed in detail in Chapter 6 while this chapter will focus on the increase in fluctuations. The top row of graphs represents data taken $0.25cm$ from the curved surface of the membrane wall. For these cases the local averaged cross section solids concentration was 0.82%, with a solids recycle rate of $5.7kg/m^2$. The bottom row represents data taken on $0.25cm$ from the flat portion of the membrane wall. It is more sheltered than the curved section and as a result the mean velocity is slightly less and the fluctuations are not as pronounced. For these cases the local averaged cross section solids concentration was 0.67%, with a average solids recycle rate of $4.2kg/m^2$. A similar set of experiments were performed except with the probe held in the perpendicular position so as to measure lateral fluctuations, see figure (5-13).

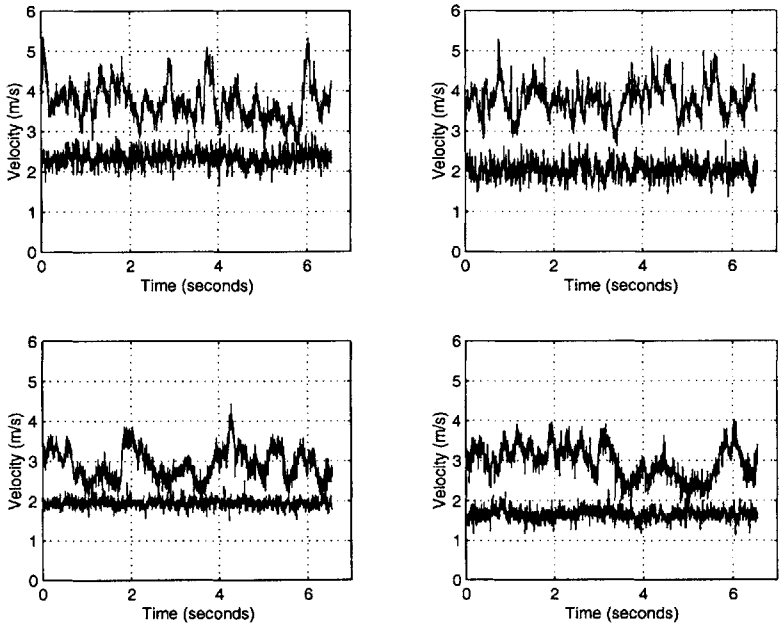

Figure 5-12: Air velocity parallel to bulk gas flow at bed wall, with and without particle flow, flow conditions in appendix C, clockwise from top left, test 17&18 test 11&12 test 5&6 test 21&22

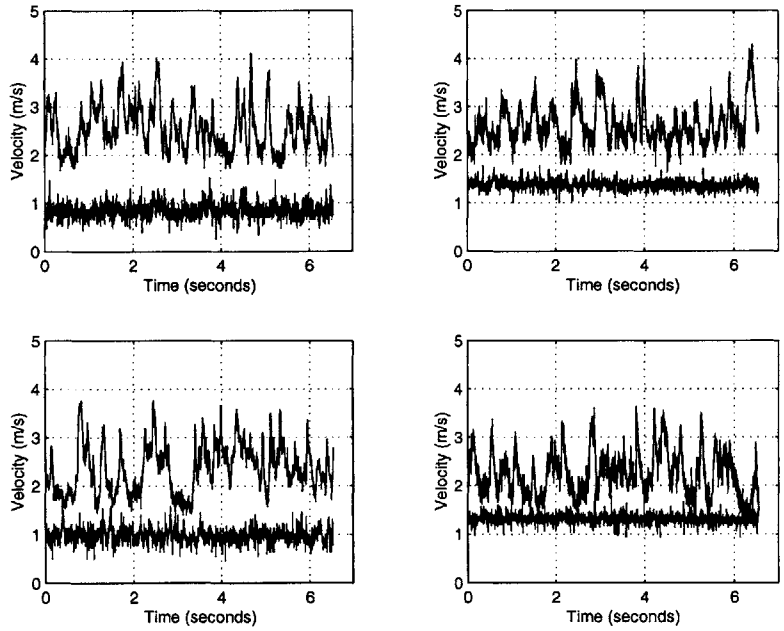

Figure 5-13: Air velocity perpendicular to bulk gas flow at bed wall, with and without particle flow, flow conditions in appendix C, clockwise from top left, test 9&10 test 19&20 test 23&24 test 7&8

Once again the data with the pronounced fluctuations corresponds to the CFB running with particles. The top row has the probe located on the curved surface and the local averaged cross section solids concentration was 0.75%, with a average solids recycle rate of $5.3kg/m^2$. The bottom row where the probe is located at the flat surface the local averaged cross section solids concentration was 0.82%, with a average solids recycle rate of $6.2kg/m^2$. In all cases the gas superficial velocity ranged from $2.0 - 2.4m/s$. Unfortunately due to pressure restrictions throughout the inlet piping system the range of superficial velocities available for these experiments was limited.

As in figure (8-2) a fast fourier transform was also performed on the velocity measurements inside the bed. This was in order to determine if the characteristic Kolmorgorov slope was obtained for velocity measurements similar to the pressure fluctuations. The probe was located 1.5m above the distributor plate, in the bed center, parallel to the flow and with the local cross sectional solids concentration 0.66%. The results of the FFT together with a characteristic $-\frac{5}{3}$ slope are shown in figure (8-1). The origin of this slope is explained in section (5.7.1).

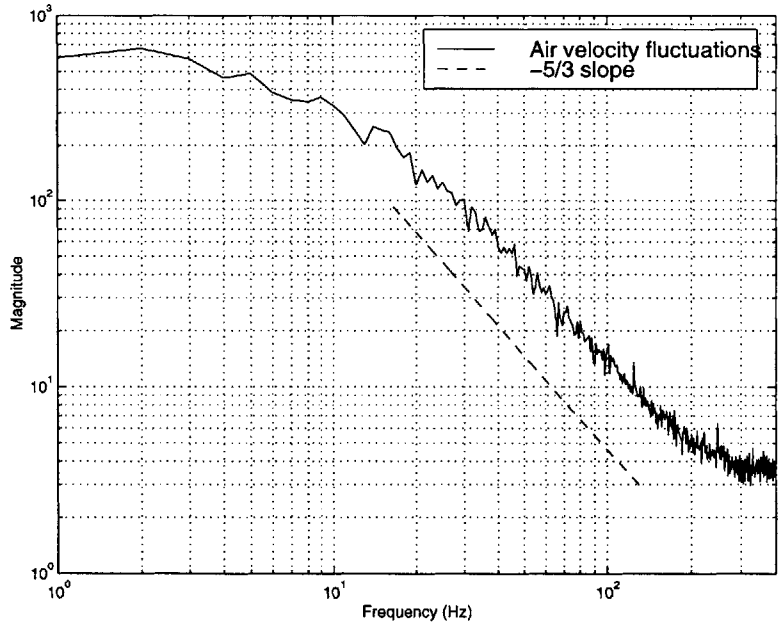

Figure 5-14: Fourier transform of fluctuating velocity measurements in CFB

Figure (8-1) demonstrates the fact that in the inertial subrange the scales of

turbulence inside our CFB are consistent with theory. Comparing the FFT for velocity fluctuations with particles and without any particles, figure (5-15) is obtained.

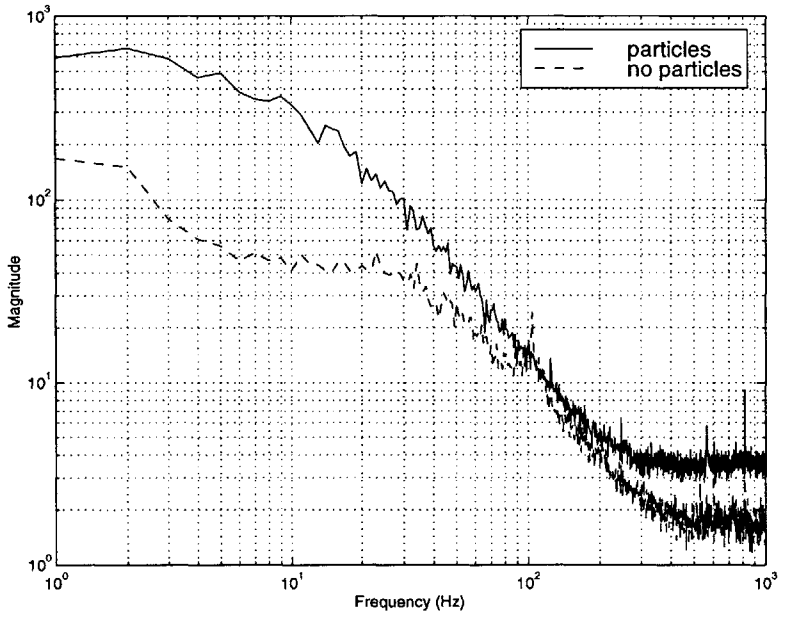

Figure 5-15: Fourier transform of fluctuating velocity measurements in CFB with and without particle flow

Figure (5-15) indicates that at low frequencies (less than 50Hz) the particle flow has more energy. The energy levels tend to converge in the range from 40Hz - 200Hz. This indicates that the large scale fluctuations occur primarily in the sub 100Hz frequency region. This interesting conclusion shall be discussed in more detail throughout the next section.

5.5 Data Analysis

Velocity modulation is the effect of particles on the velocity of the carrier phase. If the particle concentration is very low then the modulation is weak. In order to characterize this modulation Gore and Crowe [21], compiled data from a variety of sources, see figure (5-16). It is worth noting that none of the data sources had the same flow structure (core-annulus flow) as found inside a circulating fluidized bed.

The data was compiled according to a property defined as percentage change in turbulent intensity, given by:

$$\frac{\sigma_{TP} - \sigma_F}{\sigma_F} \times 100 \tag{5.7}$$

where σ is the turbulent intensity of the fluid based on the local time-averaged velocity, $\sigma = \frac{\sqrt{\overline{u'^2}}}{U_m}$ and the subscripts TP and F refer to the two-phase and single-phase flows respectively. They compared the value of turbulent intensity to the expression; $\frac{d_p}{l_e}$ where d_p is the particle diameter and l_e is the characteristic length of the most energetic eddy in the flow. Hutchinson et al. [25] developed a model for estimating l_e. At non near wall regions inside the tube l_e can be approximated by:

$$l_e \simeq 0.1 D_{tube} \tag{5.8}$$

Where D_{tube} is the diameter of the CFB riser. The critical point for this ratio was found to be:

$$\frac{d_p}{l_e} \simeq 0.1 \tag{5.9}$$

Values for $\frac{d_p}{l_e}$ below this were found to have no effect or decrease the percentage change in relative turbulent intensity while values above this were found to substantially increase the relative turbulent intensity, as can be seen in figure (5-16).

For the experiments above it is unclear whether the percentage change in turbulent intensity is the correct criteria for analyzing the data since turbulence implies a random chaotic motion. The gas velocity patterns above are not completely random as they tend to exhibit large scale fluctuations exclusively in the low frequency spectrum, see figure (5-15). To further illustrate this point the data with particles in figure (5-10) was passed through a filter which only passed frequencies within certain ranges. The filter used is a recursive filter designed using a least squares method. If a filter was desired which only allowed through frequencies between 2000Hz and 3000Hz then the filter in figure (5-17) would be used. It shows the ideal filter versus

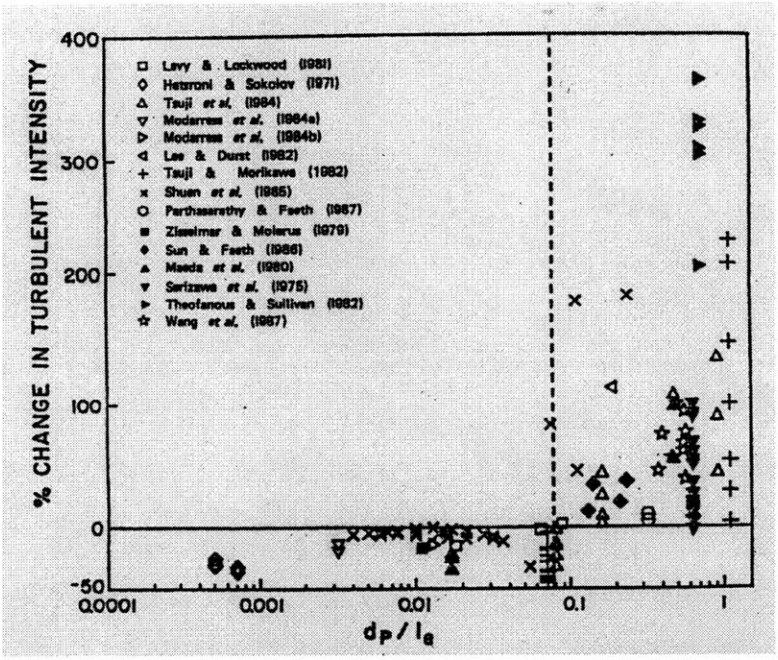

Figure 5-16: Change in turbulent intensity as a function of length scale ratio. from Gore and Crowe [21]

the actual filter. By changing the upper and lower bound of the frequency range this filter can be changed into a low or high pass filter.

Figure (5-10) was analyzed using such a filter and the results are shown in figure (5-18). The first plot ranges from $0 - 200Hz$ the second from $200 - 1000Hz$ and the third from $1000 - 4000Hz$.

As can be seen from figure (5-18) the large scale fluctuations are associated with the small (below $200Hz$) frequencies. If a bandpass filter, $1 - 4kHz$, is applied to both sets of data from figure (5-10), then figure (5-19) is obtained. This shows that at the higher frequencies there is little if any difference between the two phase and single phase air flows. This demonstrates again that the velocity differences occur in the sub 200Hz range.

If the fluctuations were truly random they would be distributed evenly throughout the inertial region of the spectrum. However, in the absence of any other common method for analyzing the data and acknowledging the uncertainties associated with this approach the experimental data shall be compared with the criteria

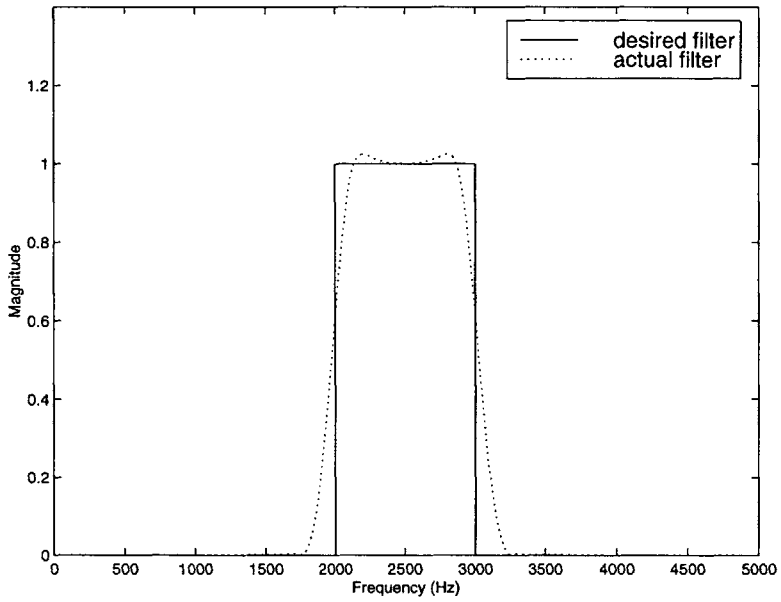

Figure 5-17: Filter used to analyze data

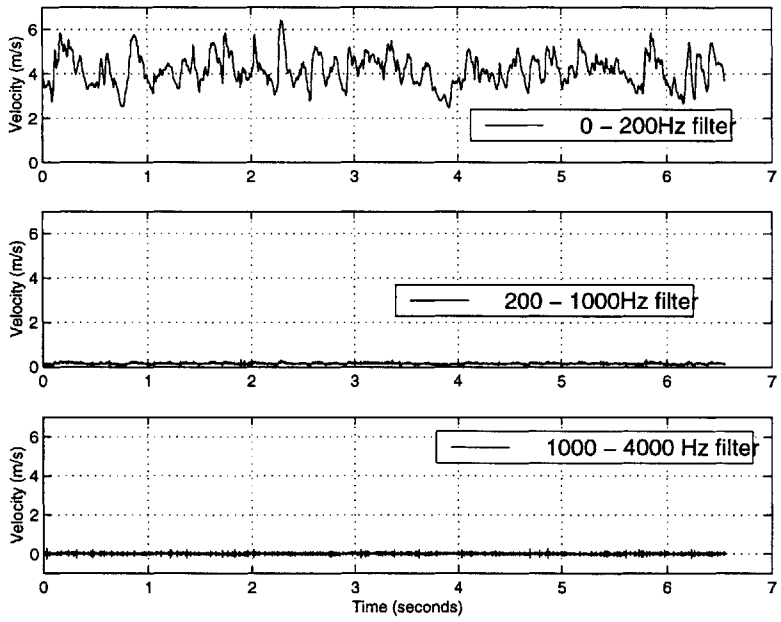

Figure 5-18: Air velocity versus time after passing through various bandpass filters, see appendix C test 1 for flow conditions

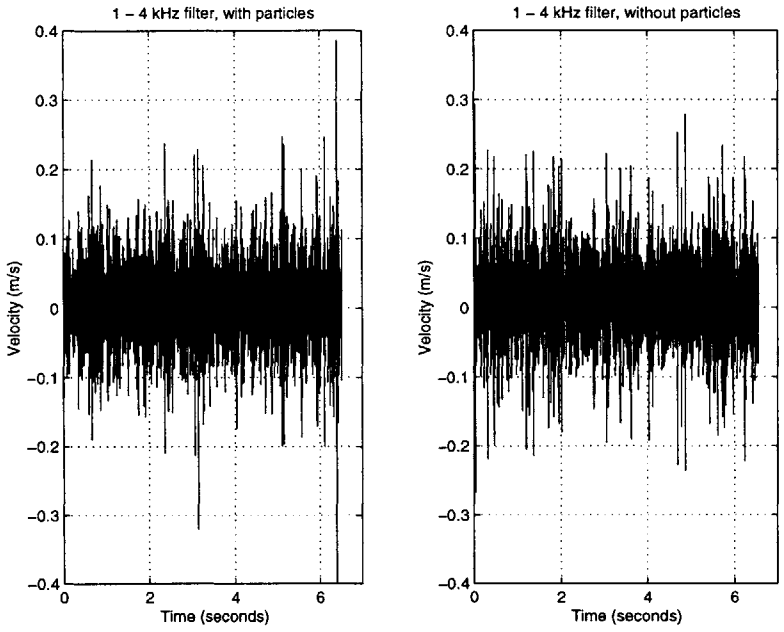

Figure 5-19: Air velocity versus time after passing through a 1 - 4 kHz bandpass filter, with and without particles, see appendix C test 1&2 for flow conditions

from equation (5.9). The average particle size inside the bed was $164\mu m$. Hutchinson et al. [25] showed that the $\frac{l_e}{R}$ ratio across a pipe of radius R, in fully developed flow was approximately constant ($\frac{l_e}{R} \simeq 0.2$) except near the wall region. This gives an eddy length of $l_e \simeq 1.6cm$. Substituting these values into equation (5.9) yields a ratio of $\frac{d_p}{l_e} = 0.01$. As this is an order of magnitude below the cutoff value of 0.1, it is expected that the addition of particles would decrease the turbulence intensity. Surprisingly, this is not the case. Using the data from figure (5-10) and equation (5.7), an increase in percentage change in turbulence intensity of 158% was found. Experiments run with different solids concentration and gas superficial velocity yielded similar results. The turbulence intensity always increased by a factor between 50% and 400%. Appendix C contains the conditions of all experiments, values of turbulence intensity for all experiments are also listed here.

M.Rashidi et al. [48] developed a separate criteria for predicting whether particles would enhance or reduce turbulence. They said particles with a Reynolds number below 100 ($Re_p < 100$) suppress turbulence while those with a Reynolds number greater than 400 ($Re_p > 400$) enhance turbulence due to vortex shedding. A

good estimate for the particle Reynolds number is given in equation 5.10:

$$Re_p = \frac{V_{air} D_{particle}}{\nu_{air}} \simeq \frac{(2.5)(164E-6)}{17.44E-6} \approx 23 \tag{5.10}$$

A particle Reynolds number of 23 implies suppression of turbulence which we quite clearly are not seeing from experimental data.

There are some problems with the above analysis. Firstly, the data compiled by Gore and Crowe [21] and M.Rashidi et al. [48] is predominantly two phase flow in pipes. No data is available for gas phase fluctuations inside a circulating fluidized beds and their unique flow structure. Comparing two dissimilar phenomena is not advisable but it still is unclear what causes such a large difference. A fluidized bed typically has a core-annulus flow. Clusters of particles are continuously formed and broken up as they travel through the riser, [24]. Due to a lack of air momentum close to the wall the clusters in that vicinity travel downwards. This leads to a possible explanation to describe the apparent increase in gas velocity fluctuations. The dominant particle structures are clusters; perhaps the dominant particle length scale is the cluster size, d_c, instead of particle size, d_p. Previous authors Lim et al. [31], and Soong et al. [54] have estimated the size of clusters in circulating beds of similar size to the one used in these experiments, $\simeq 15 - 20cm$. Although the definition of a cluster is somewhat arbitrary and larger clusters are found nearer to the wall both authors measured mean cluster diameters of approximately $2cm$. Using this as the particle length scale, a ratio of 1.25 is obtained for $\frac{d_c}{l_e}$. This is an order of magnitude greater than the cutoff value of 0.1. This predicts an increase in relative turbulence intensity. Similarly using a length scale of $2cm$ in order to obtain the particle Reynolds number gives:

$$Re_p = \frac{V_{air} D_{particle}}{\nu_{air}} \simeq \frac{(2.5)(0.02)}{17.44E-6} \approx 2867 \tag{5.11}$$

Equation (5.11) clearly places the data in the turbulence enhancement regime according to the criteria of M.Rashidi et al. [48]. All this evidence leads to the conclusion that an appropriate length scale to use for turbulence enhancement or suppression inside a CFB is the cluster length scale instead of the particle length scale

as has traditionally been the case.

5.6 Data Modeling

There are several analytical models that have been developed for attempting to predict the effect of a solid dispersed phase on the gas or carrier phase. Many provide a simple order of magnitude analysis to this issue. None of them provide a comprehensive solution to this problem. In this section a brief review of the models is presented and discussed.

5.6.1 Earlier models

One of the first models proposed was from P.Owen [47]. He allowed the turbulence energy associated with the carrier and dispersed phase to be expressed as:

$$E_k = \tilde{\rho}_f \frac{u'^2}{2} + \tilde{\rho}_d \frac{v'^2}{2} \tag{5.12}$$

If the particle Stokes number was less than one ($St << 1$) the particle will achieve near velocity equilibrium with the gas so the kinetic energy can be expressed as:

$$E_k = (\tilde{\rho}_f + \tilde{\rho}_d) \frac{u'^2}{2} \tag{5.13}$$

Assuming the rate of energy production is the same in both single and dispersed phase flow and the rate of energy decay is proportional to the kinetic energy, the turbulent fluctuating velocity would be reduced by:

$$\frac{u'}{u'_0} \approx (1 + \frac{\tilde{\rho}_d}{\tilde{\rho}_f})^{-\frac{1}{2}} = (1 + X_d)^{-\frac{1}{2}} \tag{5.14}$$

Equation (5.14) predicts that particles or droplets would reduce turbulence uniformly; the effect becoming smaller for larger particles. However this model is only valid for small Stokes numbers and does not explain the augmentation of turbulence for larger particle sizes.

Al Taweel and Landau [58] utilized the predicted particle-fluid velocity difference in a fluid oscillating sinusoidally to establish the energy dissipation as a function of frequency. They incorporated this effect into expressions for energy flux in isotropic turbulence and predicted a decrease in the energy spectrum at higher frequencies with increased mass concentration. However once again their model fails to predict an increase in turbulence intensity for larger particle size.

Besnard and Harlow [6] use the average field equations to develop equations for turbulence energy in a multiphase flow. Their model also predicts a damping of the turbulence and has no mechanism to account for turbulence augmentation.

Theofaneous and Sullivan [59] developed a model for turbulence modification with the premise that the turbulence fluctuational velocity approaches the wall shear velocity. Their model predicts that the dispersed phase will always augment the turbulence; which is clearly not experimentally accurate.

5.6.2 Later Models

Recently, Yaun and Michaelides [67] developed a model which attempts to include the turbulence attenuation due to viscous work done by the fluid on the particles and augmentation due to particle wakes. The following expression for the change in energy ($\triangle E_k$) due to the particles was derived

$$\triangle E_k = -\frac{\pi}{12} D^3 \tilde{\rho}_d U_{rel}^2 [1 - exp(-\frac{2f\tau}{\tau_a})] + \frac{\pi}{12} D^2 \rho_f f(l_w)(u^2 - v^2) \qquad (5.15)$$

where τ_a is the particle relaxation time, τ is the eddy life time or particle residence time in the eddy, whichever is smaller, U_{rel} is the relative velocity between the particle and fluid, f is the ratio of the drag coefficient to Stokes drag and $f(l_w)$ is

a function representing the wake length. the first term is attenuation due to viscous work on the particles and the second is augumentation due to the wake. There is some questionable features of the model. The wake term suggests that the energy is either added or subtracted from the flow depending on the sign of the term $(u^2 - v^2)$. In this model this term should have an absolute sign sign a wake should always augment turbulence. Also the function $f(l_w)$ is ill defined. It is supposed to be the representative length of the wake region but a precise definition was not given. The wake was assumed to be half of a complete ellipsoid and steady but as we shall see in the simulations presented in chapter 7 the wake region behind a cylinder is neither an ellipsoid nor steady even for moderate Reynolds numbers.

Yarin and Hestroni [65] utilize an idea similar to Yuan and Michaleides but employ a more detailed description of the wake. They predict that

$$\frac{\sqrt{u'^2}}{|v-u|} = \left(C \frac{\rho_c}{\rho_d} C_d^{3/2} \right)^{4/9} \tag{5.16}$$

where C_d is the drag coefficient and C is an empirical constant. This model appears to correlate data for turbulence generated solely by particles at very low particle volume fractions.

Basically the analytical models presently available are applicable to a limited range of particle sizes and/or volume concentrations. There is no general predictive model that covers all flow scenarios. Future research is needed to develop a general model that is applicable to all flow conditions including those of circulating fluidized beds where the flow simultaneously consists of both small scale particles and large scale clusters.

5.7 Turbulence scaling

In this section a turbulence scaling argument will be applied to the results obtained. In a steady, homogeneous flow there is a balance between the production rate of turbulent energy by Reynolds stresses and the rate of viscous dissipation of turbulent

fluctuations. Mathematically:

$$\mathcal{P} = \epsilon \tag{5.17}$$

Equation (5.17) is only useful for scaling of turbulence not related to diffusion. Let the production length and velocity scales for the flow be l, u respectively. These are the scales associated with the gross behavior of the flow. Let the length and velocity scales for the fluctuations be η, υ, these are called the Kolomogorov microscales, see Uriel Frisch [15]. They apply to the dissipation part of equation (5.17). The magnitude of production of velocity fluctuations can be estimated from:

$$\mathcal{P} \sim \frac{u^2}{t} \sim u^2 \frac{u}{l} \tag{5.18}$$

The magnitude of the dissipation can be estimated from:

$$\epsilon \sim \nu \frac{\upsilon^2}{\eta^2} \tag{5.19}$$

Using equation (5.17) gives:

$$\mathcal{P} \sim u^2 \frac{u}{l} \sim \nu \frac{\upsilon^2}{\eta^2} \sim \epsilon \tag{5.20}$$

This allows us to estimate viscous dissipation of energy from the large scale inviscid dynamics. Rearranging equation (5.20), as $l \to \eta$ and $u \to \upsilon$, allows us to estimate the Kolmogorov length scale and velocity;

$$\eta \sim \left(\frac{\nu^3}{\epsilon} \right)^{1/4} \tag{5.21}$$

$$\upsilon \sim (\eta \epsilon)^{1/3} \tag{5.22}$$

An estimate for u can be taken as the rms fluctuating velocity measured inside the CFB, taken to be $0.8m/s$ for this case. The length scale l can be estimated from the largest eddy size in single phase flow but for a two phase flow another estimate for l can be obtained from the dominant frequency of the velocity fluctuations. In figure (5-15) the peak frequency f_0 for the velocity fluctuations was $2Hz$. Therefore l can be estimated from:

$$l \propto \frac{u}{2\pi f_0} \sim 0.06m \tag{5.23}$$

From equation (5.24) the production term is estimated to be:

$$\mathcal{P} \sim u^2 \frac{u}{l} \sim 8.5m^2/s^3 \sim \epsilon \tag{5.24}$$

Using equation (5.21), with a value of air kinematic viscosity at $27°C$, gives a Kolmogorov length scale of:

$$\eta \sim \left(\frac{\nu^3}{\epsilon}\right)^{1/4} \sim 146\mu m \tag{5.25}$$

This length scale is similar to the particle length scale, $164\mu m$. In fact the assumption that the Kolmogorov microscale is similar to the particle length scale was postulated before by G.Palchonok et al. [16]. Using equation (5.22) to estimate the Kolmogorov velocity:

$$v \sim (\eta\epsilon)^{1/3} \sim 0.11m/s \tag{5.26}$$

The fluctuating component of the velocity field for the two-phase flow at high frequencies is approximately $0.1m/s$, see figure (5-19), which is very similar to the magnitude estimated from the scaling arguments.

Applying rough models to the scales of turbulence reveal the smallest length scales are the same order as the particle length scale. The smallest velocity scales estimated correspond to the velocities measured at the high frequencies in the flow.

5.7.1 Energy spectrum

In this section scaling arguments from the previous section will be used to demonstrate the Kolmogorov slope $-5/3$ for eddy decay. From the definition of energy, E:

$$E \sim u^2 \tag{5.27}$$

Eliminating u using equation (5.20) yields:

$$E \sim (\epsilon l)^{2/3} \tag{5.28}$$

Also by definition the energy and its spectrum are related as:

$$E \sim fE(f) \tag{5.29}$$

Eliminating E between equations (5.28, 5.29) and noting that $l \sim f^{-1}$ gives:

$$E(f) \sim \epsilon^{2/3} f^{-5/3} \tag{5.30}$$

which is the Kolmogorov energy spectrum for the equilibrium range.

5.8 Summary

The unique two-phase flow structure inside a circulating fluidized bed significantly effects the gas velocity. Hot-wire measurements taken at the bed centerline show a substantial difference between the single and two-phase air flow. The main conclusions can be summarized below:

- The mean gas velocity at the bed center is between 50-100% higher than the gas superficial velocity

- There are large scale velocity fluctuations caused by particle clustering
- The frequency of these fluctuations is in the range of 0-200Hz
- The increase in gas velocity fluctuations is consistent with previous research in two-phase flow so long as the length scale used is the typical cluster length scale as opposed to the particle diameter.
- The Kolmogorov microscale length and velocity was found to be similar to the particle length scale and the high frequency fluctuating velocity.

Chapter 6

Mean Velocity Measurements

6.1 Introduction

The results and subsequent discussion from Chapter 5 dealt primarily with the fluctuation measurements obtained from the circulating fluidized bed. Referring back to figure (5-10) there is also another interesting effect in addition to the large increase in fluctuations. The mean gas velocity had increased from $2.1m/s$ to $4.14m/s$, almost a factor of 2. This is an interesting result which shall be explored in more detail this chapter.

The objective of this chapter is to measure and model the mean gas velocities inside a cold scale model circulating fluidized bed. Results indicate that the mean gas velocity at the bed center can be up to twice as high as the gas superficial velocity. This information has never been obtained or published before. Other researchers have examined changes in the gas phase due to the presence of a second phase, most notably Tsuji [61] and Crowe [8]. However as mentioned previously this research has focused on small diameter risers ($\sim 2cm$) to enable laser light penetration, [61]. Small diameter risers do not produce the core-annulus structure found in CFB's and to compare the hydrodynamics of one with the other may not be accurate. Alternatively, to allow laser light penetration, some experiments were performed with low solids concentrations ($\sim 0.04\%$) J.S.Shuen et al. [52], D.Modarress et al. [39] and Masayuki

Horio and Hiroaki Kuroki [24]. Once again data and conclusions from these tests are not necessarily applicable to CFB's where typical solids concentrations run from $0.5\% - 5\%$.

6.2 Results

Rather than reprint the same graphs again the reader is referred to figure (5-10) in chapter 5 as a starting point. The gas superficial velocity was $2.1m/s$, solids recycle rate $6.54kg/m^2s$ and the local cross sectional solids concentration was 0.924%. The large scale fluctuations have been discussed in the previous chapter therefore the focus of this discussion shall be the increase in mean gas velocity at the bed centerline when particles are introduced. The mean centerline velocity for air flow alone is $2.1m/s$. The mean centerline velocity then becomes $4.14m/s$ with a local particle concentration of 0.924%, an increase of over 97%. This large increase was an unexpected result. To investigate this phenomena further the shielded probe was incrementally moved across the diameter of the bed starting at a point midway along the width of one wall. At each position the mean velocity was recorded. The results are shown in figure (6-1).

It can be seen from figure (6-1) that the mean velocity is largest at the bed center, although the actual data point at the bed center seems large, possibly a result of experimental uncertainty. Away from the center the mean gas velocity tapers off down to a minimum of $3.2m/s$ close to the riser wall. The experimental technique does not permit accurate velocities measurements in the vicinity ($\sim 2cm$) of the wall. This is because there is clearly cluster downflow at the wall, Moran and Glicksman [40]. The hot wire cannot distinguish the direction of air flow, only its magnitude. It is highly probable that the air flow at the wall is also moving downward with the clusters. The velocities close to the wall are probably smaller than those shown in figure (6-1). However the majority (6 out of 8) of the data points were taken outside the particle boundary layer and provide the bulk of the required information for the curve fit. Where these estimates of the particle boundary layer thickness were obtained shall be explained in the next section.

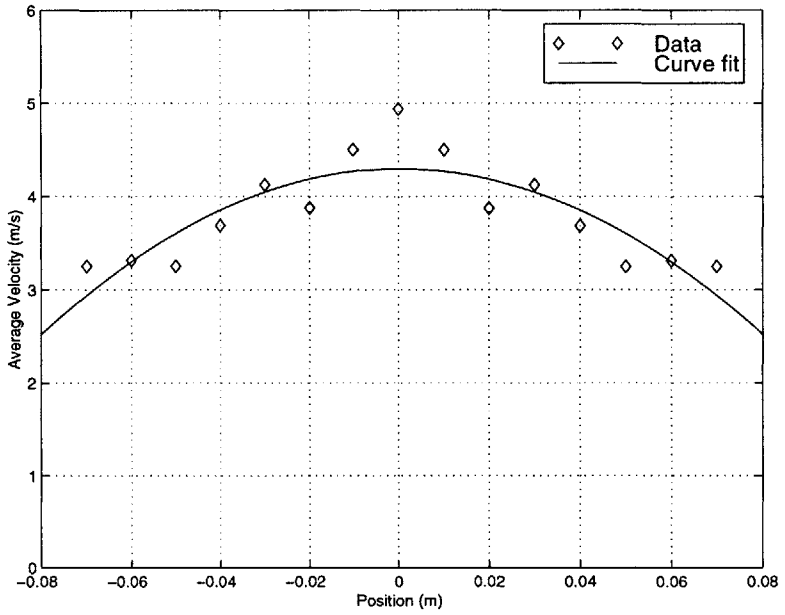

Figure 6-1: Mean air velocity across riser diameter, appendix C tests 25-32 contain the flow conditions for these experiments

6.3 Analysis

Mass conservation shall be used to help understand these results. An orifice plate outside the bed allows for accurate measurement of the air volumetric flow rate. This value must exactly equal the volume flow rate inside the bed as air does not enter from any other source. Using the functional curve fit from figure (6-1) the volume flow rate can be plotted as a function of bed radius. An upper bound for the flow rate integrates this curve fit over the bed radius to obtain a two-dimensional flow rate which is then multiplied by the bed diameter. This is an upper bound because it assumes no decrease in velocity as the bed walls are approached. A more realistic estimate is obtained using a three-dimensional model for the air velocity. The same functional curve fit is extended to three dimensions to form an elliptic paraboloid, figure (6-2).

Figure (6-2) provides a more accurate model for the velocity profile assuming that the velocity is symmetric inside the bed. It is likely that the velocity profile will not be symmetric due to local variations in solids concentration. This profile

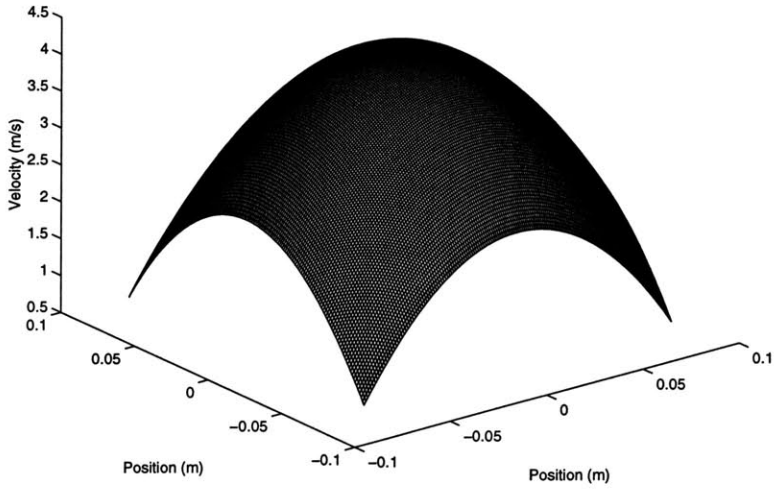

Figure 6-2: Model for air velocity inside CFB riser

integrated over two dimensions provides another (lower bound) volume flow rate plot. Both plots along with the actual volume flow rate as measured before entering the bed are shown in figure (6-3).

The actual volume flow rate is $0.059m^3/sec$. The upper bound model predicts a volume flow rate of $0.093m^3/sec$ through the whole bed diameter. The lower bound predicts a volume flow rate of $0.08m^3/sec$. An explanation is needed for the apparent addition of an extra $0.02m^3/sec$ air flow. As mentioned previously the flow structure inside the CFB is the typical core-annulus flow. A dense layer of particles/clusters flow downward at the wall with a more dilute upward flowing layer throughout the core. It seems reasonable to assume that the downward moving clusters drag and entrain a certain amount of gas causing a downward moving gas layer close to the wall. Previous researchers have estimated the thickness of the particle downflow region. Particle boundary layer thickness is defined as the distance from the wall to where the net particle flux is zero. Zhou et al. [70] used a fibre optic particle velocity measuring system in a $146mm$ square diameter riser. They found average particle boundary layers to be around $15mm$. Zhang et al. [68] used a particle flux probe in a $1720mm$ square diameter bed. An average boundary layer thickness of $90mm$ was published. Zhang also hypothesized that the particle boundary layer was dependent only on bed diameter and compiled data from eleven sources to produce

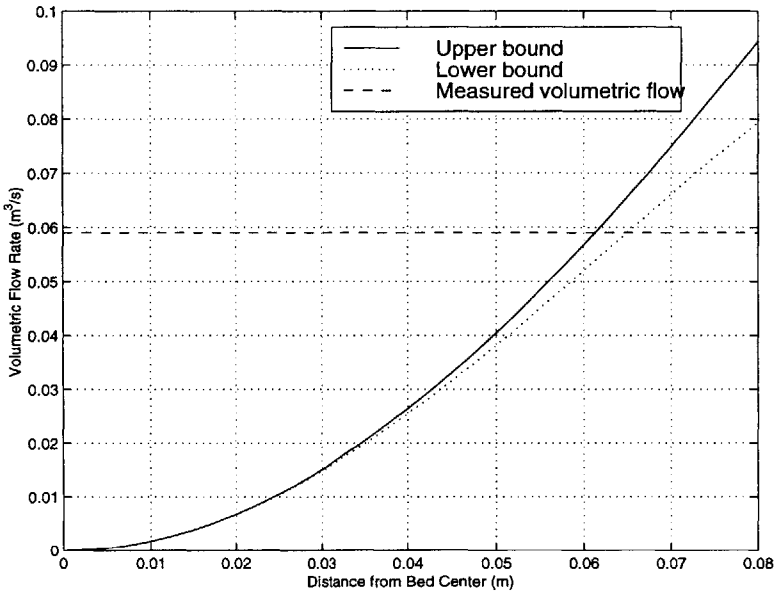

Figure 6-3: Air volumetric flow rate versus bed radius

the following correlation:

$$\delta = 0.05 D_e^{0.74}$$

Where δ is the particle boundary thickness and D_e is an effective diameter which in our case is the bed diameter ($160mm$). Substituting in gives a value of $\sim 13mm$ for the boundary layer of the bed used in these experiments. Figure (6-3) is clear evidence that there also exists a gas boundary layer. If the upper bound velocity profile is integrated from the bed center to a distance of $18.5mm$ from the wall, the true gas volume flow rate is reached. Likewise if the more realistic 3D velocity profile is integrated from the bed center to a distance of $15mm$ from the wall, the actual gas volume flow rate is achieved. These results indicate an upper bound for the gas boundary layer of $18.5mm$ with a more realistic estimate being $15mm$. This value is very close to the particle boundary layer ($13mm$). It is not surprising that the estimate for gas boundary layer is larger than the particle boundary layer as the wall clusters likely entrain a downward moving gas layer causing a net downward flow of gas inside the particle boundary layer.

6.3.1 Growth of Gas Boundary Layer with Solids Concentration

The gas velocity appears to be effected by the size of the gas boundary layer. The gas boundary layer is related to the particle boundary layer and the cross sectional solids concentration. Figure (6-4) illustrates this point. The mean gas velocity increases as the local cross sectional solids concentration increases while the volume flow rate of gas remains constant for the three different solids loadings. This suggests that the effective gas boundary layer increases with local cross sectional solids concentration causing the gas velocity in the bed core to increase.

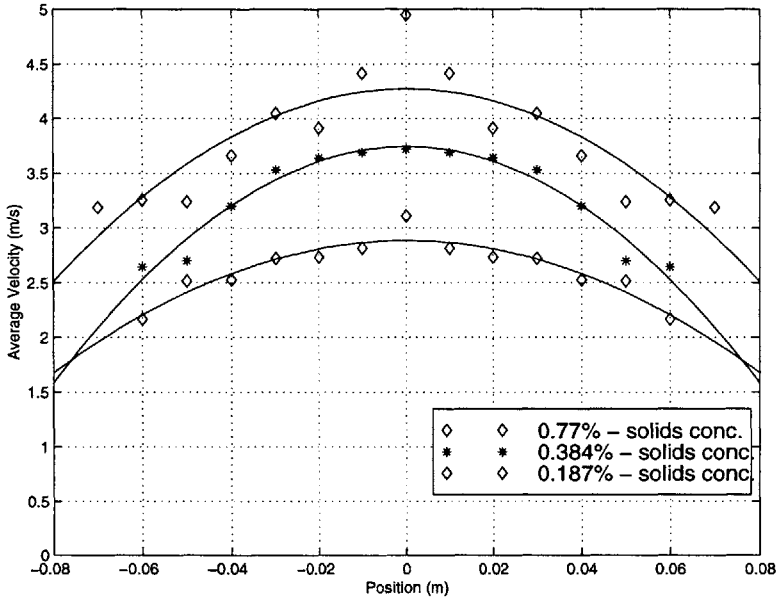

Figure 6-4: Mean air velocity versus riser diameter as a function of cross sectional solids concentration for a fixed air flow rate of $0.059 m^3/sec$

Another series of experiments were performed where the gas centerline velocity was measured as a function of the local cross sectional solids concentration. The results which are shown in figure (6-5).

For the particular bed there appears a definite relationship for a fixed volume flow rate between the centerline velocity and the local cross sectional solids concentration. The linear data curvefit $y = 2.79x + 2.55$, is a first order approximation. The measurement of solids concentrations by pressure transducers outside the

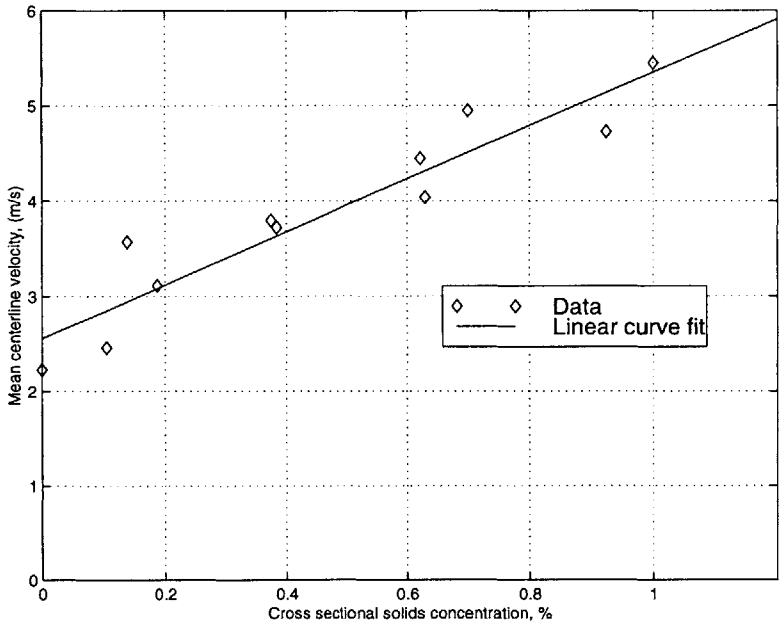

Figure 6-5: Cross sectional solids concentration versus mean centerline velocity for an air flow rate of $0.059 m^3/sec$

bed is an easier procedure than direct measurement of gas velocities inside the bed. These relationships may be exploited in the future to provide information on the gas flow using existing instrumentation. Additional work on different geometry risers is required to determine if a more universal relationship between gas velocity and solids concentration exists.

6.4 Summary

The unique two-phase flow structure found inside a circulating fluidized bed effects the gas velocity. Hot-wire measurements taken throughout the bed cross section yielded average velocities that are up to 100% higher than those taken during single phase flow. This is explained by the annulus layer which effectively causes a reduction in the cross section and higher gas velocities through a narrower region. The main conclusions can be summarized below:

- Using a shielded hot wire can produce accurate measurements for average gas

velocities in circulating fluidized beds

- The average gas velocity at the bed center can be over twice as high as the gas superficial velocity
- In addition to a particle boundary layer at the wall there is also a gas boundary layer
- The gas and particle boundary layer thickness are the same order of magnitude
- There appears to be a relationship between the mean gas centerline velocity and the local cross sectional solids concentration
- The presence of the solids in the fluidized bed causes a larger variation in gas velocity from the wall to the centerline than a single phase gas flow

Chapter 7

Single Cluster Experiments and Analysis

7.1 Introduction

The preceding two chapters dealt with the hot-wire experiments performed on the square cross section cold scale model circulating fluidized bed at MIT. When preliminary results were obtained considerable effort was expended in verifying that the results were accurate and not experimental error. For example, perhaps the vibration caused by the clusters impacting the hot wire support was causing the fluctuations. Initial simple experiments such as manually dropping clusters of particles onto the shield and vibrating the shield manually yielded results which suggested otherwise. However something more qualitative was needed to erase these doubts. It was decided therefore to construct an experiment that could accurately analyze the effect of one single cluster on the shielded hot wire probe. In addition to answering concerns over the experimental accuracy of the data from the preceding two chapters more information on the influence of clusters on the gas phase can be obtained by this approach. In particular it was hoped to obtain information on how the gas phase velocity fluctuated with the passing of a cluster. By simplifying the flow inside a large CFB, where there are many particles and clusters all interacting with each other, to a riser with just one single cluster useful information may be obtained. It was therefore

decided to analyze experimentally the air flow around a single cluster of particles. This chapter studies this phenomena.

7.2 Experimental Method

In order to achieve our stated goals a small experiment was set up. A 2m long riser with a 10cm diameter was used, see figure (7-1). Particle free air travels vertically upwards through the riser. The average velocity of the air is obtained from the air flow meters located in the supply lines.

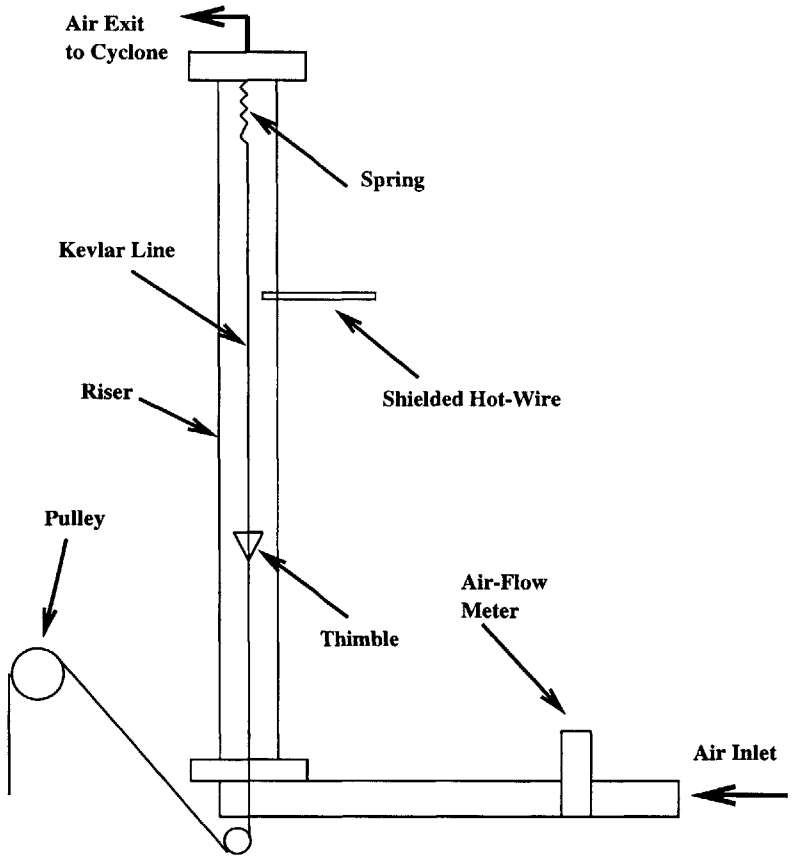

Figure 7-1: Schematic of single cluster experiment

A thimble was located at the riser centerline. It was attached to a spring at the top of the riser via a kevlar line. Kevlar was chosen because of its high strength. Single clusters were introduced to the riser by placing a quantity of particles inside

the thimble. The cluster was released by extending the kevlar line a certain distance and then releasing. At one end of the kevlar line a metal grip was attached which allowed the line to be easily extended. A meter stick was attached to the dexion support so the distance extended by the grip was known. A mechanical stop was located on the kevlar line. The grip is located at the stop when it is at rest. Upon release from extension the grip travels vertically before it impacts the stop. This also causes the thimble to stop abruptly and launches the cluster from the thimble into the riser. There is no exact definition of how big or small a cluster is supposed to be. The volume of the thimble was approximately $3cm^3$, which produced an adequately sized cluster. The ratio of the riser area to the thimble area is 25:1. This is small enough so that blockage effects caused by the thimble are negligible. The amount that the kevlar line was extended determined the initial velocity of the cluster. A larger extension produced a larger initial velocity.

A short distance above the cluster release point the shielded hot-wire anemometer probe was located. It was attached to the riser via a swagelok fitting. Initially the probe was positioned away from the centerline so that the particles did not impact it. This provided measurements of the instantaneous gas velocity as the cluster passed by. These results were compared to results when the probe was positioned at the centerline. In this situation the particles struck the probe. Figure (7-2) shows a cluster traveling vertically through the riser, the hot wire is located at the wall a short distance above the cluster.

During certain experiments the high speed video camera was also used to record images of the cluster as it passed by the anemometer probe. Information such as cluster velocity and whether or not the cluster struck the probe or not was gathered by slow motion analysis of the videos. In addition the high speed camera was used to calibrate our system, see section (7.2.1).

7.2.1 Calibration Procedure

The cluster tosser needs to be calibrated so that the initial velocity of the cluster as it exits the thimble is known. This allows the cluster to be launched at the same velocity as the gas superficial velocity. The thimble was filled with a $2cm^3$ volume of sand

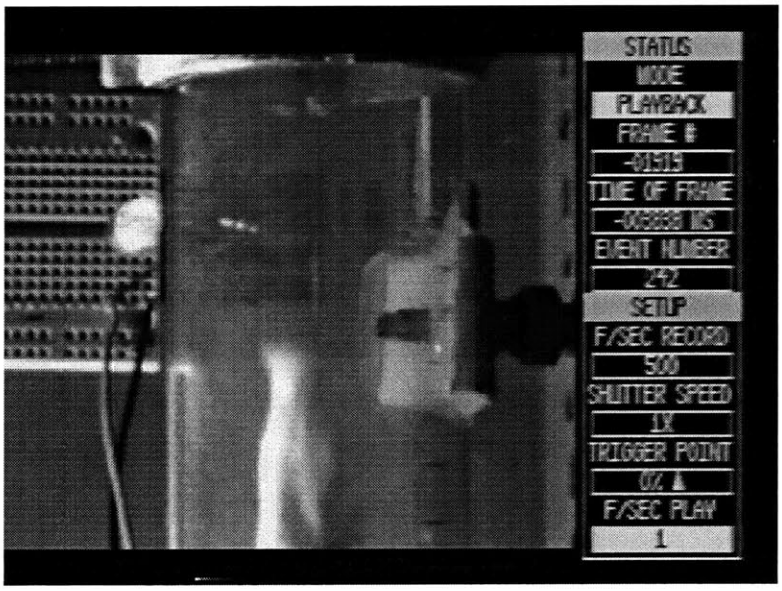

Figure 7-2: Cluster traveling towards shielded hot wire

particles. The cluster tosser was calibrated by correlating the distance the spring is stretched to the cluster release velocity. The velocity was determined by tracking the leading edge of the particles leaving the thimble with the high speed video system over a short $5cm$ distance when there is no gas flowing. For these short distances the distance-time relationship for the motion of a sphere is nearly linear. Therefore the velocity can be approximated as the distance traveled divided by the elapsed time. The elapsed time is determined from the video images. Figure (7-3) presents the calibration curve representing the spring extension versus the initial cluster velocity.

The curve in figure (7-3) can be used to allow the clusters to be launched at a velocity equal to the gas superficial velocity. The superficial velocities used were kept in the range between $2 - 3m/s$ as this is also the velocity range in the larger CFB. The shielded hot wire probe was located at a position $30cm$ above the thimble release point.

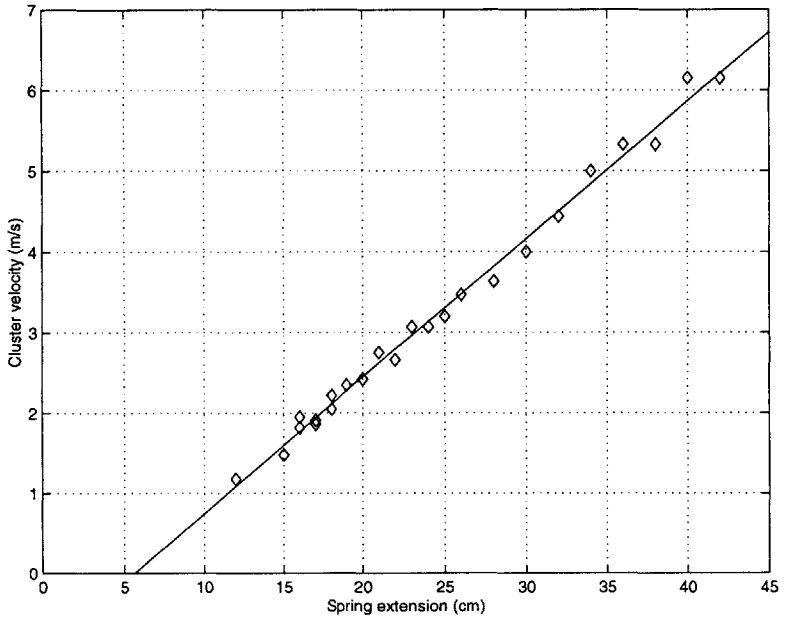

Figure 7-3: Spring extension versus initial cluster velocity

7.3 Results

Experiments were performed to see the effect a cluster has on the air flow surrounding itself. Points were sampled at a rate of $8192Hz$ for a time period between 8 seconds and 13 seconds. This allowed adequate time for the cluster and the wake to pass by the hot wire. Some representative graphs are shown in figures (7-4, 7-5, 7-6).

In figure (7-4) the hot-wire is located at the centerline of the riser facing the direction of the air flow. In figure (7-5) the hot wire is also oriented parallel to the air flow and is located $0.5cm$ from the wall edge so that the cluster which travels up the center of the riser does not strike the probe. In figure (7-6) the hot wire is oriented perpendicular to the air flow and is also located $0.5cm$ from the wall edge. Once again the cluster does not strike the probe at this position. The fact that the velocity deviates substantially from its mean value when the cluster does not strike the probe verifies the assumption that it is the air flow surrounding the cluster which is being measured in the CFB experiment and not some error due to clusters striking the shielded probe.

The air surrounding the cluster fluctuates substantially. In some cases it

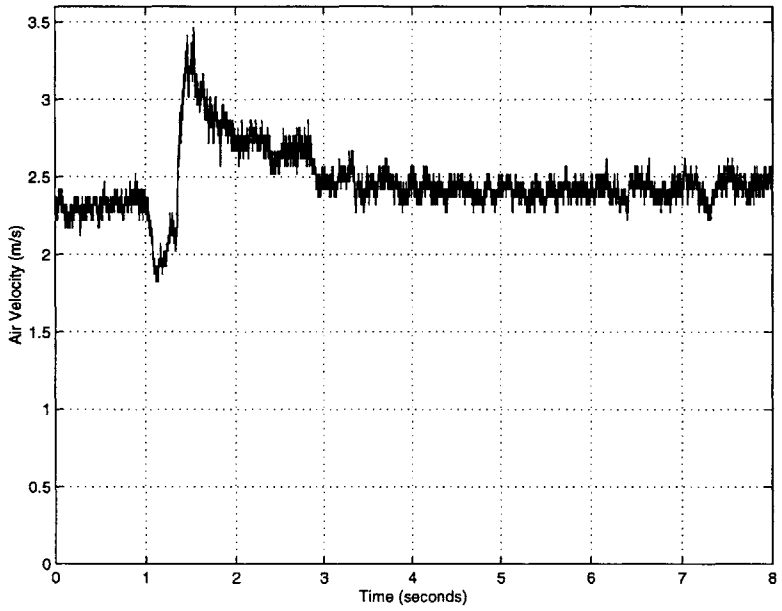

Figure 7-4: Air velocity versus time with the hot wire located at the center of the riser, see appendix C, table 2, test 1 for flow conditions

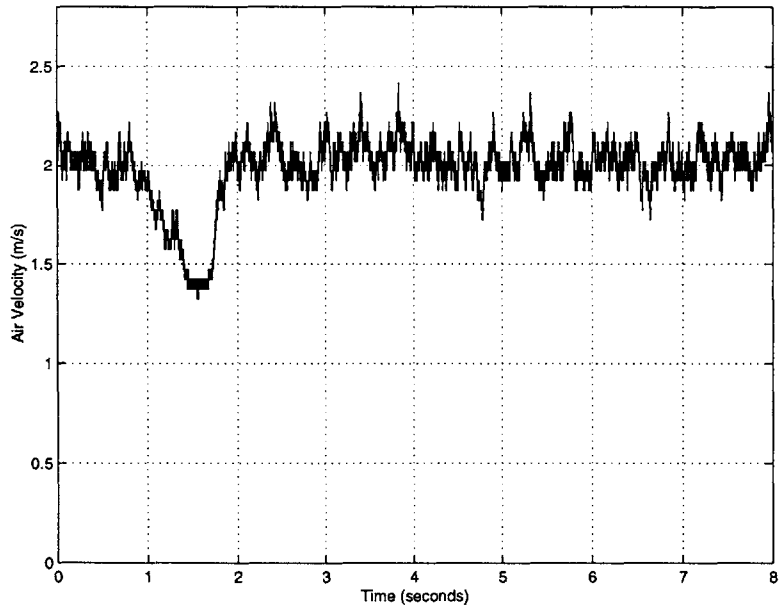

Figure 7-5: Air velocity versus time with the hot wire located at the riser wall, parallel to the flow direction, see appendix C, table 2, test 8 for flow conditions

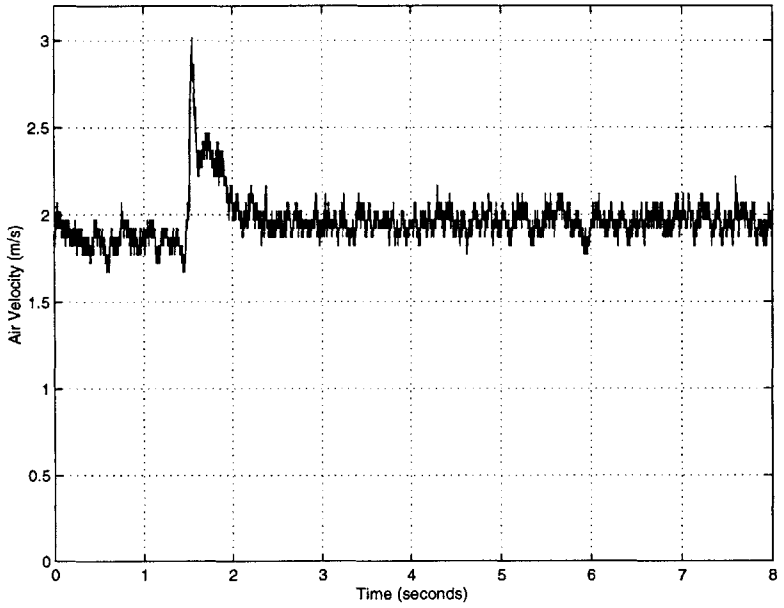

Figure 7-6: Air velocity versus time with the hot wire located at the wall of the riser perpendicular to the flow direction, see appendix C, table 2, test 21 for flow conditions

causes a "spike" in the velocity of approximately $1m/s$ while in figure (7-5) a reduction in air velocity of $0.6m/s$ is found. It is interesting to note that these fluctuations caused by single clusters are of similar order of magnitude to the fluctuations obtained from the larger bed as shown for example in figure (5-10). This gives further verification that the air fluctuations in the bed center are caused by clusters.

A series of experiments were performed with the shielded hotwire located at the center of the riser facing the air flow direction. Some of the results from these experiments are presented in figure (7-7). Sometimes an increase in velocity is observed, sometimes a decrease and sometimes a decrease followed by an increase is observed.

At the center of the riser the clusters always struck the shield. Another series of experiments were performed this time with the shielded hotwire located $0.5cm$ from the wall edge so that the clusters did not strike the shield. The direction of the probe was also facing into the flow. Results for these tests are presented in figure (7-8).

Other experiments were performed with the shielded hotwire located at $0.5cm$ from the wall but oriented 90° from the main flow direction, i.e. perpendicular

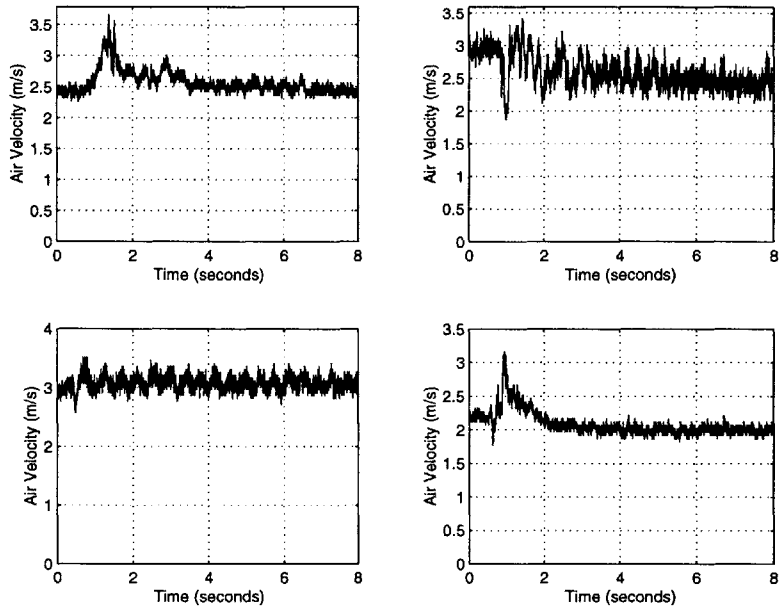

Figure 7-7: Air velocity versus time with the hot wire located at the center of the riser parallel to the flow direction (4 separate experiments), flow conditions in appendix C, table 2, clockwise from top left, test 3 test 11 test 18 test 2

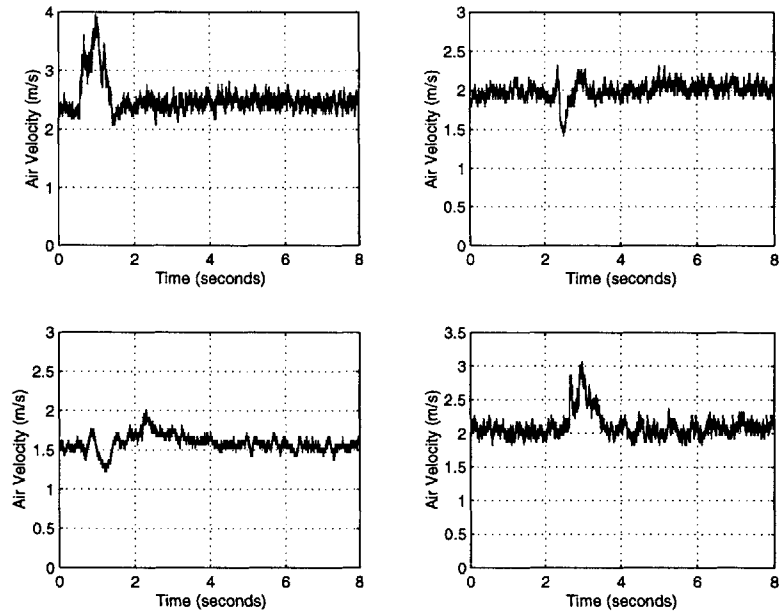

Figure 7-8: Air velocity versus time with the hot wire located at the riser wall, parallel to the flow direction (4 separate experiments), flow conditions in appendix C, table 2, clockwise from top left, test 19 test 12 test 9 test 7

to the direction in the above tests. Some results for these tests are presented in figure (7-9).

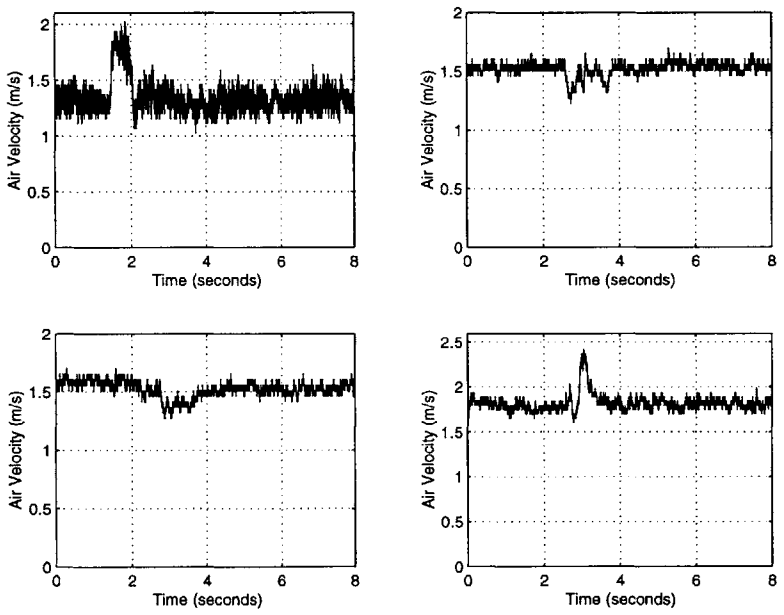

Figure 7-9: Air velocity versus time with the hot wire located at the riser wall, perpendicular to the flow direction (4 separate experiments), flow conditions in appendix C, table 2, clockwise from top left, test 23 test 13 test 15 test 16

As can be seen sometimes the cluster produces a positive "spike" in the velocity, sometimes a decrease in the velocity and sometimes a little bit of both. An interesting observation is that in the direction parallel to the airflow the positive increases in velocity are on the order of $1-1.5m/s$ while in the perpendicular direction they are on the order of $0.5-0.8m/s$. This could be because the wall has a dampening effect in that direction but it is still a significant fluctuation - capable of transporting particles to and from the wall. To better clarify this information tables (C.1, 7.2, 7.3) were compiled.

These tables show that the majority of experiments (approx $50-60\%$) caused a velocity peak in the data.

	Probe location: center Probe orientation: parallel	Mean fluc. (m/s)	STD (m/s)
% tests causing an increase in airflow	44%	1.06	0.12
% tests causing a decrease in airflow	28%	0.7	0.3
% tests causing both an increase and decrease	28%	1.45	0.05

Table 7.1: Effect of cluster on airflow with probe at center of riser, parallel to the air stream, sample size of 7 experiments

	Probe location: riser wall Probe orientation: parallel	Mean fluc. (m/s)	STD (m/s)
% tests causing an increase in airflow	62%	1.04	0.35
% tests causing a decrease in airflow	25%	0.75	0.05
% tests causing both an increase and decrease	13%	0.7	n/a

Table 7.2: Effect of cluster on airflow with probe at riser wall, parallel to the air stream, sample size of 8 experiments

	Probe location: riser wall Probe orientation: perpendicular	Mean fluc. (m/s)	STD (m/s)
% tests causing an increase in airflow	66%	0.725	0.22
% tests causing a decrease in airflow	17%	0.3	n/a
% tests causing both an increase and decrease	17%	0.9	0.1

Table 7.3: Effect of cluster on airflow with probe at riser wall, perpendicular to the air stream, sample size of 9 experiments

7.3.1 High speed video experiments

In order to view the cluster in slow motion as it passes by the hot wire probe the following experimental procedure was performed. The high speed video camera described in chapter 4 was used to record images of the cluster as it traveled through the riser. An led was connected to the data acquisition system. At the instant the data acquisition began recording voltage signals from the hot-wire it applied a voltage to the hot-wire. The exact time this occurred was obtained through the digital clock on the digital camera. Therefore the cluster motion could be correlated with the instantaneous air velocity. The first observation was that when the hot-wire was located at the wall of the riser the cluster did not make contact with it. This is important as the air velocity obtained without cluster contact was equal in magnitude to the air velocity with cluster contact. In the large CFB the impact of clusters on the probe should not effect the results. Although the velocity fluctuation began before the cluster reached the probe, the fluctuation continued to increase/decrease after the cluster had passed. This can also be demonstrated using some rough numbers. The length of each cluster was approximately $15cm$, the average velocity was $1.5m/s$ giving a cluster time scale of:

$$t_{cluster} \approx \frac{L_{cluster}}{V_{cluster}} \approx 0.1 \tag{7.1}$$

The time scales for the velocity fluctuations was 0.5 seconds to 1.0 seconds meaning that there was still considerable activity after the cluster had passed. The assumption was verified with the high speed camera. A region behind each cluster consisting of dilute particle concentration was observed. Substantial variation in velocity occurred in this region. More experiments, where the mechanism for releasing clusters is varied and a larger diameter riser is used so that larger clusters can be released, are needed to further quantify this effect.

7.3.2 Discussion on experiments

Every cluster was found to have a marked effect on the air velocity. Roughly more than half the time it caused the instantaneous air velocity to peak at a value up to 50% higher than the average air velocity. This corresponded to an actual increase of between $0.5m/s$ and $1.2m/s$. At other times it caused the instantaneous air velocity to decrease by a smaller factor. Occasionally (18%)both a reduction and an increase in velocity were observed. The instantaneous air velocity was always affected in some way, it never remained unchanged. This behavior suggests that a cluster of particles behaves in certain ways like a solid body. As the air flows around such a body vortices are probably formed in front of the body while a sizeable wake region exists behind the body. The vortex/wake structures are the likely cause of the velocity fluctuations. Further research is required to quantify these effects thoroughly. Numerical studies will be used to try to quantify these effects.

7.4 Numerical Modeling

To arrive at a more complete understanding of the experimental observations, a numerical model was built. Isolating a single cluster as the object to be analyzed, there is flow past it and flow through it. The most effective way of incorporating all those effects in the analysis is to employ a computational model. The results from this can be used to examine the velocity flow field around a cluster and determine if the observed fluctuations are correct. This section of the thesis is structured as follows: the computational model and methods are described, the computational model is

validated for flow past a solid cylinder, the model is used to determine the effect of permeability and porosity on the flow field around a cluster.

7.4.1 CFD Model

A commercially available program for computational fluid dynamics was used in this study. The CFD program is Adina-F, version 7.4, produced by ADINA R&D Inc. Adina-F is a finite element analysis program that allows fluid flow problems to be solved. The system includes the pre-processor Adina-in, the fluid flow program Adina-F and the post processor Adina-plot. The finite element model is defined in Adina-in, analyzed in Adina-F and the results displayed in Adina-plot. It employs finite element methods for the solution of the governing equations for fluid dynamics and the output is the pressure and velocity fields on the user specified discrete computational domain. Internal to Adina is some built in functions that allows for the effects of heat transfer or permeability to be accounted for. The use of these is discussed later. Appendix D contains an Adina input file for one of the simulations.

7.4.2 Computational Domain

For simplicity, the cluster is modeled as a round two dimensional cylinder. Although results from this will not match exactly the results obtained from clusters inside a CFB, the results will indicate the general velocity field and fluctuation levels. Turbulence modeling was not used because of software limitations. Figure (7-10) gives the computational domain defined for this problem. In this figure the air flows around a 2cm solid cylinder. The upper, lower and left hand outer surfaces were given an constant velocity which served as the boundary conditions for the flow. In later simulations a porous fluid will be used to model the cluster and those velocity fields shall be compared to the solid cylinder case.

The domain itself was discretized in two distinct regions. The inner region, occupies approximately 3 cylinder diameters and is divided into 40 evenly spaced circumferential divisions. It also has evenly spaced radial divisions. This means that the closer one is to the cylinder the finer the mesh. This design allows for higher

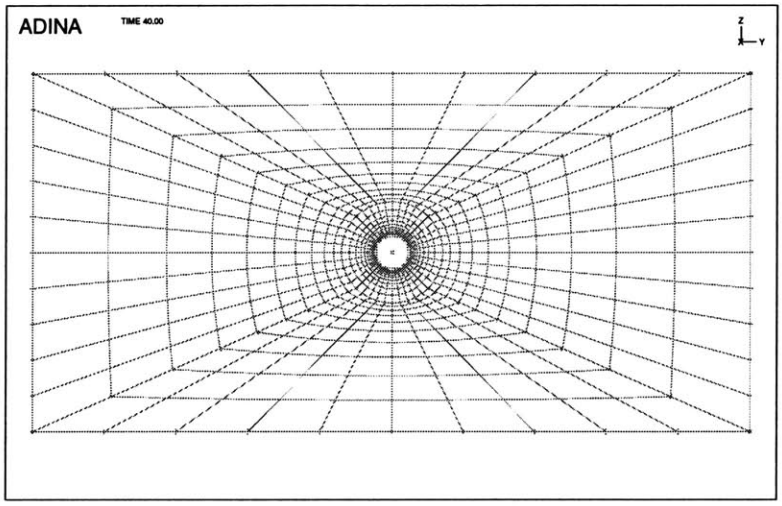

Figure 7-10: Finite element mesh for air flow around a solid cylinder

accuracy in the region close to the cylinder while not compromising solution speed by allowing the mesh to become more coarse away from the cylinder. The outer region occupies 20 cylinder diameters and the mesh is subdivided in a similar manner to the inner region. This allows for continuity. The cylinder itself is modeled as a no slip rigid boundary. We are not interested in the stress distribution throughout the cylinder so it does not need to be meshed.

When a porous body, which models a cluster, replaces the solid cylinder in later simulations this will need to be meshed as the velocity distribution throughout the cluster needs to be obtained. In reality the cluster would deform and change shape which will have an effect on the wake region but to a first approximation the cluster is modeled as a cylinder. This porous body had its porosity and permeability specified. Clusters in fluidized beds have been measured to have porosity levels of about 70% to 85%, Lints and Glicksman [33]. The porosity (or volumetric void fraction), ε, can be related to the permeability, κ, by the Carmen-Kozeny relation, Scheidegger [50].

$$\kappa = \frac{1}{180} \frac{\varepsilon^2 d_p^2}{(1-\varepsilon)^2} \tag{7.2}$$

where d_p is the diameter of the particles in the fluidized bed. In our case the mean diameter is 164 microns, which is the value that was always used in equation (7.2). This relationship between porosity and permeability is best expressed in

graphical form.

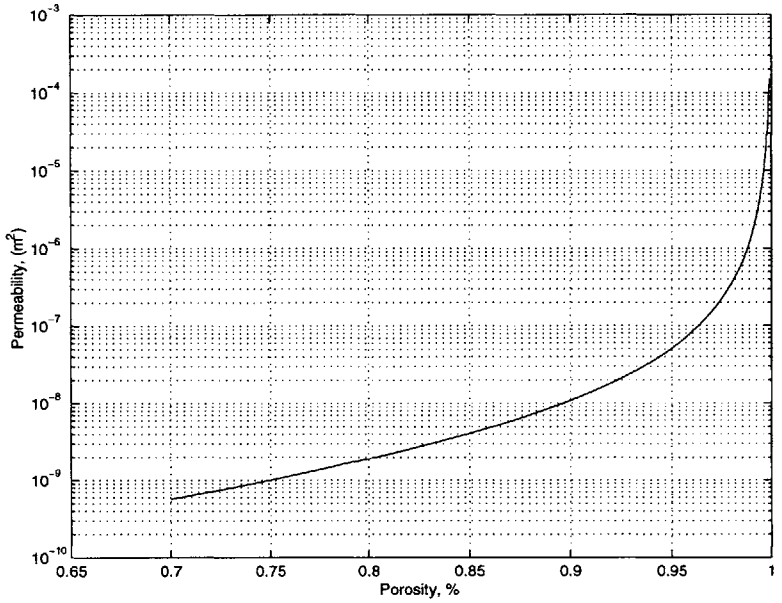

Figure 7-11: Porosity versus permeability for 164 micron particles

It is worth noting the small value of the permeability ($\sim 10^{-7}m^2$) when the porosity is relatively high $\sim$ 95%. As the pressure drop across the cluster can be related to the free stream velocity a small value of permeability indicates that the velocity through the cluster is small compared to the air free stream velocity. There will be further discussion on this later.

The porous body which models a cluster is given a specified porosity and permeability. It is meshed following a similar technique described above using 40 evenly spaced circumferential divisions. The mesh is shown in figure (7-12).

7.4.3 Governing equations and boundary conditions

Throughout the cluster mass conservation and Darcys law for flow in a permeable body are applied in order to solve for the pressure and velocity fields. The mass conservation equation for two dimensional incompressible flow is given by the following expression, e.g. White [64].

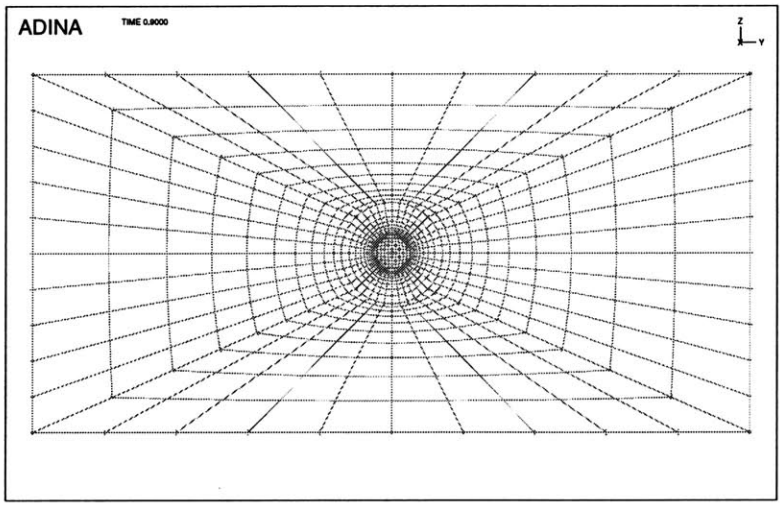

Figure 7-12: Finite element mesh for air flow around a cluster

$$\vec{\nabla} \cdot \vec{v} = 0 \tag{7.3}$$

and the conservation of momentum is expressed in D'Arcys law, e.g. Scheidegger [50]

$$\vec{\nabla} P = \frac{\mu \vec{v}}{\kappa} \tag{7.4}$$

In the region outside the cluster, mass conservation is applied while the two dimensional, incompressible form of the Navier-Stokes equation is used to solve for the momentum of the fluid flow.

$$\vec{v} \cdot \nabla \vec{v} = -\vec{\nabla} P + \mu \nabla^2 \vec{v} \tag{7.5}$$

The solutions for the pressure and velocities are matched at the interface of the two regions. An initial pressure of zero is specified throughout the entire domain. A velocity field is applied at the left most surface of the mesh which causes a velocity to flow over the cluster, see figure (7-16) for a plot of the velocity vectors. The cluster is kept fixed at the center so the velocity corresponds to the relative velocity between the cluster and the air.

7.4.4 Validation of CFD model

In order to establish a benchmark for all of the computational results, the drag for a solid cylinder in unbounded flow is considered first. Figure (7-13) presents the computational results for drag coefficient,c_d, versus Reynolds number. The drag coefficient is given by:

$$c_d = \frac{F_y}{\frac{1}{2}\rho u^2 D} \tag{7.6}$$

where F_y is the drag force acting in the direction of fluid flow, u is the free stream velocity, D is the cylinder diameter. The output is compared to a wide body of empirical data for this flow configuration. The figure shows that the computational model is accurate within about 10% near Re=1000 which is the range of interest. To gauge the integrity of the computational model further, figure (7-14) presents the computational results for the angle of flow separation from the cylinder versus Reynolds number, where the separation angle is measured from the nose to the leading separation point. Excellent agreement is seen between the computational and empirical results.

To further demonstrate the accuracy of the model the pressure distribution around the cluster was examined. It should be continuous if the model is physically accurate. The shear stress in the air at the surface of the cluster should match the shear stress in the cluster. Taking the pressure distribution after a time period of 9 seconds yields the results shown in figure (7-15). The pressure is continuous at the boundary providing further confidence in the model.

7.4.5 Results

Both models predict a steady wake behind the cylinder/cluster for all Reynolds numbers. This is not physically accurate as random noise and perturbations in experimental situations produce an unsteady wake behind bluff bodies for Reynolds numbers greater than 50. In order to produce an unsteady wake a perturbation to the flow must be introduced early in the flow. This perturbation can take the form of a slight

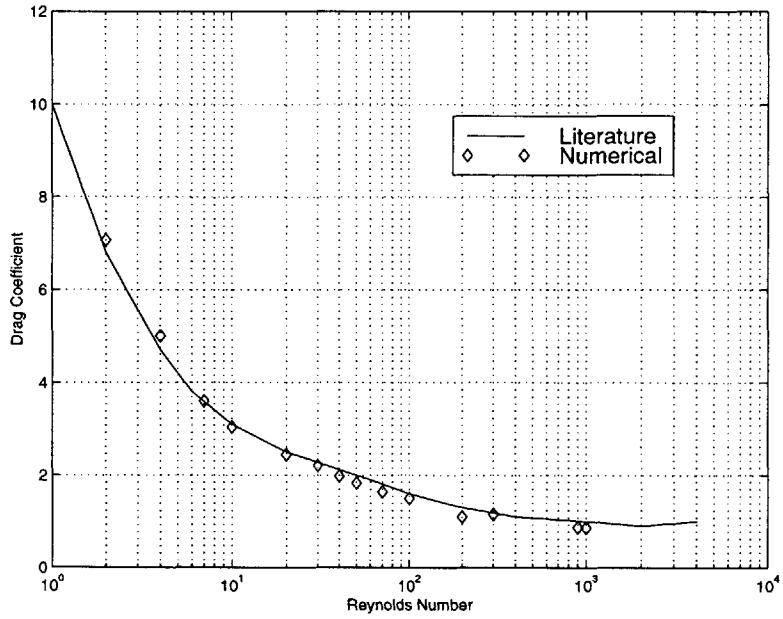

Figure 7-13: Drag coefficient on a solid cylinder, computed vs. empirical, for literature reference see H.Schlichting [51]

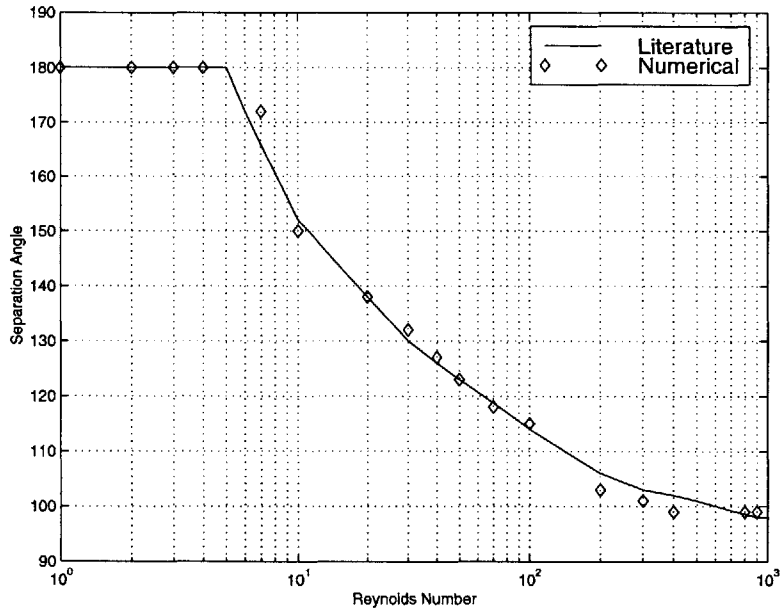

Figure 7-14: Separation angle for flow past a solid cylinder, computed vs. empirical, for literature reference see H.Schlichting [51]

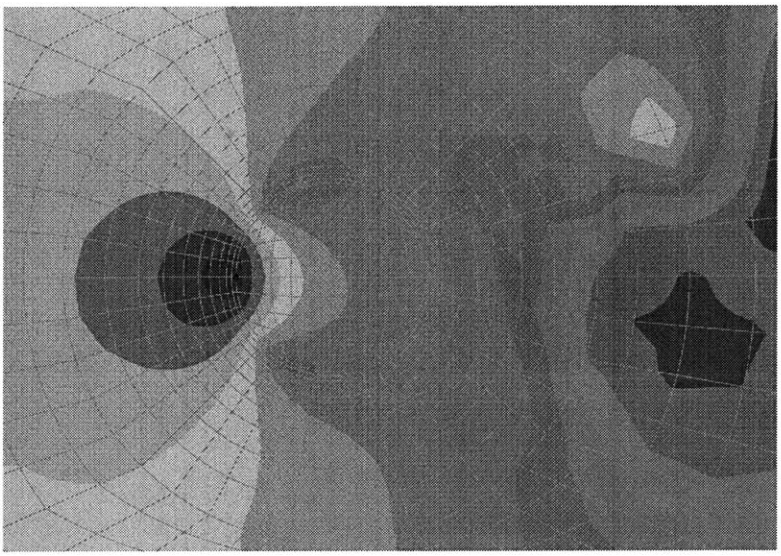

Figure 7-15: Pressure distribution around cluster for a Reynolds number of 1000, porosity of 75%

oscillation of the cylinder/cluster or a small disturbance applied to the velocity field, see appendix D for the simulation program.

The velocity field at an instant in time behind the cylinder is shown in figure (7-16), for a Reynolds number of 1000. Figure (7-17) shows the velocity field around a cluster with a Reynolds number of 1000 and a porosity level of 75%. The free stream velocity in both cases was 0.783m/s. As can be seen both sets of velocity profiles are very similar, indicating that at a porosity level of 75% the flow around a cluster is similar to the flow around a solid.

Figure (7-18) and figure (7-19) show a more close up view of the velocity profiles behind a solid cylinder and a cluster with a 75% porosity level. The profiles correspond to a time of 0.9 seconds after the flow begins. There is very little, if any, difference between the two flow structures.

7.4.6 Velocity through cluster

Central to the assumption that the porous cluster has an equivalent velocity field to a solid cylinder is the fact that the velocity flowing through the cluster is negligible.

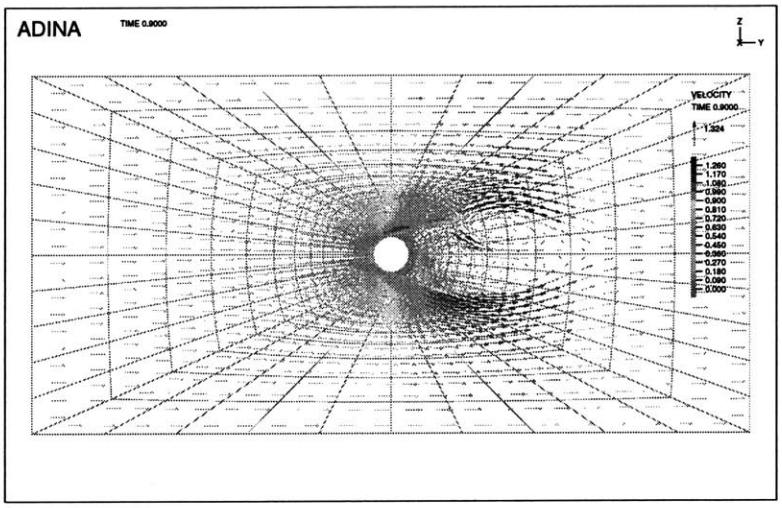

Figure 7-16: Velocity field around a solid cylinder for Re=1000

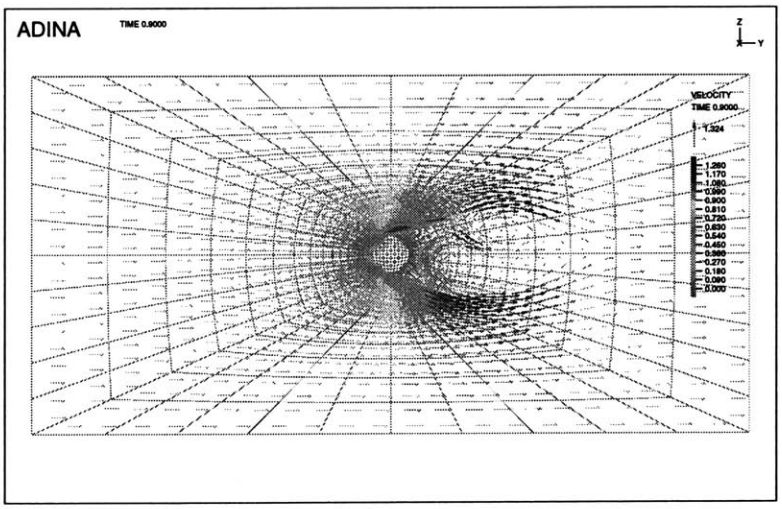

Figure 7-17: Velocity field around a porous media, with a porosity of 75% and Re=1000

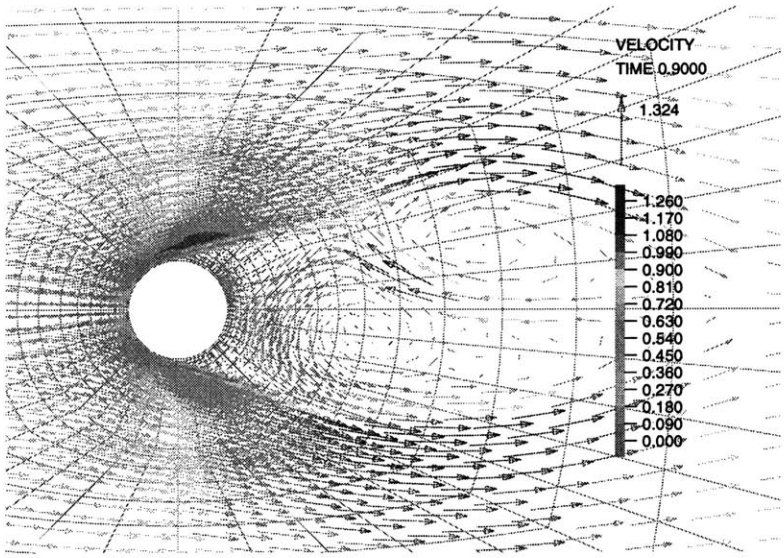

Figure 7-18: Close up of velocity field around a solid cylinder for Re=1000

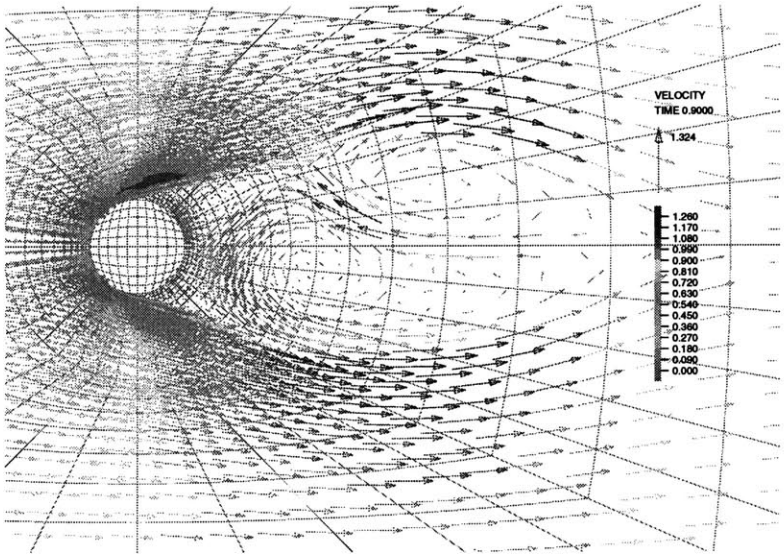

Figure 7-19: Close up of velocity field around a porous media, with a porosity of 75% and Re=1000

The numerical simulations can yield the velocity through the cluster but before such data is presented it is prudent to perform a rough calculation to obtain a 'back of the envelope' estimate beforehand. Using the following version of Darcy's Law:

$$\nabla P_l = \frac{\mu_l L_{eff} V_{cl}}{\kappa} \tag{7.7}$$

where L_{eff} is the effective length of the porous medium, in the case it is the radius of the cluster $1cm$, $\kappa(m^2)$ is the permeability which for a porosity of 75% is given by equation (7.2), for a particle diameter of $164\mu m$, to be $1.01x10^{-9}m^2$, μ_l is the viscosity of the air, V_{cl} is the velocity through the porous medium and V_∞^2 is the free stream velocity, $0.783m/s$ for a Reynolds number of 1000. Modeling the pressure drop from the free stream stream to the stagnation point using Bernoulli gives:

$$\frac{1}{2}\rho_l V_\infty^2 = \frac{(18.43x10^{-6})(0.01)V_{cl}}{1.01x10^{-9}} \tag{7.8}$$

This gives an approximate value for the velocity through the cluster as:

$$V_{cl} \approx 0.002m/s \tag{7.9}$$

Using the numerical simulations for an equivalent porosity level and Reynolds number yields a velocity through the cluster of $0.004m/s$. This is similar order of magnitude to our back of the envelope solution above which lends credibility to these results. Figure (7-20) shows a plot of the velocity through the cluster as a function of porosity. It is plotted for two separate Reynolds numbers (1000 and 100) based on cluster diameter. These Reynolds numbers correspond to free stream velocities of 0.783m/s and 0.0783m/s respectively.

For a Reynolds number of 1000 and a relatively high porosity level of 90% the velocity through the cluster is only $0.05m/s$ which is still an order of magnitude less that the oncoming free stream velocity. As the Reynolds number increases the velocity through the cluster increases also. Perhaps after a certain critical velocity is reached the throughput causes the breakup of the cluster. However this important effect is not possible to model using the software presently available.

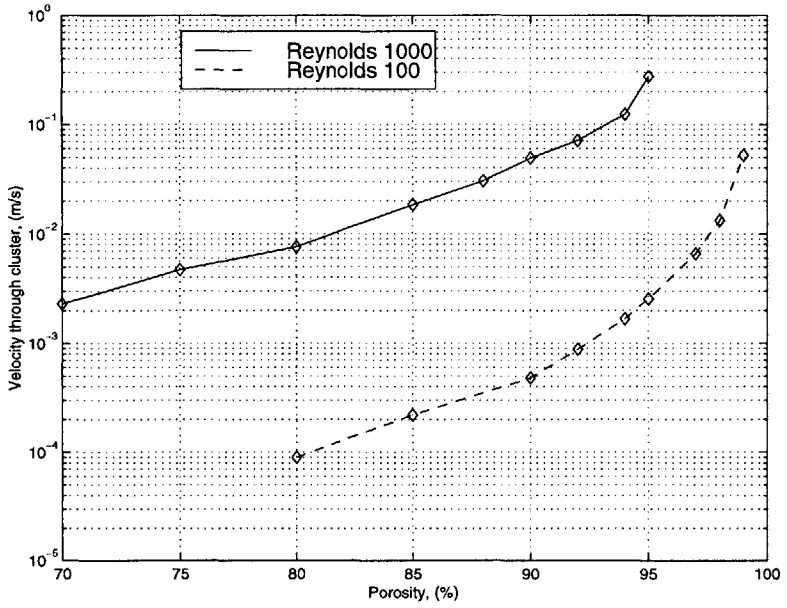

Figure 7-20: Air velocity through cluster versus porosity, for two separate Reynolds numbers

7.4.7 Velocity around cluster

The next question to be answered is how do the simulations compare with the single cluster experiments. The velocity along the centerline of the figure (figure (7-21)), one diameter above the centerline (figure (7-22)), two diameters above the centerline (figure (7-23)). The velocity in all figures is the absolute velocity of air. For a Reynolds number of 1000 the relative velocity between the cluster and the air was $0.783m/s$, the velocity of the cluster was $1.5m/s$ which is the average cluster velocity measured using the high speed video camera used in the single cluster experiments. The gives an absolute free stream air velocity of $2.283m/s$ which roughly corresponds to the air velocity in the experiments.

Figure (7-21) shows a decrease in the air velocity along the centerline of approximately $1.9m/s$. The average drop from our experiments was $0.5m/s$. The are several explanations for this apparent discrepancy between the simulations and experiment. First of all the simulations are all two dimensional. This leads to a vortex structure in front of the cluster which produces a decrease in the velocity. This decrease along the centerline is not always observed experimentally. In fact, along

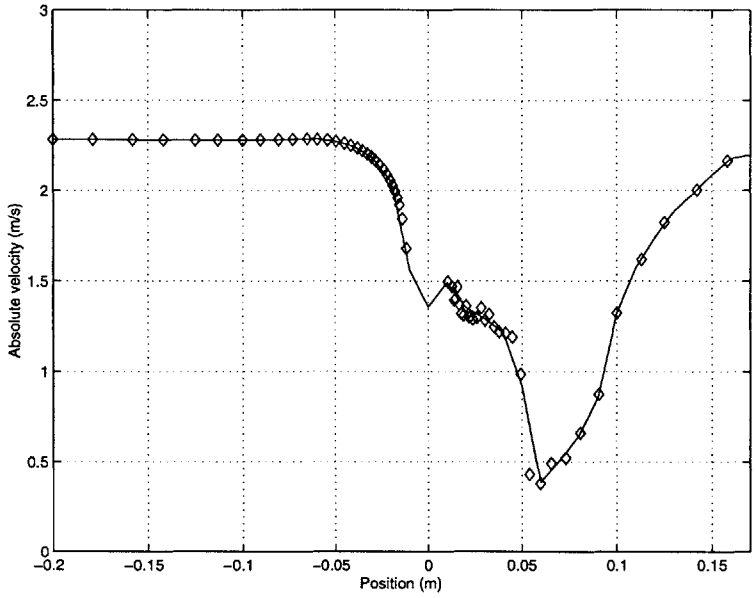

Figure 7-21: Numerical simulation of actual air velocity, 20cm upstream and downstream from cluster centerline, for Re=1000, porosity=75%

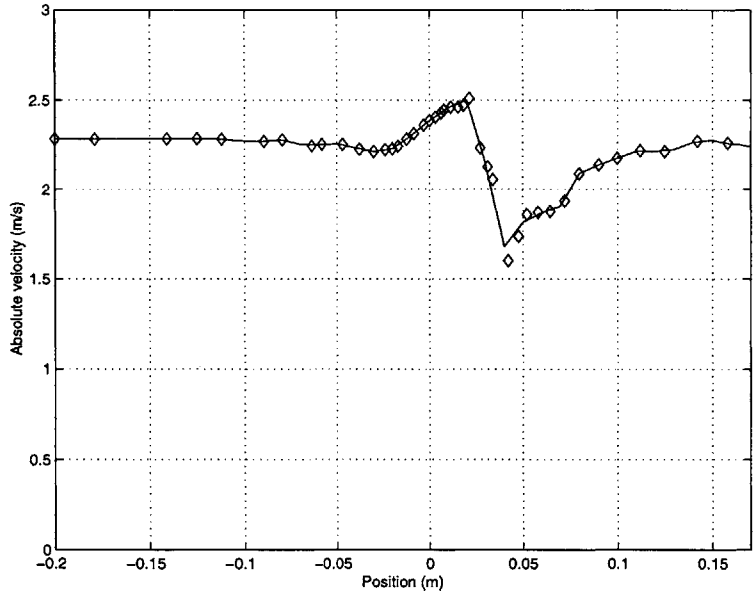

Figure 7-22: Numerical simulation of actual air velocity, 20cm upstream and downstream from a location 1 diameter away from cluster centerline, for Re=1000, porosity=75%

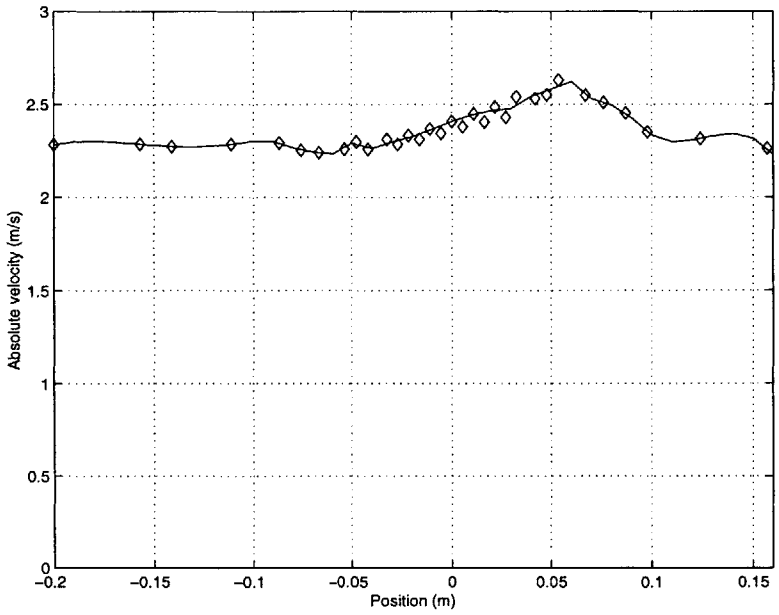

Figure 7-23: Numerical simulation of actual air velocity, 20cm upstream and downstream from a location 2 diameters away from cluster centerline, for Re=1000, porosity=75%

the centerline a decrease in velocity was observed only 40% of the time. A three dimensional simulation would provide more information because the vortices would shed in three dimensions and so produce a velocity pattern along the centerline that may be more indicative of our experiments. Another factor is that in the experiments the cluster broke over the hot-wire when it was located at the centerline which could have affected results.

Figure (7-22) shows both a decrease of $0.6m/s$ followed by a velocity increase of $0.2m/s$. This velocity decrease is comparable with the experimental results however the velocity increase is smaller than anticipated. Indeed the increase in velocity varied from $0.5m/s$ to $1.0m/s$ experimentally. However, due to the unsteady nature of the flow, if the velocity distribution is taken at a different instant of time but at the exact same location a profile such as that in figure (7-24) is obtained.

In figure (7-24) a velocity increase of $0.5m/s$ is detected with no decrease in the velocity. This indicates that the velocity profile is a function of position and because of the unsteady nature - time. This increase is comparable with experimen-

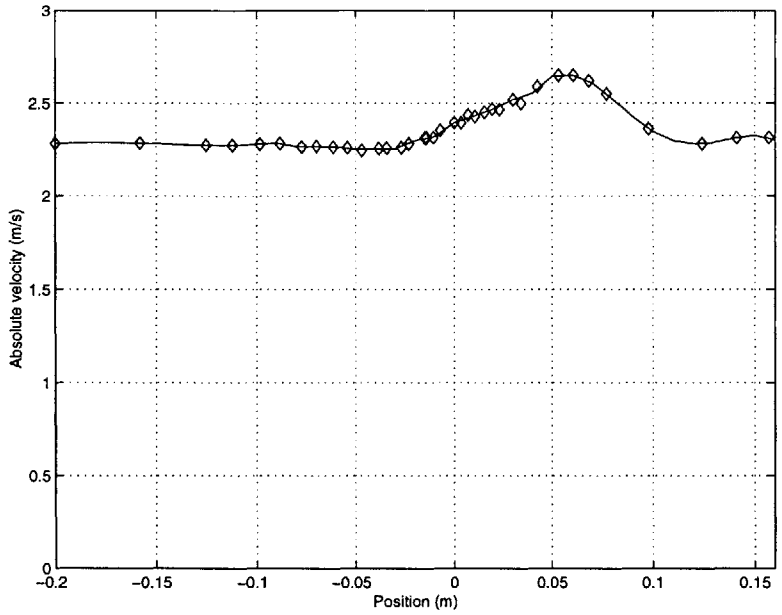

Figure 7-24: Actual air velocity, 20cm upstream and downstream from a location 1 diameter away from cluster centerline, for Re=1000, porosity=70%

tal data. Larger fluctuations would be produced by increasing the relative velocity between the cluster and the air but by doing so increases the computational time considerably.

Further away from the cluster, the fluctuations are less extreme as can be seen in figure (7-23). Here a velocity increase of approximately $0.4m/s$ is detected which compares well with some of the experiments but once again perhaps a larger relative velocity between the cluster and air in the simulation would produce larger fluctuations. Further away again very little disturbance is observed on the air. At a distance of 3 diameters from the cluster an increase in velocity of $0.2m/s$ is observed with a barely noticeable fluctuation observable 4 diameters away.

7.4.8 Numerical versus Experimental

The fluctuation level obtained during the numerical can be compared with the fluctuation level obtained in the large bed. Figure (7-25) shows the comparison between the experimental result over a quarter of a second time period using data from figure (5-9)

versus a numerical simulation with a Reynolds number of 2000 and a distance of 1 diameter away from the cluster centerline.

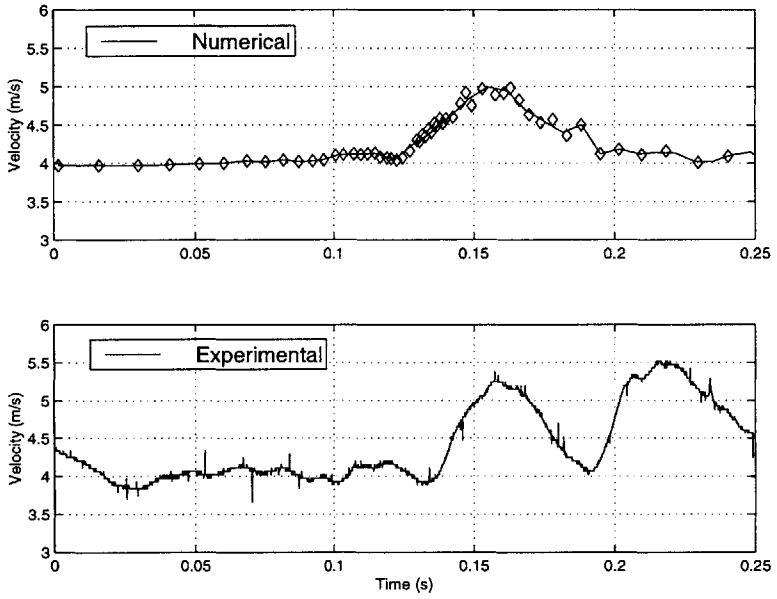

Figure 7-25: Numerical simulation versus experimental data

As can be seen from figure (7-25) the magnitude of the fluctuations are remarkably similar indicating that a Reynolds number of 2000 may be the most accurate. Incidentally using a cluster size of 2cm and a relative velocity between the cluster and the air of 1.5m/s, which is the terminal velocity of an individual particle, gives a theoretical result of a Reynolds number very close to this result. Also the time scale of the fluctuations are of the same order as the experimental data, $\sim 0.05 seconds$. The fluctuation levels of the single cluster experiments are similar to both of these results however the time scale is much larger, $\sim 0.5 seconds$. The cause for this discrepancy is presently not understood.

7.4.9 Discussion

There are limitations with the model. The limitations associated with its two dimensionality have already been discussed. The model takes a porous medium as the equivalent of a cluster. The porous medium maintains its mechanical structure through the simulations. Therefore cluster breakup and particle shedding behind the

cluster are not simulated. This is a problem as the single cluster experiments indicate that a large velocity fluctuation occurs behind the cluster where there is dilute particle flow in this wake region. There is not presently a commercially available software package that can simulate this breakup/shedding phenomena although there are several groups worldwide (e.g. Y.Tsuji et al., J.Sinclair et al.) working on performing this and other related simulations. There is also the assumption that the cluster is shaped as a circular object. This is a good basis for the start of the simulations but it certainly is an approximation. Clusters have been observed as being either 'arch-shaped', Lim et al. [31], or being shaped like a 'paraboloid', Horio and Kuroki [24].

These limitations not withstanding the model does provide useful insight into the mechanism behind the large scale velocity fluctuations observed in the CFB. The first lesson is that the velocity of air that flows through a cluster is negligible throughout the porosity range of interest, 70% - 90%. Above this range the velocity through the cluster becomes more significant and could possibly be a mechanism which causes cluster breakup. If the vast majority of air flow travels around a cluster then this is further evidence that the length scale of the cluster needs to be considered for velocity fluctuations inside a CFB instead of the particle length scale.

The magnitude of the velocity fluctuations is similar to the experimental data. Depending on the position and time velocity measurements are made sometimes an increase in velocity is detected, sometimes a decrease and sometimes both an increase and decrease is observed. When the position where the air velocity is measured is chosen randomly then the fraction of time a pure velocity increase is detected is approximately 62% for the simulations. This corresponds well with the fraction of time a pure increase was experimentally observed - 59%. Although for the experiments this fraction appeared independent of position which is not the case for these two dimensional simulations.

The simulations involving a solid cylinder produced a similar velocity field as the simulations around a 75% porous medium. Therefore to conclude, the simulations although simplified in nature, produce evidence to suggest that the cluster can be treated as a solid, having the same shape, when it comes to identifying the flow field surrounding the cluster. The relative air velocity over the cluster and the ensuing

flow disturbance appear to be the same as the fluctuations obtained in the circulating bed.

Chapter 8

Future developments and conclusions

8.1 Future developments

There are two potentially interesting lines of enquiry that may evolve directly from the work presented here. The first involves the capability of measuring mean gas velocities inside a CFB and the second involves measuring mean cluster length scales inside a CFB. The capability to measure the pressure along the riser is usually present in circulating fluidized beds. These pressure measurements are used to obtain local cross sectional solids concentrations. Presently there is only one facility that can measure mean gas velocities - that is the facility here at MIT. Likewise there is only one facility with the capability of measuring mean cluster length scales - that is the research group at Lehigh University. They use a dual sensor capacitance probe to obtain simultaneous measurements of solid concentrations in two small sensing volumes [54]. It may be possible to estimate both the mean centerline velocity and mean cluster size from pressure measurements taken outside the bed.

8.1.1 Mean centerline velocities

In our CFB as described in section 3.1 there appears a definite linear relationship between the mean centerline velocity and the local cross sectional solids concentration, (see figure (6-5) for example). This means that a linear relationship exists between the mean centerline velocity and the mean pressure measurements. The solids concentration increases causing an increase in the gas boundary layer which forces the air to flow through a smaller area, thus raising its centerline velocity. If a model could be developed which accounted for this effect for a variety of riser geometries then by simply measuring the outside pressure an estimate of the centerline velocity could be made .

8.1.2 Mean cluster size

Estimating the mean cluster size from outside measurements is another exciting prospect. This requires more fundamental work but the potential benefits are substantial. If an assumption is made, that the peak or dominant frequency in the velocity spectrum is related in some way to the dominant frequency that vortices are shed in front of a cluster then interesting conclusions can result. For a start the peak frequency from the velocity spectrum (see figure (8-1)) is the same as the peak frequency from the pressure spectrum (see figure (8-2)). In both cases the peak frequency is $\approx 2Hz$. This result should not be too surprising as pressure fluctuations can produce velocity fluctuations. If this peak frequency is related to the shedding frequency in front of a average cluster then the Strouhal number (see figure (8-3)) can be used to estimate mean cluster size.

Above a Reynolds number of 1000 the Strouhal number is fairly constant at 0.2 as can be seen from figure (8-3). Assuming that the relative velocity between the airflow and the cluster produces a Reynolds number of this magnitude then the following equation can be used to estimate the cluster length scale:

$$\frac{fL_{cluster}}{V_{rel}} = 0.2 \tag{8.1}$$

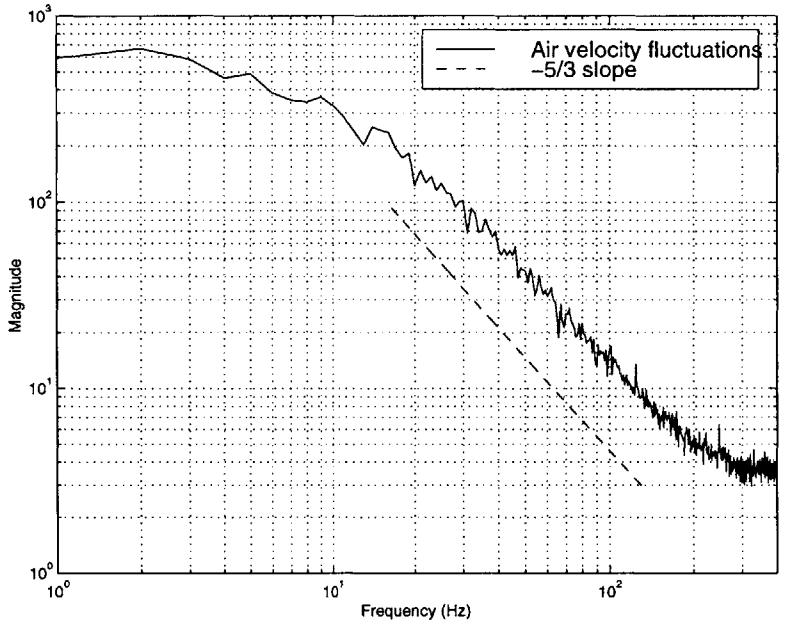

Figure 8-1: Fourier transform of fluctuating velocity measurements in CFB

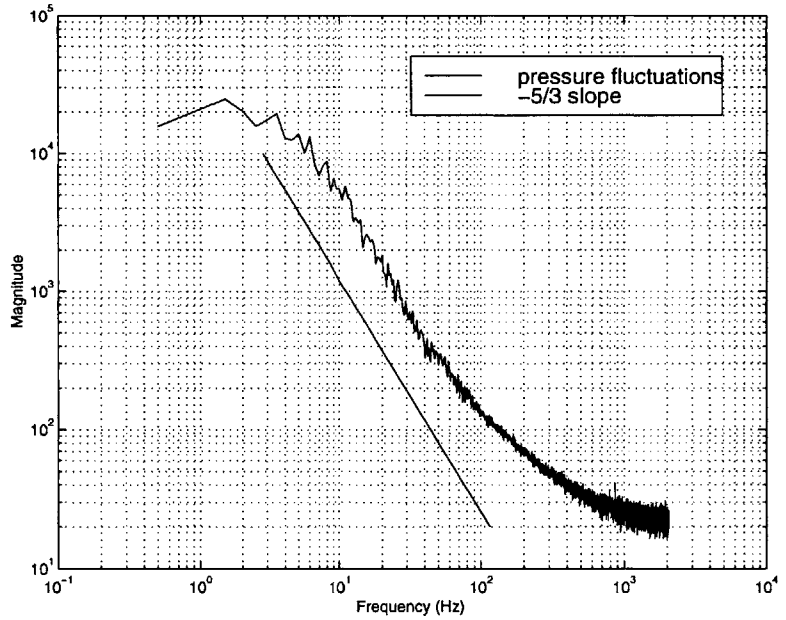

Figure 8-2: Fourier transform of fluctuating pressure measurements in CFB freeboard

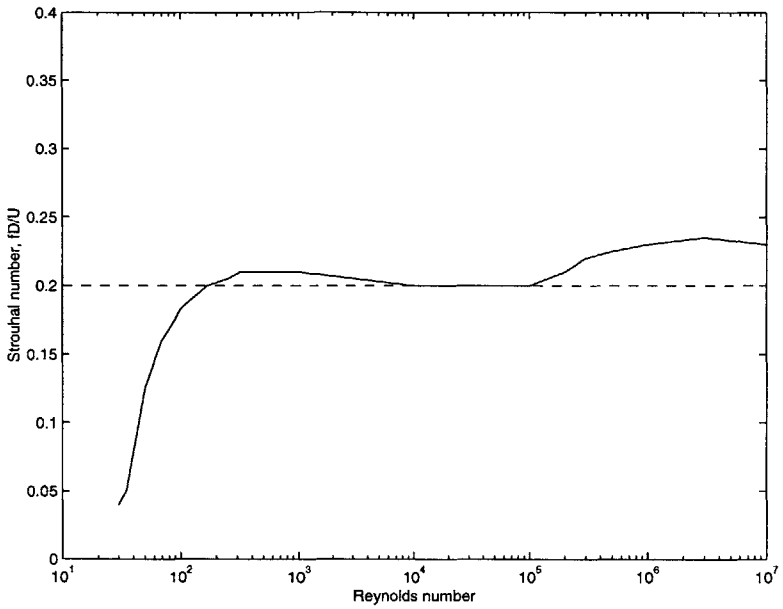

Figure 8-3: Strouhal number versus Reynolds number

Where V_{rel} is the relative velocity between the cluster and the air. As a first estimate this is equal to the air velocity minus the particle terminal velocity. The frequency f is related to the peak frequency obtained from the pressure measurements and $L_{cluster}$ is the cluster length scale. Unfortunately though using this criteria yields a cluster length scale of $10cm$ for our CFB which is almost five times larger than our expected value of $2cm$. There is clearly potential for a significant amount of useful future research in this area.

8.1.3 Numerical modeling

Some simplifications were made in using the CFD model to investigate the velocity field surrounding itself. The application of Darcy's law to describe the flow within the cluster is one. It is unclear whether or not Darcy's law applies at relatively low solid fractions and, even if so, it is unclear if the distribution of particles throughout the cluster is sufficiently uniform to allow the use of a single value of permeability. A more accurate model would consider the cluster region to contain individual solid particles, rather than a permeable continuum. Then there is the issue already touched upon as to the correct shape to use for a cluster. More in-depth experimental data is

required to answer this question and even then there is a good chance it varies from system to system, although a suitable starting point is the cluster shape observed in these experiments.

8.1.4 Modeling particle motion

The effect of an eddy on the motion of a particle is crucially important for a CFB. Especially in light of the results presented throughout this thesis it becomes even more important to examine what happens when a particle interacts with a large scale eddy. For some numerical models this interaction is ignored as there was evidence from previous two-phase flow research that the particle phase will damp out turbulence. Our observations that the unique flow structure inside a CFB will not damp out turbulence but will in fact cause substantial increase in the fluctuations puts modeling particle/eddy interactions back in the spotlight. Typically a scaling argument is used where if the particle Stokes number is large, (> 10), then the eddies have no effect of its motion, whereas if the particle Stokes number is small, (< 0.1), then it is said to follow the eddy trajectory exactly. For intermediate Stokes numbers, as found typically is CFBs, there is no satisfactory technique used to model their motion. The Stokes number for our particles inside the large CFB is 0.3 seconds. This is very important to do so as the motion and deposition of particles from the core to the wall of a CFB, as discussed in section (2.3.1), is the dominant heat transfer mechanism. A first principle numerical model to predict heat transfer needs to take into account this particle/eddy motion.

8.2 Summary

The motivation behind this research was a desire to investigate the gas phase behavior inside a CFB and its influence on bed to wall heat transfer. Initially experiments observing clusters on a transparent membrane wall led to an interest in the mechanism by which particles are transported and removed from the walls. After a literature search revealed a distinct lack of prior research in this area, an experimental procedure was designed that allowed adequate measurements be made of gas phase mean and fluctuating velocities inside a cold scale model CFB. Calibration experiments indicated that this was a valid technique.

Measurements were made using the instrumentation developed and the results were surprising in that they predicted an increase in turbulent intensity between 100% and 400%. This was a revelation because little if any increase was expected. If anything, a decrease was expected. The effects of these fluctuations potentially have a profound effect on particle dispersion and heat transfer. After investigating the differences between the hydrodynamics of standard low particle concentration two phase flows and CFB flows it was postulated that dense concentrations of particles, known as clusters, which form throughout the riser were responsible for the increase in gas fluctuations as a result of their large length scale.

In order to verify if this suggestion was correct a simple experiment was designed and built. The effects of a single cluster on the surrounding air flow could be studied and observed. It was found that gas velocity fluctuations of similar magnitude to the CFB experiments were observed. Using a high speed video camera to photograph the cluster as it passed by the probe useful information could be obtained. The increase or decrease in velocity occurred as the cluster approached but after the cluster had passed the velocity continued to increase or decrease and only returned to normal after 3-5 cluster length scales had passed. This provided evidence that the cluster wake region in which there exists gas and dilute solids flow contains significant velocity variations.

An approximate numerical model was developed to simulate the velocity field surrounding a cluster. The cluster was modeled as a porous continuum have a porosity and permeability comparable to the porosity and permeability of an actual

cluster. The length scale of this body was taken as the estimated length scale found inside the CFB. The velocity flow through the structure was very small in comparison to the free stream flow. The porous body caused vortices to shed which caused velocity fluctuations of comparable magnitude to those in both the single cluster experiment and CFB experiments.

The evidence from the experiments and simulations points to a mechanism for vortex generation inside a CFB that has never been considered before. The clustering of particles, and subsequent vortex shedding, raises the gas fluctuations substantially which has significant implications for heat transfer inside a CFB.

8.3 Conclusions

The general conclusions from this work are:

- The velocities of clusters on the surface of the membrane wall is independent of bed operating conditions.
- Significantly higher particle concentrations were observed on the fin sections in comparison with the tube sections.
- The average velocity of clusters on the fin was 1.76m/s while the average cluster velocity on the tube was 1.02m/s. The difference between these two is attributed to cluster acceleration.
- The distance traveled by a cluster on the tube section before leaving the wall was approximately 5.5cm while clusters on the fins traveled much further.
- Using a shielded hot wire can produce accurate measurements for gas velocities in circulating fluidized beds
- The average gas velocity at the bed center can be over twice as high as the gas superficial velocity
- There appears to be a relationship between the mean gas centerline velocity and the local cross sectional solids concentration
- In addition to a particle boundary layer at the wall there is also a gas boundary layer
- The gas and particle boundary layer thickness are the same order of magnitude
- The presence of the solids in the fluidized bed causes a steep gradient in gas velocity from the wall to the centerline in comparison to the gradient resulting from a single phase gas flow
- There are large scale velocity fluctuations most probably caused by particle clustering
- The frequency of these fluctuations is in the range of 0-300Hz

- The Kolmogorov microscale length and velocity was found to be similar to the particle length scale and the high frequency fluctuating velocity.
- Experiments and simulations using single clusters indicate that there are significant air velocity variations surrounding a cluster.
- The air velocity that flows through a cluster is negligible in comparison to the air velocity that flows around the cluster for values of porosity, particle diameter and cluster size typically found inside CFB's.
- The magnitude of the variations surrounding a cluster is consistent with the air velocity fluctuations observed in the CFB.
- The cause of these fluctuations is vortex shedding around a cluster.
- The increase in gas velocity fluctuations is consistent with previous research in two-phase flow so long as the length scale used is the typical cluster length scale as opposed to the particle diameter - usually there is two orders of magnitude difference between these two scales.

Appendix A

A.1 Calibration curves for anemometers used in experiments

All calibration curves are for anemometers which were surrounded by the protective shield. The anemometers used were all Model 1201 disposable probes from TSI incorporated.

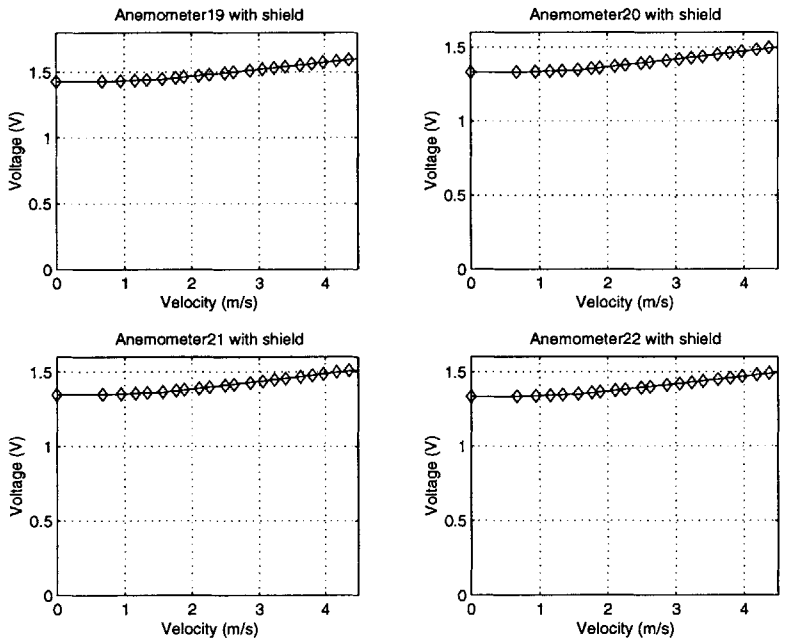

Figure A-1: Calibration curves for hot-wire anemometers with protective shield

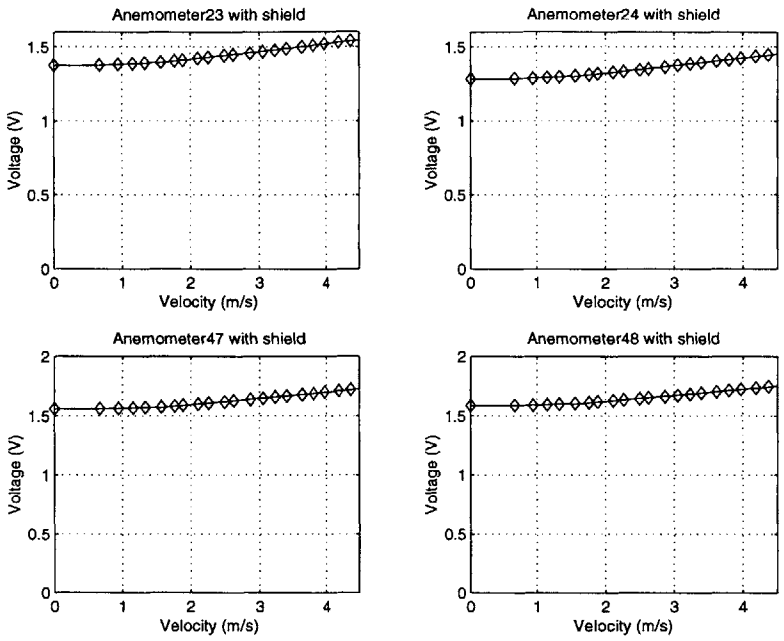

Figure A-2: Calibration curves for hot-wire anemometers with protective shield

Certain calibration curves for anemometers without the protective shield.

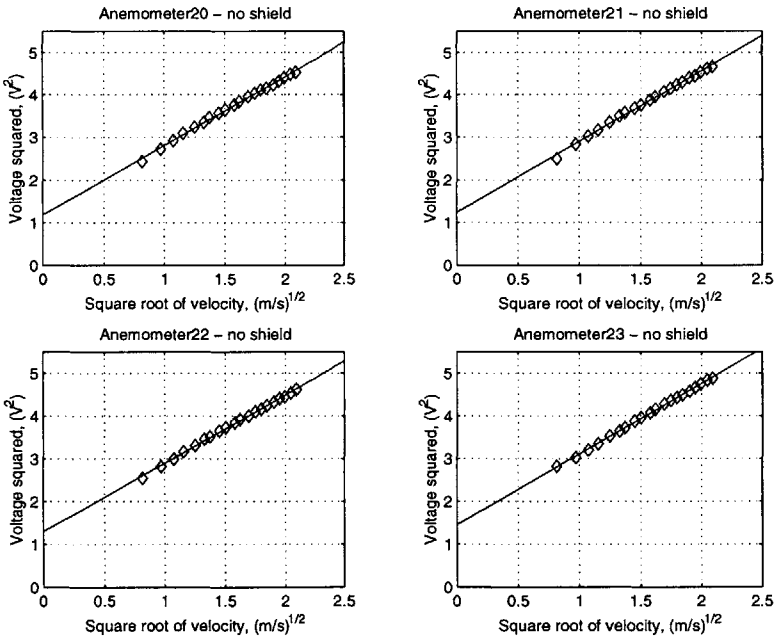

Figure A-3: Calibration curves for hot-wire anemometers without protective shield

Appendix B

B.1 Design Data for Pressure Transducers

The CFB has eleven pressure taps along its length. This allows for ten differential pressure measurements. These measurements allow for the calculation of average solid concentration as a function of riser height as described in section (3.1.3). The transducers are numbered from the bottom of the riser: the rated range is quoted from the manufacturer: the high/low tap locations are those corresponding to the high and low pressure readings: the dimensionless location is the fraction of riser height corresponding to the midpoint between two taps measured from the air distributor: the calibration function converts the voltage signal from the transducer into pressure expressed in inches of water.

transducer number	transducer rated range	high/low tap location	dimensionless location	calibration function
1	1240Pa	1.9/10.4 cm	0.025	$\triangle P = 1.236V - 1.356$
2	1240Pa	10.4/17.3 cm	0.057	$\triangle P = 1.233V - 1.351$
3	1240Pa	17.3/34.9 cm	0.11	$\triangle P = 1.220V - 1.332$
4	500Pa	34.9/54.9 cm	0.18	$\triangle P = 0.4815V - 0.6171$
5	500Pa	54.9/80.6 cm	0.28	$\triangle P = 0.4799V - 0.5769$
6	500Pa	80.6/108 cm	0.39	$\triangle P = 0.4779V - 0.5329$
7	500Pa	108/138 cm	0.50	$\triangle P = 0.4818V - 0.6174$
8	500Pa	138/168 cm	0.63	$\triangle P = 0.4751V - 0.5448$
9	500Pa	168/199 cm	0.75	$\triangle P = 0.4821V - 0.6005$
10	500Pa	199/229 cm	0.88	$\triangle P = 0.4764V - 0.6001$

Table B.1: Pressure tap and transducer characteristics

Appendix C

C.1 Experimental Conditions

The following tables contain the experimental conditions for the experiments performed in both the circulating fluidized bed and the single cluster tosser. Some abbreviations used in the table are:

- mean vel, m/s : average air velocity recorded by the hotwire, m/s
- T.I.% : turbulence intensity, defined by the root mean square fluctuating component divided by the mean velocity component, $\frac{\sqrt{U'^2}}{\bar{U}}$
- Local cssc, % : local averaged cross sectional solids concentration, %
- $U_o, (m/s)$: Gas superficial velocity, m/s
- $G_s, (kg/m^2s)$: Solids recycle rate, kg/m^2s
- probe position : the position of the probe in the bed(s). It can be at the center, at the wall, a certain fixed distance from the center (e.g. center + 1cm), on the flat surface of the membrane wall (flat) or on the curved surface of the membrane wall (curve).
- probe orientation : orientation of probe. Either parallel to the direction of the air flow or perpendicular (perpend) to the air flow direction

- mean cluster vel, m/s : the mean absolute velocity of the cluster as recorded by the high speed digital camera, m/s
- increase/decrease : a velocity increase or decrease detected

test #	mean vel (m/s)	T.I. (%)	local cssc (%)	U_o (m/s)	G_s (kg/m^2s)	probe position	probe orientation
1	4.15	16.5	0.924	2.1	6.54	center	parallel
2	2.06	6.4	0	2.1	0	center	parallel
3	1.60	21	0.75	2.05	4.68	center	perpend
4	1.01	7.0	0	2.12	0	center	perpend
5	1.84	16.0	0.646	2.05	3.92	flat	parallel
6	1.65	5.9	0	2.06	0	flat	parallel
7	1.82	26.5	0.887	2.1	6.51	flat	perpend
8	0.97	10.3	0	2.1	0	flat	perpend
9	2.01	22.5	0.767	2.09	5.45	curve	perpend
10	0.85	9.6	0	2.07	0	curve	perpend
11	3.22	11.3	0.979	2.01	6.29	curve	parallel
12	2.03	8.2	0	2.02	0	curve	parallel
13	5.45	14.2	1.0	2.43	8.1	center	parallel
14	2.58	4.4	0	2.36	0	center	parallel
15	2.8	9.8	0.803	2.4	4.94	center	perpend
16	1.65	3.1	0	2.37	0	center	perpend
17	3.73	11.5	0.781	2.38	5.06	curve	parallel
18	2.33	4.8	0	2.48	0	curve	parallel
19	2.62	15.0	0.743	2.38	5.11	curve	perpend
20	1.83	3.8	0	2.47	0	curve	perpend
21	2.92	12.4	0.69	2.38	4.75	flat	parallel
22	2.43	3.6	0	2.53	0	flat	parallel
23	2.24	19.5	0.786	2.42	5.84	flat	perpend
24	1.75	2.68	0	2.4	0	flat	perpend
25	4.95	19.2	0.699	2.4	4.8	center	parallel
26	4.41	16.5	0.887	2.41	6.63	center+1	parallel
27	3.91	13.8	0.74	2.37	4.87	center+2	parallel
28	4.05	12.4	0.745	2.39	4.61	center+3	parallel

test #	mean vel (m/s)	T.I. (%)	local cssc (%)	U_o (m/s)	G_s (kg/m^2s)	probe position	probe orientation
29	3.66	16.9	0.698	2.44	4.76	center+4	parallel
30	3.24	19.9	0.778	2.36	5.25	center+5	parallel
31	3.25	19.6	0.827	2.39	5.95	center+6	parallel
32	3.18	19.3	0.784	2.41	5.93	center+7	parallel
33	2.13	6.7	0	1.86	0	center	parallel
34	3.35	22.9	n/a	1.9	4.59	center	parallel
35	1.23	9.3	0	1.97	0	center	perpend
36	0.96	20.8	n/a	1.87	4.76	center	perpend
37	1.76	9.3	0	1.88	0	center	parallel
38	2.18	25.7	n/a	1.92	4.75	curve	perpend
39	0.71	7.4	0	1.9	0	curve	perpend
40	1.38	29.6	n/a	1.88	4.29	curve	perpend
41	1.41	7.15	0	1.92	0	flat	parallel
42	1.38	20.2	n/a	1.94	3.57	flat	parallel
43	0.57	5.6	0	1.84	0	flat	perpend
44	1.08	40.8	n/a	1.89	3.55	flat	perpend
45	2.15	7.6	0	2.38	0	center	parallel
46	2.45	23.1	0.104	2.39	1.7	center	parallel
47	3.57	14.6	0.138	2.39	4.76	center	parallel
48	3.79	13.2	0.374	2.39	6.26	center	parallel
49	4.44	10.7	0.622	2.41	9.68	center	parallel
50	4.03	8.75	0.629	2.41	10.31	center	parallel
51	3.72	19.2	0.384	2.34	4.84	center	parallel
52	3.69	22.2	0.384	2.34	4.84	center+1	parallel
53	3.64	17.3	0.384	2.34	4.84	center+2	parallel
54	3.53	20.5	0.384	2.34	4.84	center+3	parallel
55	3.2	22.3	0.384	2.34	4.84	center+4	parallel
56	2.70	16.9	0.384	2.34	4.84	center+5	parallel

test #	mean vel (m/s)	T.I. (%)	local cssc (%)	U_o (m/s)	G_s (kg/m^2s)	probe position	probe orientation
57	2.64	15.4	0.384	2.34	4.84	center+6	parallel
58	3.11	19.9	0.187	2.30	3.28	center	parallel
59	2.81	20.1	0.187	2.30	3.28	center+1	parallel
60	2.73	22.6	0.187	2.30	3.28	center+2	parallel
61	2.72	20.2	0.187	2.30	3.28	center+3	parallel
62	2.52	28.1	0.187	2.30	3.28	center+4	parallel
63	2.52	24.3	0.187	2.30	3.28	center+5	parallel
64	2.16	27.0	0.187	2.30	3.28	center+6	parallel

Table C.1: Experimental conditions for data taken in circulating fluidized bed

test #	mean air vel (m/s)	mean cluster vel (m/s)	probe position	probe orientation	increase decrease
1	2.4	1.32	center	parallel	both
2	3.1	2.27	center	parallel	decrease
3	2.5	2.0	center	parallel	increase
4	2.2	n/a	center	parallel	increase
5	2.5	n/a	center	parallel	increase
6	2.6	0.5	wall	parallel	increase
7	2.2	0.6	wall	parallel	both
8	2.9	1.66	wall	parallel	decrease
9	3.0	2.08	wall	parallel	increase
10	2.9	1.66	wall	parallel	increase
11	2.8	n/a	center	parallel	decrease
12	2.4	n/a	wall	parallel	decrease
13	2.1	n/a	wall	perpend	decrease
14	2.2	n/a	wall	perpend	increase
15	2.4	n/a	wall	perpend	increase
16	2.4	n/a	wall	perpend	decrease
17	2.2	1.9	wall	perpend	increase
18	2.1	1.9	center	parallel	both
19	2.8	2.5	wall	parallel	increase
20	1.8	2.5	wall	perpend	increase
21	2.75	0.78	wall	perpend	increase
22	3.5	n/a	wall	parallel	increase
23	2.5	n/a	wall	perpend	increase
24	3.1	n/a	wall	perpend	both
25	2.5	n/a	wall	parallel	both
26	2.5	n/a	wall	perpend	increase
27	2.3	n/a	center	perpend	increase
28	2.5	n/a	wall	parallel	increase

test #	mean air vel (m/s)	mean cluster vel (m/s)	probe position	probe orientation	increase decrease
29	3.2	n/a	center	parallel	both
30	2.4	n/a	center	perpend	increase
31	1.6	n/a	center	parallel	both
32	1.8	n/a	wall	perpend	increase

Table C.2: Experimental conditions for data taken in single cluster experiments

Appendix D

D.1 Adina input file for vortex shedding simulation

```
****ADD:BATCH *PLSYSTEM NULL
        *FILEECHO OPTION=FILE FILE='f7401.ilog'
        *FILELOG OPTION=FILE FILE='f7401.ilog'
        ****END:BATCH
        ****ADD:INTERACTIVE
        FILEECHO OPTION=NONE
        ****END:INTERACTIVE
        CONTROL PROMPT=NO
        FEPROGRAM PROGRAM=ADINA-F
        HEADING 'f7401: VORTEX SHEDDING FROM A CYLINDER'
        *
        MASTER ANALYSIS=TRANSIENT MODEX=EXECUTE TSTART=0.00000000000000,
```

IDOF=10001 TURBULEN=NO IROTA=0 HYDRO=YES STREAM=YES, TRACTB=DEFAULT IRINT=DEFAULT AUTOMATI=NO SOLVER=5 COMPRESS=NO, FSINTERA=NO NMASS=0 MASSCOUP=NO MAP-OUTP=NONE MAP-FORM=NO, NONDIMEN=NO MAXSOLME=0

*

TIMESTEP NAME=DEFAULT

CLEAR

* TO ENTER THE LIMITING CYCLE OF VORTEX SHEDDING, AT LEAST RUN 100 STEPS.

* 100 0.4

* BUT TO SAVE TIME, HERE ONLY RUN 15 STEPS

15 0.02 * PORTHOLE SAVEDEFAULT=YES FORMATTED=NO INPUT=0 * PRINT-STEPS ENT BLOCK FIRST LAST INCREMENT * 1 100 100 1 1 15 15 1 NODESAVE-STEPS ENT BLOCK FIRST LAST INCREMENT * 1 1 100 1 1 1 15 1 ELEMSAVE-STEPS ENT BLOCK FIRST LAST INCREMENT * 1 100 100 1 1 15 15 1 *

TIMEFUNCTION NAME=2

0.0 0.0

5.0 -0.1

10. 0.1

20. 0.0

1.E+10 0.0 @ * * COORDINATES POINT SYSTEM=0

1 0 0.000000 0.000000 0

2 0 -0.00707107 -0.00707107 0

3 0 0.00707107 -0.00707107 0

4 0 0.00707107 0.00707107 0

5 0 -0.00707107 0.00707107 0

6 0 -0.02000000 -0.02000000 0

7 0 0.02000000 -0.02000000 0

8 0 0.02000000 0.02000000 0

9 0 -0.02000000 0.02000000 0

10 0 -0.2000000 -0.10000000 0

11 0 0.2000000 -0.10000000 0

12 0 0.2000000 0.10000000 0

13 0 -0.2000000 0.10000000 0

@ * * LINE ARC NAME=1 MODE=1 P1=2 P2=3 CENTER=1

LINE ARC NAME=2 MODE=1 P1=3 P2=4 CENTER=1

LINE ARC NAME=3 MODE=1 P1=4 P2=5 CENTER=1

LINE ARC NAME=4 MODE=1 P1=5 P2=2 CENTER=1

LINE ARC NAME=5 MODE=1 P1=6 P2=7 CENTER=1

LINE ARC NAME=6 MODE=1 P1=7 P2=8 CENTER=1

LINE ARC NAME=7 MODE=1 P1=8 P2=9 CENTER=1

LINE ARC NAME=8 MODE=1 P1=9 P2=6 CENTER=1

LINE STRAIGHT NAME=9 P1=10 P2=11

LINE STRAIGHT NAME=10 P1=11 P2=12

LINE STRAIGHT NAME=11 P1=12 P2=13

LINE STRAIGHT NAME=12 P1=13 P2=10

LINE STRAIGHT NAME=13 P1=6 P2=2

LINE STRAIGHT NAME=14 P1=7 P2=3

LINE STRAIGHT NAME=15 P1=8 P2=4

LINE STRAIGHT NAME=16 P1=9 P2=5

LINE STRAIGHT NAME=17 P1=10 P2=6

LINE STRAIGHT NAME=18 P1=11 P2=7

LINE STRAIGHT NAME=19 P1=12 P2=8

LINE STRAIGHT NAME=20 P1=13 P2=9 * SURFACE PATCH NAME=1 EDGE1=5 EDGE2=14 EDGE3=1 EDGE4=13

SURFACE PATCH NAME=2 EDGE1=6 EDGE2=15 EDGE3=2 EDGE4=14

SURFACE PATCH NAME=3 EDGE1=7 EDGE2=16 EDGE3=3 EDGE4=15

SURFACE PATCH NAME=4 EDGE1=8 EDGE2=13 EDGE3=4 EDGE4=16

SURFACE PATCH NAME=5 EDGE1=9 EDGE2=18 EDGE3=5 EDGE4=17

SURFACE PATCH NAME=6 EDGE1=10 EDGE2=19 EDGE3=6 EDGE4=18

SURFACE PATCH NAME=7 EDGE1=11 EDGE2=20 EDGE3=7 EDGE4=19

SURFACE PATCH NAME=8 EDGE1=12 EDGE2=17 EDGE3=8 EDGE4=20

* * MATERIAL CONSTF NAME=1 XMU=18.4333E-6 RHO=1.177 *

LOAD VELOCITY NAME=1 VY=0.783 VZ=0.

LOAD NORMAL-TRACTION NAME=1 MAGNITUD=0. * APPLY-LOAD

BODY=0

1 'VELOCITY' 1 'LINE' 12 0 1 0. 0 0. 0. 0

2 'VELOCITY' 1 'LINE' 11 0 1 0. 0 0. 0. 0

3 'VELOCITY' 1 'LINE' 9 0 1 0. 0 0. 0. 0

4 'NORMAL-TRACTION' 1 'LINE' 10 0 1 0. 0 0. 0. 0 *

BOUNDARY-CON WALL NAME=1 GTYPE=LINES SLIPC=0. MOV-
ING=YES NCURZ=2 1 2 3 4 @ *

INITIAL-COND NAME=I1 'Y-VELOCITY' 0.783 'Z-VELOCITY' 0.00 'PRES-
SURE' 0.00 @ * SET-INITCOND SURFACES CONDITIO=I1 5 'I1' 0

1 'I1' 0

6 'I1' 0

2 'I1' 0

7 'I1' 0

3 'I1' 0

8 'I1' 0

4 'I1' 0 @ * EGROUP TWODFLUID NAME=1 SUBTYPE=PLANAR MA-
TERIAL=1 INT=3,RESULTS=FORCES DEGEN=NO DISSP=NO SOLID=NO *
SUBDIVIDE SURFACE NAME=1 MODE=DIVISIONS NDIV1=10 NDIV2=10, RA-
TIO1=1.00000000000000 RATIO2=10.0000000000000, PROGRESS=GEOMETRIC
EXTEND=NONE 1 2 3 4 5 6 7 8 @ * GSURFACE NODES=9 PATTERN=AUTOMATIC
NCOINCID=BOUNDARIES NCEDGE=1234, NCVERTEX=1234 NCTOLERA=1.00000000000000
05 SUBSTRUC=0 GROUP=1, PREFSHAP=AUTOMATIC MESHING=MAPPED
SMOOTHIN=NO DEGENERA=NO, COLLAPSE=NO MIDNODES=CURVED 1
2 3 4 5 6 7 8 @ * * LEADER-FOLLO

1 2 6 1.00000000000000 0

2 3 7 1.00000000000000 0

3 4 8 1.00000000000000 0

4 5 9 1.00000000000000 0 @ * SAVENODES LINE 1 / 2 / 3 / 4 @ * FRAME
* MESHPLOT BOUNDEPI=ALL * ADINA-F FILE='f7401.dat'

****ADD:SNAPSHOT *SNAPSHOT 'f7401.ps' APPEND=NO ****END:SNAPSHOT
****ADD:BATCH *QUIT IMMEDIATE=YES ****END:BATCH

Bibliography

[1] Bengt-Åke Andersson and Bo Leckner. Experimental methods of estimating heat transfer in circulating fluidized bed boilers. *International Journal of Heat and Mass Transfer*, 35(12):3353–3362, 1992.

[2] Bengt-Åke Andersson and Bo Leckner. Local Lateral Distribution of Heat Transfer on Tube Surface of Membrane Walls in CFB Boilers. In *4th Int. Conf. on Circulating Fluidized Beds*, pages 311–318, Somerset PA, 1993.

[3] A.P. Baskakov. The Mechanism of heat Transfer between a Fluidized-Bed and a Surface. *International Chemical Engineering*, 4(320), 1964.

[4] P. Basu and P.K. Nag. Heat Transfer to Walls of a Circulating Fluidized-Bed Furnace. *Chemical Engineering Science*, 51(1):1–26, 1996.

[5] Thomas G. Beckwith, Roy D. Marangoni, and John H. Lienhard V, editors. *Mechanical Measurements.* Addison-Wesley, 5 edition, 1995.

[6] D.C. Bensard and F.H. Harlow. Turbulence in multiphase flow. *Intl. Jnl. Multiphase Flow*, 14:679–699, 1988.

[7] H. Chang and M. Louge. Fluid Dynamic Similarity of Circulating Fluidized Beds. *Powder Tech.*, 70:259–270, 1992.

[8] Clayton Crowe, Martin Sommerfield, and Yutaka Tsuji. *Multiphase Flows with Droplets and Particles.* CRC Press, New York, 1998.

[9] C.T. Crowe. On Models for Turbulence Modulation in Fluid-Particle Flows. *Intl. Jnl. of Multiphase Flow*, 26:719–727, 2000.

[10] Leon Douglas and David Platt, editors. *Pulverized-coal combustion and gasification: theory and applications for continuous flow processes.* Plenum Press, New York, 1979.

[11] T. Ebert, L.R.Glicksman, and M. Lints. Determination of Particle and Gas Convective Heat Transfer Components in a Circulating Fluidized Bed. *Chemical Engineering Science*, 48(12):2179–2188, 1993.

[12] H. Enwald and A.E. Almstedt. Fluid dynamics of a pressurized fluidized bed: comparison between numerical solutions from two-fluid models and experimental results. *Chemical Engineering Science*, 54:329–342, 1999.

[13] Paul A. Farrell. *Hydrodynamic Scaling and Solids Mixing in Pressurized Bubbling Fluidized Bed Combustors.* PhD thesis, Massachusettes Institute of Technology, June 1996.

[14] James A. Fay. *Introduction to Fluid Mechanics.* MIT Press, 1 edition, 1994.

[15] Uriel Frisch. *Turbulence: the legacy of A.N.Kolmogorov.* Cambridge University Press, 1 edition, 1995.

[16] G.I.Palchonok, C.Breitholtz, V.A.Borodulya, and B.Leckner. Effect of Turbulance on Heat Transfer in the Freeboard of Stationary and Circulating Fluidized Beds. In *Fluidization IX*, pages 413–420, Durango, Colorado, May 1998.

[17] G.K.Batchelor. *The Theory of Homogeneous Turbulence.* Cambridge University Press, 1953.

[18] Leon R. Glicksman and Peter D. Noymer. Measurements of the Velocity and Acceleration of Clusters at the Wall of a Circulating Fluidized Bed. In *AIChE Annual Meeting*, November 1996.

[19] L.R. Glicksman. Circulating Fluidized Bed Heat Transfer. In P.Basu and J.F.Large, editors, *Circulating Fluidized Bed Technology 2.* Pergamon Press, 1988.

[20] L.R. Glicksman, M. Hyre, and P. Farrell. Dynamic Simularity in Fluidization. *International Journal of Multiphase Flow*, 20:331–386, 1994.

[21] R.A. Gore and C.T. Crowe. Effect of Particle Size on Modulating Turbulent Intensity. *Int. J. Multiphase Flow*, 15(2):279–285, 1989.

[22] J.R. Grace, A.A. Avidan, and T.M. Knowlton, editors. *Circulating Fluidized Beds.* Blackie Academic & Professional, New York, 1997.

[23] Elias P. Gyftopoulos and Gian Paolo Beretta. *Thermodynamics: foundations and applications.* Collier Macmillan, New York, 1991.

[24] Masayuki Horio and Hiroaki Kuroki. Three-Dimensional Flow Visualization of Dilutely Dispersed Solids in Bubbling and Circulating Fluidized Beds. *Chemical Engineering Science*, 49(15):2413 – 2421, 1994.

[25] P. Hutchinson, G. Hewitt, and A.E. Dukler. Deposition of Liquid or Solid Dispersion from Turbulent Gas Streams: a Stochastic Model. *Chemical Engineering Science*, 26:419 – 439, 1971.

[26] Matthew R. Hyre. *Aspects of Hydrodynamics and Heat Transfer in Circulating Fluidized Beds.* PhD thesis, Massachusettes Institute of Technology, September 1995.

[27] Frank P. Incropera and David P. Dewitt. *Fundamentals of Heat Transfer.* John Wiley & Sons, 1981.

[28] A. Kokko, R. Karvinen, and H. Alstedt. CYMIC - boiler scale up and full scale demonstration experiences. In K.J.Heinschel, editor, *Proceedings of the 13th International Conference on Fluidized Bed Combustion*, volume 1, page 219, 1995.

[29] J.A.M. Kuipers, B.P.B. Hoomans, and W.P.M. van Swaaij. Hydrodynamic Models of Gas-Fluidized Beds and Their Role for Design and Operation of Fluidized Bed Chemical Reactors. In *Fluidization IX*, pages 15–30, Durango, Colorado, May 1998.

[30] D. Kunii and O.L. Levenspiel, editors. *Fluidization Engineering*, volume 1. Robert E. Krieger, 1977.

[31] K.S. Lim, J. Zhou, C. Finley, J.R. Grace, and C.M.H. Brereton. Cluster Descending Velocity at the Wall of Circulating Fluidized Bed Risers. In *Circulating Fluidized Bed Technology V*, pages 218–223, Beijing, China, May 1996.

[32] M. Lints. *Particle-to-Wall Heat Transfer in Circulating Fluidized Beds.* PhD thesis, Massachusettes Institute of Technology, February 1992.

[33] M. Lints and L.R. Glicksman. The Structure of Particle Clusters Near the Wall of a Circulating Fluidized Bed. In *AIChE Symposium Series*, volume 89 of *296*, pages 35–47, 1993.

[34] M.C. Lints and L.R. Glicksman. Parameters Governing Particle-to-Wall Heat Transfer in a Circulating Fluidized Bed. In A. Avidan, editor, *Circulating Fluidized Bed Technology IV.* Pergamon Press, 1993.

[35] C. Lockhart, J. Zhu, C.M.H. Brereton, C.J. Lim, and J.R. Grace. Local Heat Transfer, Solids Concentration and Erosion around Membrane Tubes in a Cold Model Circulating Fluidized Bed. *Int. J. Heat Mass Transfer*, 38(13):2403–2410, 1995.

[36] L.R.Glicksman. Scaling Relationships for Fluidized Beds. *Chemical Engineering Science*, 39:1373–1379, 1984.

[37] L.R.Glicksman, M. Hyre, and K. Woloshun. Simplified Scaling Relationships for Fluidized Beds. *Powder Tech.*, 77:177, 1993.

[38] H.S. Mickley and D.F. Fairbanks. Mechanism of Heat Transfer to Fluidized Beds. *AIChE Journal*, 1:374, 1955.

[39] D. Modarress, J. Wuerer, and S. Elghobshi. An Experimental Study of a Turbulent Round Two-Phase Jet. *Chem. Engng Commun.*, 28:341–354, 1984.

[40] James C. Moran and Leon R. Glicksman. Observations of Clusters on a Membrane Wall of a Circulating Fluidized Bed. In *AIChE Annual Meeting*, Dallas, TX, November 1999.

[41] N.I.Gelperin and V.G. Einstein. *Heat Transfer in Fluidized Beds.* Academic Press, 1971.

[42] Peter Noymer and Leon R. Glicksman. Measurement of Cluster-Wall Contact Times in a Scale Model Circulating Fluidized Bed. In *ASME Winter Annual Meeting*, 1996.

[43] Peter Noymer and Leon R. Glicksman. Cluster motion and Particle Convection Heat Transfer at the Wall of a Circulating Fluidized Bed. *Int. J. Heat Mass Transfer*, 41(1):147–158, 1998.

[44] Peter Noymer, Matthew R. Hyre, and Leon R. Glicksman. The Influence of Bed Diameter on Hydrodynamics and Heat Transfer in Circulating Fluidized Beds. In *AIChE Annual Meeting*, pages 117–121, Florida, 1995.

[45] Peter D. Noymer. *Heat Transfer by Particle Convection at the Wall of a Circulating Fluidized Bed.* PhD thesis, Massachusettes Institute of Technology, June 1997.

[46] Jie Ouyang and Jinghai Li. Particle-motion-resolved discrete model for simulating gas-solid fluidization. *Chemical Engineering Science*, 54:2077–2083, 1999.

[47] P.R. Owen. Pneumatic transport. *Jnl. Fluid Mech.*, 39:407–432, 1969.

[48] M. Rashidi, G. Hetsroni, and S. Banerjee. Particle-turbulence interaction in a boundary layer. *Int. J. Multiphase Flow*, 16(6):935–949, 1990.

[49] M. Rhodes, H. Mineo, and T. Hirama. Particle Motion at the Wall of a Circulating Fluidized Bed. *Powder Technology*, 70:207–214, 1992.

[50] A.E. Scheidegger. *The Physics of Flow Through Porous Media.* University of Toronto Press, 1960.

[51] Hermann Schlichting. *Boundary-Layer Theory.* McGraw-Hill, 6 edition, 1968.

[52] J. S. Shuen, A. S. P. Solomon, Q. F. Zhang, and G. M. Faeth. Structure of Particle-Laden Jets - Measurements and Predictions. *AIAA Jl*, 23:396–404, 1985.

[53] C.H. Soong, K. Tuzla, and J.C. Chen. Identification of Particle Clusters in Circulating Fluidized Beds. In *4th Int. Conf. on Circulating Fluidized Beds*, page 137, Somerset PA, 1993.

[54] C.H. Soong, K. Tuzla, and J.C. Chen. Experimental Determination of Cluster Size and Velocity in Circulating Fluidized Bed. In *Fluidization VIII*, May 14-19 1995.

[55] J. Sterneus, F. Johnsson, B. Leckner, and G.I. Palchonok. Gas and solids flow in circulating fluidized beds - discussion on turbulence. *Chemical Engineering Science*, 54:5377–5382, 1999.

[56] Johan Sterneus, Filip Johnsson, and Bo Leckner. Gas mixing in circulating fluidized-bed risers. *Chemical Engineering Science*, 55:129–148, 2000.

[57] D. Subbarrao and P. Basu. A Model for Heat Transfer in Circulating Fluidized Beds. *Int. J. Heat Mass Transfer*, 29(3):487–489, 1986.

[58] A.M. Al Taweel and J. Landau. Turbulence modulation in two-phase jets. *Intl. Jnl. Multiphase Flow*, 3:341–351, 1977.

[59] T.G. Theofaneous and J. Sullivan. Turbulence in two-phase dispersed flows. *Jnl. Fluid Mech.*, 116:434–462, 1982.

[60] Y. Tsuji, T. Kawaguchi, and T. Tanaka. Discrete Particle Simulation of a Two-Dimensional Fluidized Bed. *Powder Tech.*, 77:79–87, 1993.

[61] Y. Tsuji, Y. Morikawa, and H. Shiomi. Ldv Measurements of an Air-Solid Two-Phase Flow in a Vertical Pipe. *J. Fluid Mechanics*, 139:417–434, 1984.

[62] D. Westphalen. *Scaling and Lateral Solids Mixing in Circulating Fluidized Beds.* PhD thesis, Massachusettes Institute of Technology, June 1993.

[63] D. Westphalen and L.R. Glicksman. Experimental verification of scaling for a commercial size CFB combustor. In A. Avidan, editor, *Circulating Fluidized Bed Technology IV.* Pergamon Press, 1993.

[64] Frank M. White. *Viscous Fluid Flow.* McGraw-Hill, 2 edition, 1991.

[65] L.P. Yarin and G. Hetsroni. Turbulence intensity in dilute two phase flows: the particles-turbulence interaction in dilute two-phase flow. *Int. J. Multiphase Flow*, 20:27–44, 1994.

[66] J. Yerushalmi and N.T.Cankurt. Further studies of the regimes of fluidization. *Powder Technology*, 24:187, 1979.

[67] Z. Yuan and E.E. Michaelides. Turbulence modulation in particulate flows - a theoretical approach. *Intl. Jnl. Multiphase Flow*, 18:779–785, 1992.

[68] Wennan Zhang, Filip Johnsson, and Bo Leckner. Fluid-Dynamic Boundary Layers in CFB Boilers. *Chemical Engineering Science*, 50(2):201–210, 1995.

[69] J. Zhou, J. R. Grace, C. M. H. Brereton, and C. J. Lim. Influence of Membrane Walls on Particle Dynamics in a Circulating Fluidized Bed. *AIChE Journal*, 42(12), December 1996.

[70] J. Zhou, J.R. Grace, C.J. Lim, and C.M.H. Brereton. Particle Velocity Profiles in a Circulating Fluidized Bed of Square Cross-Section. *Chem. Eng. Sci.*, 50:237, 1995.

[71] J. Zhou, J.R. Grace, S. Qin, C.M.H. Brereton, C.J. Lim, and J. Zhu. Voidage Profiles in a Circulating Fluidized Bed of Square Cross-Section. *Chem. Eng. Sci.*, 49:3217, 1994.